

NASA CR-139171

S-BAND PARAMETRIC AMPLIFIER MODEL A-471

(NASA-CR-139171) DEVELOPMENT AND
FABRICATION OF S-BAND CHIP VARACTOR
PARAMETRIC AMPLIFIER Final Report, Aug.
1973 - Nov. 1974 (Airborne Instruments Lab.)
182 p HC

N75-14961

Unclas

CSCL 09A G3/33 06932

E. H. Kraemer
AIL, a division of Cutler-Hammer
Deer Park, N.Y. 11729

November 1974

Final Report for Period August 1973 - November 1974

Prepared for:
GODDARD SPACE FLIGHT CENTER
Greenbelt, Maryland 20771

Reproduced by
**NATIONAL TECHNICAL
INFORMATION SERVICE**
U.S. Department of Commerce
Springfield, VA. 22151

AIL a division of
CUTLER-HAMMER
DEER PARK, LONG ISLAND, NEW YORK 11729



PRICES SUBJECT TO CHANGE

TECHNICAL REPORT STANDARD TITLE PAGE

1. Report No.		2. Government Accession No.		3. Recipient's Catalog No.	
4. Title and Subtitle Final Report on Development and Fabrication of S-Band Chip Varactor Parametric Amplifier				5. Report Date November 1974	
				6. Performing Organization Code	
7. Author(s) Erich Kramer				8. Performing Organization Report No.	
9. Performing Organization Name and Address AIL, a division of Cutler-Hammer Melville, L. I., N. Y. 11746				10. Work Unit No.	
				11. Contract or Grant No. NAS5-20460	
12. Sponsoring Agency Name and Address Goddard Space Flight Center Greenbelt, Maryland 20771 Mr. Pio Dalle-Mura				13. Type of Report and Period Covered	
				14. Sponsoring Agency Code	
15. Supplementary Notes					
16. Abstract <p>A noncryogenic, S-band parametric amplifier operating in the 2.2 to 2.3 GHz band and having an average input noise temperature of less than 30 K has been built and tested. The parametric amplifier module occupies a volume of less than 1-1/4 cubic feet and weighs less than 60 pounds. The module is designed for use in various NASA ground stations to replace larger, more complex cryogenic units which require considerably more maintenance because of the cryogenic refrigeration system employed. The amplifier can be located up to 15 feet from the power supply unit. Optimum performance has been achieved through the use of high-quality unpackaged (chip) varactors in the amplifier design. The attainment of these requirements constitutes a significant advancement in low-noise amplifier design and associated semiconductor technology.</p>					
17. Key Words Parametric Amplifiers S-Band			18. Distribution Statement		
19. Security Classif. (of this report) Unclassified		20. Security Classif. (of this page)		21. No. of Pages 180	
				22. Price *	



PREFACE

An S-Band Parametric Amplifier achieving a 30 K input noise temperature without use of cryogenics is described. The entire paramp module has a volume of less than 1-1/4 cubic feet and weighs less than 60 pounds. The following is a summary of the major electrical performance characteristics.

Frequency Range	2.2 to 2.3 GHz
Minimum Gain	30 dB
Maximum Gain Ripple	0.25 dB
Input Noise Temperature	28 K average
Phase Linearity	± 1.5 degrees
Delay Distortion	1.4 nanoseconds maximum
Intermodulation for two -65 dBm carriers	51 dBm down
Gain Compression (-1 dB)	-46.5 dBm input
Gain Stability	± 0.08 dB over 8 hours
Phase Stability	± 3.5 degrees over 12 hours

The unit operates from a 115 volt ac power source with a maximum input power requirement of 650 watts. The details are reported herein. The unit is designed to replace some cryogenic units in various NASA earth stations.

Preceding page blank



TABLE OF CONTENTS

	<u>Page</u>
I. Introduction	1-1
A. General	1-1
B. Requirements	1-2
C. Functional Description	1-6
II. Technical Discussion	2-1
A. Basic Noise Considerations in Ultra Low-Noise Noncryogenic Paramp Systems	2-1
B. Parametric Amplifier	2-5
C. Varactor	2-26
D. Circulator	2-40
E. Pump Source	2-50
F. Environmental Considerations	2-54
G. Packaging Requirements	2-63
H. Reliability Prediction	2-66
III. Measured Performance	3-1
A. General	3-1
B. Breadboard System	3-1
C. Measured Performance - Prototype System	3-3
IV. New Technology Developments	4-1
V. Conclusions and Recommendations	5-1
A. Conclusions	5-1
B. Recommendations	5-1
VI. References	6-1

Preceding page blank

	<u>Page</u>
VII. Appendixes	7-1
A. Computer Model of Parametric Amplifier Circuit	A-1
B. Gain Changes as a Function of Circulator Isolation Changes	B-1
C. Noise Transfer Analysis--Single Stage Parametric Amplifier	C-1
D. Test Procedure for Evaluation of Nonhermetically Sealed Gallium Arsenide Varactor	D-1
E. Summary of Diode Evaluation Data	E-1
F. Noise Transfer Analysis--General Case for Multistage Parametric Amplifier System	F-1



LIST OF ILLUSTRATIONS

<u>Figure</u>		<u>Page</u>
1-1	Specified Mechanical Outline of Paramp Enclosure	1-4
1-2	Simplified Functional Block Diagram of S-Band System	1-7
1-3	Remote Control/Power Supply Unit Block Diagram	1-8
1-4	Paramp Module and Remote Control/Power Supply Unit Comprising A471 System	1-11
2-1	Simple Equivalent Circuit for Calculating Noise	2-4
2-2	Noise Degradation Versus Antenna Return Loss	2-7
2-3	Final System Gain/Noise Temperature Budget	2-8
2-4	Schematic Diagram of Balanced Parametric Amplifier With Propagating Idler	2-9
2-5	Varactors in Waveguide	2-9
2-6	Parametric Amplifier Configuration	2-11
2-7	Block Diagram of Broadband Parametric Amplifier Theoretical Model	2-11
2-8	Noise Temperature as a Function of Pump Frequency and M	2-16
2-9	Theoretical Single Stage Gain for Proposed Balanced Parametric Amplifier With Ideal Circulator	2-16
2-10	Parametric Amplifier Mount	2-19
2-11	Least Squares Error Fit of Theoretical Paramp Phase Characteristic to Third-Order Polynomial	2-24
2-12	Varactor Holder	2-27
2-13	Assembled Quanar Varactor	2-28
2-14	Typical Varactor I Versus V Trace	2-29
2-15	Varactor C Versus V	2-30

<u>Figure</u>		<u>Page</u>
2-16	Impedance Plot of M-S Junction	2-32
2-17	Equivalent Circuit of Chip Varactor and Holder	2-33
2-18	Effect of Temperature on Varactor Contact	2-35
2-19	Various Circulator Paramp Configurations	2-41
2-20	Circulator Representation at $T = T_O$ and $T = T_O + \Delta T$	2-44
2-21	Magnetization as Function of dc Field and M_S	2-46
2-22	Degradation of Tangential Sensitivity as a Function of Absolute Power of Interfering Signal	2-52
2-23	Typical Bipolar Temperature Controllers	2-55
2-24	Paramp Module, Site Interface Outline	2-56
2-25	Paramp Module	2-60
2-26	First-Stage Circulator-Paramp Assembled to Thermo-electric Chill Plate and Input Transition	2-61
2-27	Lower Compartment Components Drawer (Partially Wired)	2-65
2-28	Remote Control/Power Supply Chassis	2-67
3-1	Measured Breadboard Room Temperature Performance	3-6
3-2	Measured Breadboard System Saturation Characteristics	3-7
3-3	Prototype Components for S-Band Chip Varactor System - Breadboard Tests	3-8
3-4	Gain-Bandwidth Characteristics	3-9
3-5	Noise Temperature Versus Frequency	3-10
3-6	Input-Output VSWR Versus Frequency	3-11
3-7	Dynamic Range Versus Frequency	3-12
3-8	Phase Linearity Versus Frequency	3-13
3-9	Envelope Delay Distortion Versus Frequency	3-14
3-10	Gain Stability Under Thermal Cycling	3-15
5-1	Comparison of the Prototype System With a Typical Equivalent Cryogenic Unit	5-2

<u>Figure</u>		<u>Page</u>
5-2	Proposed Production Model - LNA Configuration	5-5
5-3	Proposed Production Model - Front View	5-7
5-4	Proposed Production Model - Lower Compartment	5-9



I. INTRODUCTION

A. GENERAL

This report describes an S-band Parametric Amplifier System (AIL Model A-471) that has achieved a 30 K effective input noise temperature without using cryogenic refrigerators. The entire paramp unit has a volume of less than 1-1/4 cubic feet and is designed to meet the site interface requirements of various NASA ground stations. The remote power supply unit fits in a standard 19-inch rack and occupies only 7 inches of rack space. The amplifier is capable of operating over long periods of time with minimum maintenance. Since production versions of this prototype will eventually be required, the unit has been engineered so that only a minimum of engineering effort will be needed to evolve a production design of high reliability.

A number of approaches were considered in an effort to determine the optimum configuration that could be used for the paramp system that would meet the required specifications. The overall size limitations normally associated with a system when mounted in operational antenna structures, the thermal and vibration environment encountered, and the desirability for a high degree of long-term stability, power requirements, and the human engineering factors associated with operating and maintaining the system have been assessed. With these design criteria and constraints taken into account, the following approach was formulated for the ultra low-noise non-cryogenic S-band paramp system.

The approach evolved for this program is both simple and practical and has a high probability of success. The system consists of two identical stages of parametric amplification, each stage consisting of a single-ended parametric amplifier employing the proven AIL passivated quasiplanar (QUANAR) chip-type varactor coupled to a four-port circulator. The pump source consists of a separate 50-GHz fundamental Gunn oscillator for each stage. The first stage parametric amplifier and circulator are temperature-stabilized at -20°C using thermoelectric modules, while the remainder of the enclosure is stabilized at a temperature of +50°C.

The unit exceeds the following original electrical performance requirements with the exception of gain stability versus ambient temperature which deviates slightly more than (1 dB) from the design goal specification (below 10°C).

B. REQUIREMENTS

NASA Contract NAS-5-20460 defines the following requirements for the S-band paramp system:

- Two-stage paramp system, all solid state in design, packaged in a temperature controlled enclosure which includes all necessary power supplies
- Center frequency 2250 \pm 10 MHz
- Bandwidth (-1 dB point) 100 to 150 MHz
- Midband gain 30 dB (minimum)
- Noise temperature 30 K (maximum) from 2210 to 2290 MHz
35 K (maximum) from 2200 to 2300 MHz
- Gain ripple 0.5 dB peak-to-peak (maximum) over band pass, except 1.0 dB peak-to-peak (maximum) at band edges
- Gain compression (1-dB point) -50 dBm (minimum) (referred to input)
- Input/output VSWR 1.5:1 (maximum) with amplifier operating at full gain conditions and terminated with a load having a return loss of 10 dB or greater
- Phase linearity \pm 2 degrees from 2215 to 2285 MHz
 \pm 5 degrees from 2200 to 2215 MHz
 \pm 5 degrees from 2285 to 2300 MHz
- Phase slope (deviation from linearity) 0.5 degree/MHz (maximum) from 2200 to 2300 MHz
- Envelope delay distortion 5 ns (maximum) from 2200 to 2300 MHz
- Delay slope 1 ns/MHz (maximum) from 2200 to 2300 MHz
- Phase stability \pm 5 degrees over a 12 hour period
- Gain stability \pm 0.5 dB over an 8 hour period at an ambient temperature of 60 to 80°F

- Ambient temperature range -15°C to +50°C
- Gain stability over ambient temperature range ±1 dB (maximum)
- Spurious response -100 dBm (maximum) at f_p
-125 dBm (maximum) at other frequencies
- Intermodulation products At least 50 dB below the output of two carriers with equal input powers of -65 dBm
- Primary power 117 volts ac ±10 percent, 58 to 62 Hz
- Reliability The paramp system shall exhibit an MTBF of 16,000 hours
- Humidity 10 to 95 percent
- Orientation Any
- Vibration and shock The paramp system shall operate within specification when subjected to vibration and shock normally encountered in an antenna system employing a hydraulic drive.

A change in scope after the breadboard phase added the following requirements.

- Figure 1-1 indicates the maximum dimensions permissible for the proposed paramp. In addition to the stated dimensions, the enclosure shall have no protrusions on the sides except for mounting lugs. The unit will be mounted with the back adjacent to a bulkhead surface. Interior access for normal maintenance shall be from the front. All connections and controls will be located on the front or top surface. They shall be positioned in such a manner that they will not interfere with other equipment when installed in the system nor shall they interfere with the ability to perform normal maintenance on the paramp.
- The paramp will be installed as a dual system in two configurations. The 28-meter antenna installation requires close dimensional tolerances on the paramp to be physically integrated into the antenna system. This dictates tight design requirements for the mechanical configuration.

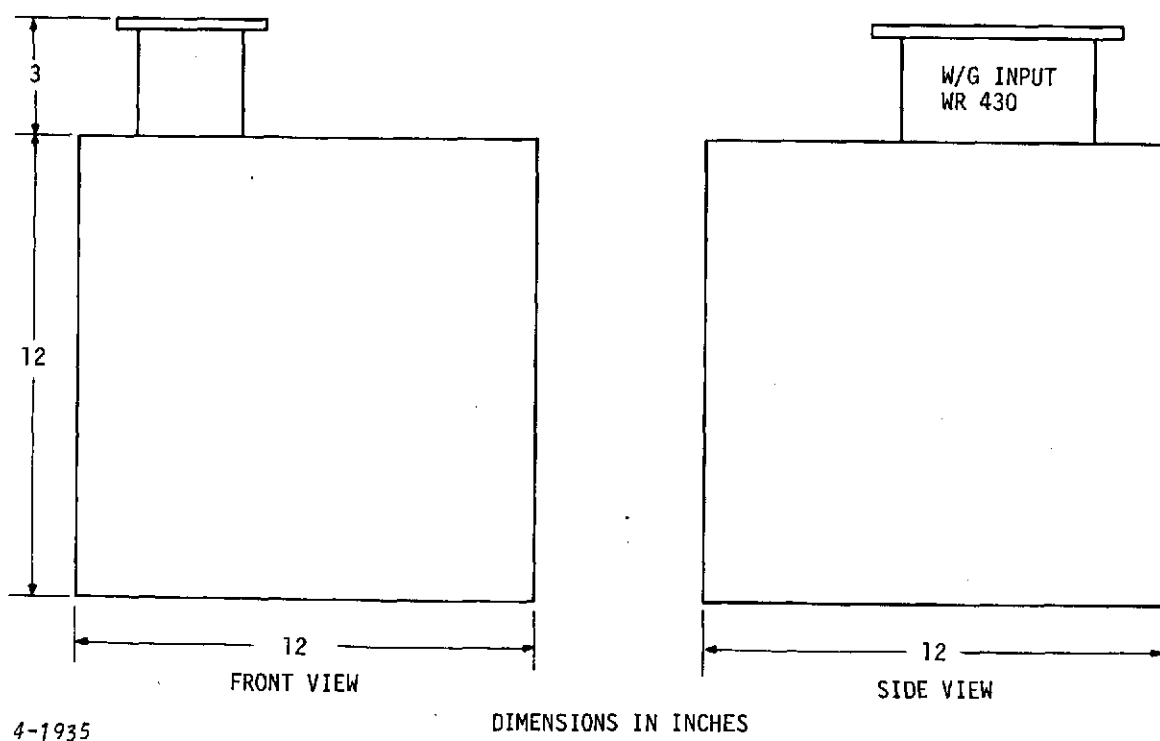
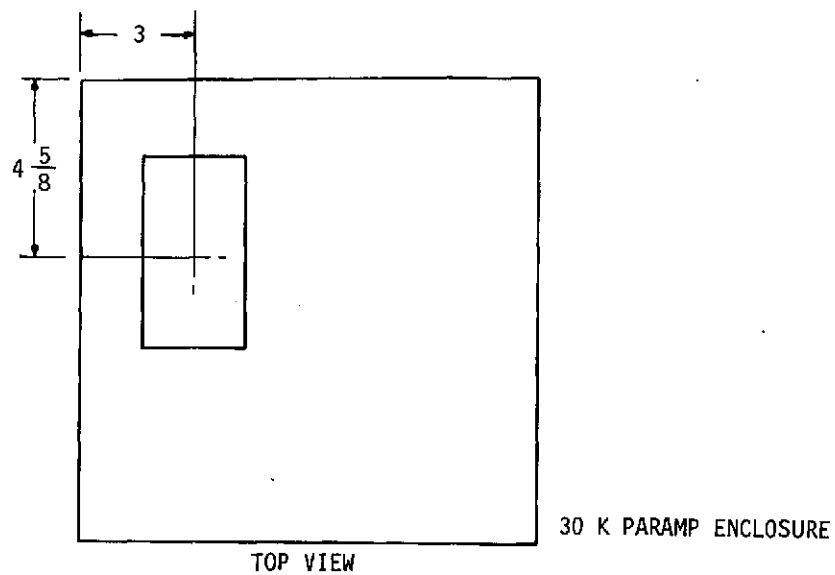


Figure 1-1. Specified Mechanical Outline of Paramp Enclosure

These requirements have been reviewed in detail. The significant areas of design and development that were essential to the successful completion of the program were as follows.

1. VARACTOR

In order to obtain the specified operational levels (primarily noise performance), a varactor of superior quality was required. Standard commercial packaged varactors provide performance that falls far short of the minimum program requirements. The NASA work statement explicitly noted this in advising the use of a chip varactor.

2. PARAMP/CIRCULATOR

Assuming the availability of a superior varactor, it was essential to minimize all signal circuit losses (including circulator input loss) in the first-stage paramp in order to meet the required noise performance. Idler circuit losses were minimized and varactor current flow at the sum frequency sideband was controlled to prevent the transfer of a positive resistance component from the idler to the signal circuit. Neglect of these important factors would have resulted in degraded noise performance.

3. PUMP SOURCE

In addition to the previously listed requirements, it was essential to provide a millimeter-wave pump source to obtain the noise performance specified. Additionally, the pump source was all solid state for prolonged life and high reliability.

4. PHYSICAL REQUIREMENTS

System components have been selected to provide a high degree of long-term stability. The temperature-controlled enclosure was designed to provide the required gain stability of ± 1 dB over the ambient temperature range of -15°C to $+50^{\circ}\text{C}$ for a continuous period of 30 days.

5. QUALITY ASSURANCE AND RELIABILITY REQUIREMENTS

Quality Assurance and Reliability groups were involved in all phases of this program from design, procurement, and assembly to acceptance testing.

C. FUNCTIONAL DESCRIPTION

The AIL Type A-471 S-band parametric amplifier system meets the system performance specifications. A functional description of the system follows.

A number of approaches were considered in an effort to determine the optimum configuration that could be used for the paramp system that would meet the required specifications. The overall size limitations normally associated with a system mounted in operational antenna structures, the thermal and vibration environment encountered, the desirability for a high degree of long-term stability, the power requirements, and the human engineering factors associated with operating and maintaining the system have been assessed. With these design criteria and constraints taken into account, the following approach was formulated for the ultra low-noise noncryogenic S-band paramp system.

The approach evolved for this program was both simple and practical. The system consists of two identical stages of parametric amplification, each stage consisting of a balanced parametric amplifier employing a proven passivated quasiplanar chip-type varactor coupled to a four-port circulator. The pump source consists of separate 50-GHz fundamental Gunn oscillators for each stage. The first stage parametric amplifier and circulator are temperature stabilized at -20°C using thermoelectric modules, while the remainder of the enclosure is stabilized at a temperature of $+50^{\circ}\text{C}$. Figure 1-2 shows a block diagram of the paramp module of the system. Figure 1-3 shows the remote control/power supply block diagram.

In Figure 1-2 the RF signal is introduced into the first-stage circulator through a low-loss waveguide to coaxial transition which also serves as a thermal isolator. A single pass of isolation between the input port and the amplifier is used to obtain improved noise performance.

For this approach to be successful, a circulator with at least 40-dB isolation per input pass is required. Isolation levels of this magnitude are generally conceded to be highly impractical using normal design techniques. A simple and practical technique for accomplishing the desired isolation level to the input and providing the overall stability required has been applied to this program.

A balanced (two-varactor) parametric amplifier configuration with a reduced bandwidth idler circuit was selected for very specific reasons. Noise performance requirements dictated the use of a relatively high pump frequency ($\sim 50\text{ GHz}$). The high pump frequency in conjunction with the low signal frequency results in a relatively narrow separation between the idler

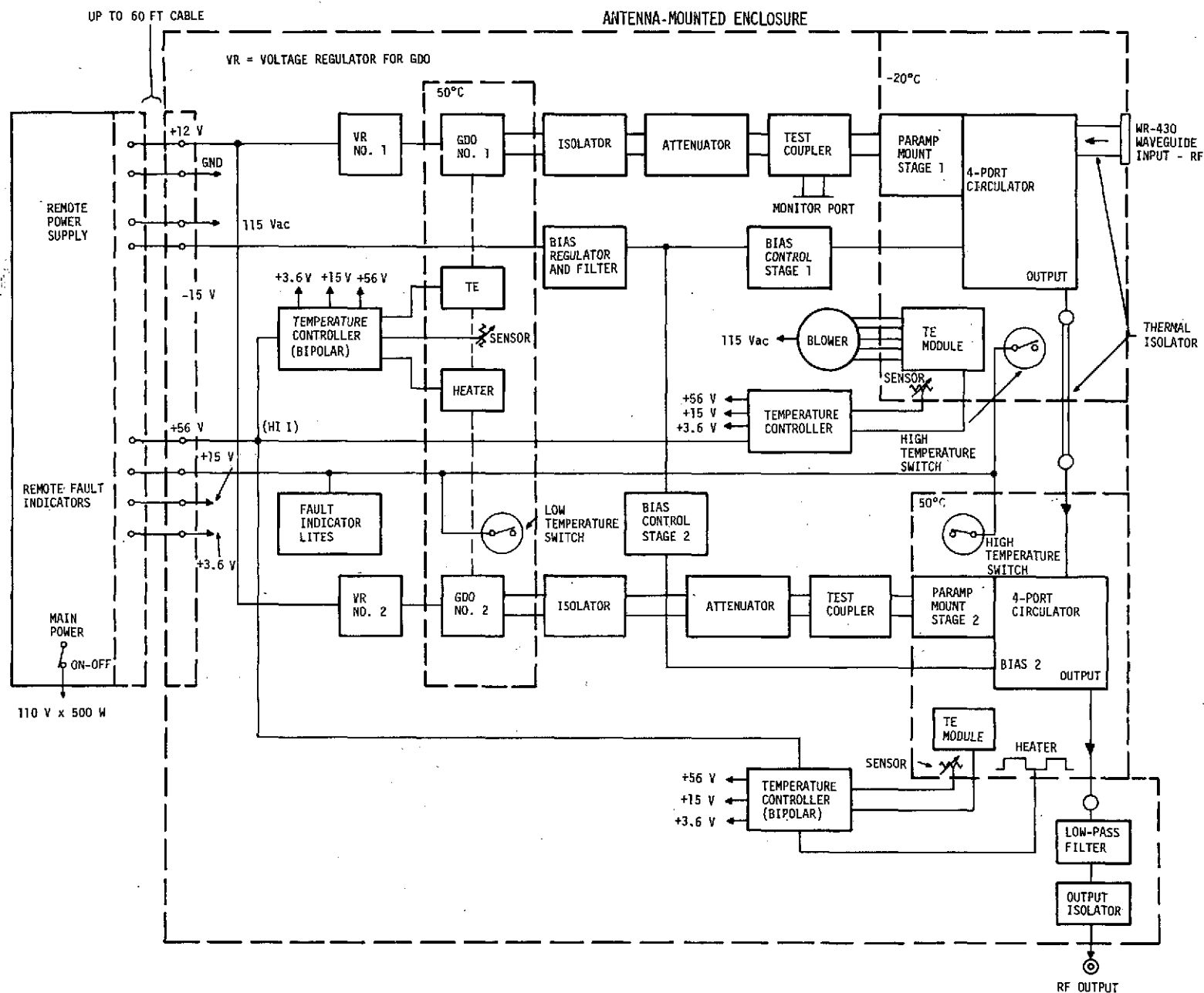
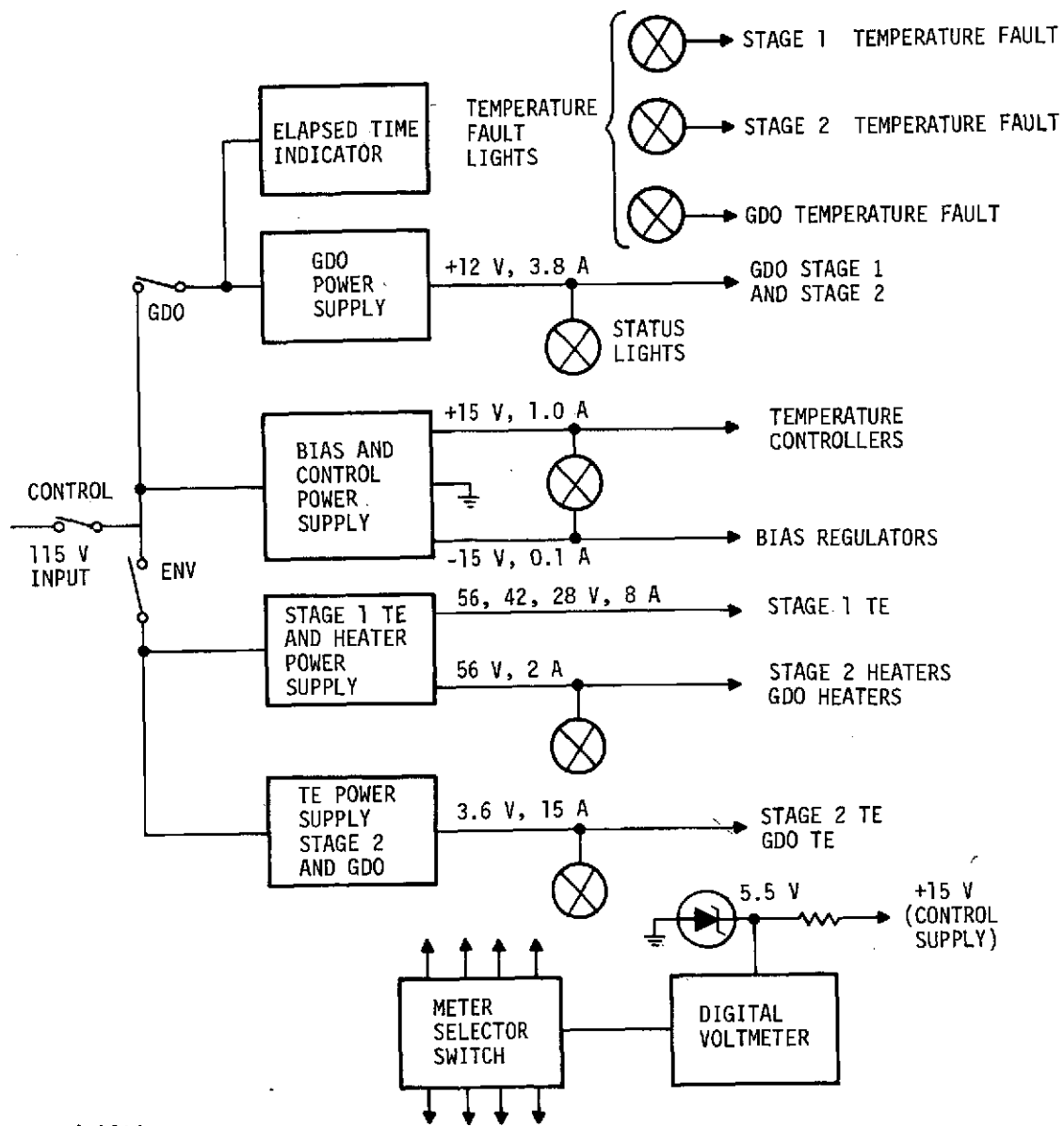


Figure 1-2. Simplified Functional Block Diagram of S-Band System



4-1937

Figure 1-3. Remote Control/Power Supply Unit Block Diagram

(difference-frequency) sideband and the sum-frequency sideband. Varactor current flow at the sum-frequency sideband is detrimental and results in degraded noise and gain-bandwidth performance. For this reason, the idler circuit bandwidth has been controlled and cannot be arbitrarily widened. The balanced amplifier configuration is capable of a wider idler bandwidth than a single-ended design, resulting in greater inherent stability, since less double-tuning is required to achieve the required gain bandwidth product.

Since the signal frequency is relatively low, large-diameter coaxial lines were used for signal-circuit tuning and to achieve the required signal-circuit impedance transformations. The propagation of higher-order modes in the coaxial lines, which presents problems in the signal circuit design of higher signal frequency paramps such as K_u -band, is not a problem at S-band. The large-diameter lines which were used minimize signal circuit losses and result in a high effective varactor quality factor (M_{eff}) in the signal circuit.

A fundamental Gunn oscillator at a frequency of ~ 50 GHz was chosen for the pump source. The Gunn device was chosen primarily because of noise considerations; suitable Gunn oscillators with the required power output level are available commercially at the present time. The millimeter wave pump circuit is simple and reliable, since a frequency multiplier is not required. Elaborate stabilization schemes which would be required for an avalanche device are not necessary with a Gunn oscillator.

The choice of a separate pump source for each stage was a judicious one. This type of operation eliminates interfering signals coupling from one stage to the other which can happen when a single source is utilized. In addition, for the same stability attained for the source, the overall gain and phase stability of the system is improved over that of a common source since changes add on an rms basis rather than on a linear basis.

The two stages are coupled with a dc block, which provides the required dc bias isolation between stages. The output of the system also contains a dc block and isolator, as well as a low-pass filter to ensure compliance with the spurious output requirement by providing rejection at the pump and idler frequencies.

The thermoelectric modules used to stabilize the first stage paramp/circulator at a temperature of -20°C also provide an enhancement in noise temperature for this stage. It is theoretically possible to stabilize the first stage at a somewhat higher temperature and meet the noise performance requirement by pumping at a higher frequency. This would, however, introduce serious problems in providing low loss separation of the idler and pump frequencies, as well as aggravate the sum frequency problem. To

obtain sufficient pump power at a higher pump frequency with sufficient spectral purity, it would be necessary to resort to a Gunn oscillator followed by a varactor multiplier (doubler). Besides complicating the pump network, this approach would be more complex.

A remote control is provided on the power supply unit for both control and monitoring system performance. It contains the system on/off switch and standby/operate switches. Tuning controls on the paramp module consist of a bias voltage adjustment (10-turn pot) and a mechanical adjustment of the pump power attenuator for each stage, as well as a vernier control of the GDO voltage. A digital meter is provided on the remote control/power supply unit for checking the following:

- Paramp bias voltage of each stage
- Gunn oscillator voltage of each stage
- Gunn and thermal stabilization power supply voltages
- Thermal fault indicator voltages

The design concept that was utilized for this program is a modular approach. This enables simple, rapid, and efficient fault location as well as repair of the equipment, if required. Figure 1-4 shows the paramp module (with second stage control access cover removed). Also shown in this figure is the remote control and power supply unit.

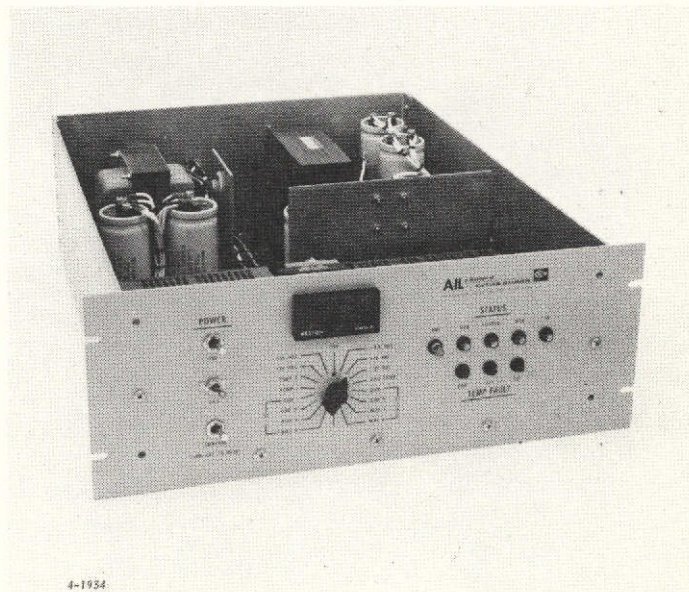
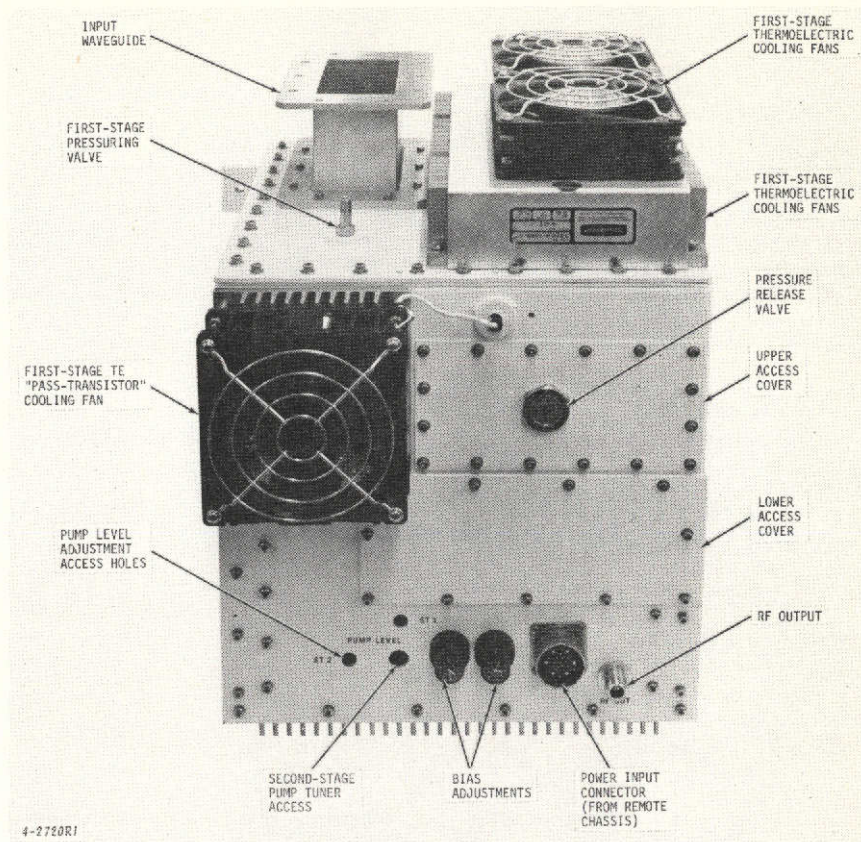
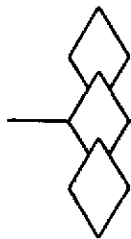


Figure 1-4. Paramp Module and Remote Control/Power Supply Unit Comprising A471 System



II. TECHNICAL DISCUSSION

A. BASIC NOISE CONSIDERATIONS IN ULTRA LOW-NOISE NON-CRYOGENIC PARAMP SYSTEMS

Theoretically, paramps at lower microwave signal frequencies having millimeter-wave pumps can exhibit ultra low-noise temperature even when operated at or near room temperature because of the high idler-to-signal frequency ratio. Practically, however, at least three interdependent sources of noise temperature degradation must be considered before these ultra low values can be realized. These effects are:

- System input losses
- Sum frequency noise
- Antenna mismatch noise degradation

Two of these effects are direct functions of the physical temperature, which is why they are particularly important in a noncryogenic amplifier. Each of these considerations is discussed in detail in the following paragraphs.

1. SYSTEM INPUT LOSSES

Input circuit losses between the antenna port and the pumped varactor or varactors of the first stage paramp directly degrade the noise temperature in accordance with the relation:

$$\Delta T = (L - 1) (T_L + T_{amp}) \quad (2-1)$$

where

L = total loss

T_L = physical temperature of losses

T_{amp} = noise temperature of amplifier in the absence of losses

As an example, some typical values of $L = 0.2$ dB, $T_L = 300$ K, and $T_{amp} = 15$ K yield $\Delta T = 14.8$ K. The principal source of this loss is forward loss of the usual input circulator. Minimization of this loss was accomplished by the use of only one pass ahead of the amplifier as discussed in paragraph D. A possible alternative design, namely the use of a pair of identical amplifiers connected to a 90-degree hybrid coupler, while having the advantage of lower losses, would be severely degraded by antenna mismatch (paragraph A.3) and this approach was therefore ruled out early in the program.

2. SUM FREQUENCY NOISE

The simple noise temperature formula to be presented in paragraph B assumes that the varactor or varactors see an open circuit at the sum frequency, $f_{sum} = f_p + f_s$. Qualitatively, this is a good assumption only as long as $f_{sum} - f_i = 2f_s \approx (BW)_i/2$, where $(BW)_i$ equals the idler circuit 3-dB bandwidth. For high values of idler to signal frequency ratios, such as were considered for this program, this condition can easily be violated. The result is that Johnson noise in the sum frequency band originating from the varactor series resistance is converted by the pump back to the signal band and can seriously degrade the noise temperature. A complicated analysis of this effect is included in Appendix A, but a simple approximation is given by the relation:

$$\frac{\Delta T}{T_{amp}} \approx \frac{f_{i0}}{4Q_i f_{s0}} = \frac{(BW)_i}{4f_{s0}} \quad (2-2)$$

where Q_i is the idler circuit Q . As an example, some values typical of a balanced high idler paramp designed for maximum gain-bandwidth product, namely, $Q_i = 10$, $f_{i0} = 50$ GHz, $f_{s0} = 2.25$ GHz, and $T_{amp} = 15$ K yield $\Delta T \approx 5.6$ K.

The obvious cure for this sum frequency noise degradation is to narrow the idler bandwidth. Then, however, to achieve the desired overall bandwidth performance, the amount of multiple (double) tuning compensation in the signal circuit must be increased. This results in increased signal circuit loss with consequent noise temperature degradation (paragraph A.1).

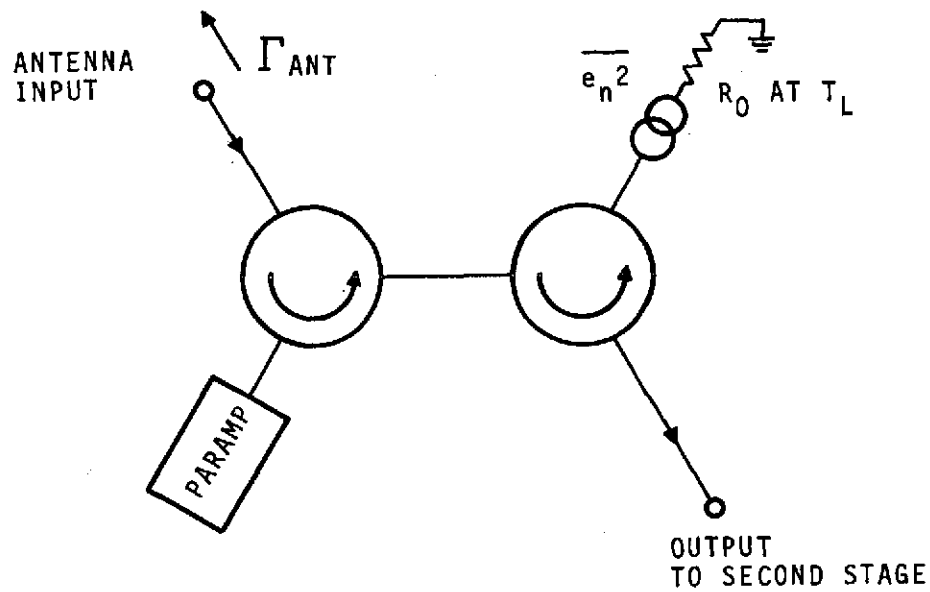
3. ANTENNA MISMATCH NOISE DEGRADATION

Ordinarily, amplifier noise temperature is specified using a theoretically perfectly matched antenna. Practically, however, some antenna mismatch must be expected, and, if the amplifier noise temperature is severely degraded by a relatively small antenna mismatch, the effect should be considered by the system designer. Figure 2-1 is a simple representation of how this degradation arises in the usual circulator-coupled parametric amplifier for the case of either one or two passes ahead of the amplifier.

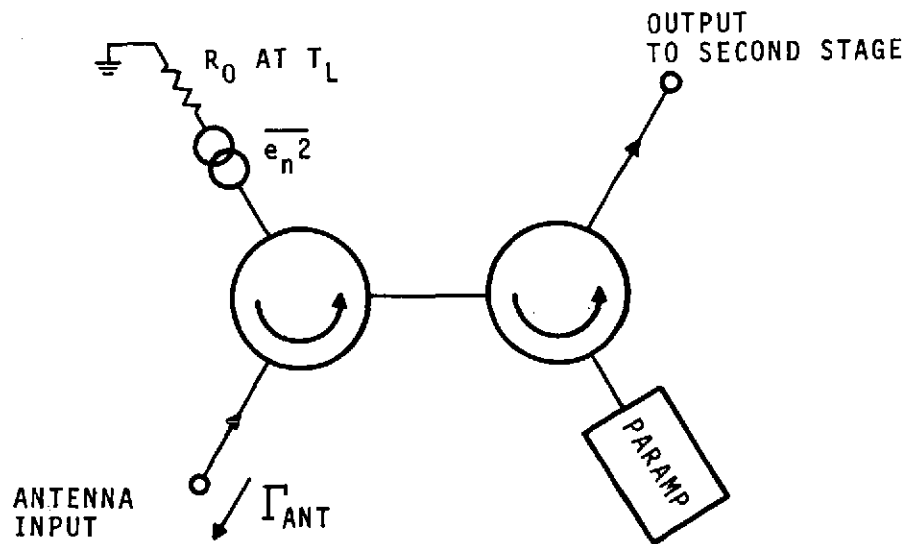
Referring to the figure, for either case (A) or (B) and assuming ideal circulators, noise power from the termination R_0 at physical temperature T_L is directly transmitted to the antenna port where it encounters reflection coefficient Γ_{ant} . The resultant reflected noise power then enters the normal signal channel to degrade the noise temperature. The magnitude of this effect can be calculated as follows. The additional noise power referred to the amplifier input terminals is proportional to $|\Gamma_{ant}|^2 T_L$, while the signal channel suffers a loss in gain by the factor $(1 - |\Gamma_{ant}|^2)$. Thus the noise temperature degradation is:

$$\begin{aligned}\Delta T &= \frac{|\Gamma_{ant}|^2 T_L + T_{amp}}{1 - |\Gamma_{ant}|^2} - T_{amp} \\ &= \frac{|\Gamma_{ant}|^2}{1 - |\Gamma_{ant}|^2} [T_L + T_{amp}]\end{aligned}\tag{2-3}$$

As an example, using the typical numbers $|\Gamma_{ant}|^2 = 0.04$ (corresponding to a VSWR of 1.5), $T_L = 300$ K, and $T_{amp} = 15$ K yields $\Delta T = 13.1$ K. Additionally, if the passive circulator match at the antenna port is not perfect, it can phase with the antenna mismatch to give an effective larger value of $|\Gamma_{ant}|$.



A. ONE PASS AHEAD OF AMPLIFIER



B. TWO PASSES AHEAD OF AMPLIFIER

3-1018

Figure 2-1. Simple Equivalent Circuit for Calculating Noise

Figure 2-2 shows the noise temperature as a function of antenna return loss according to equation 2-3 for two values of $T_L + T_{amp} = 258$ and 315 K. Figure 2-3 shows the system gain/noise budget. Also shown for comparison are the corresponding values for a hybrid-coupled amplifier with 17-dB gain. This figure clearly shows the extreme sensitivity of the hybrid-coupled amplifier to antenna mismatch. For this reason, only the circulator-coupled amplifier was considered.

B. PARAMETRIC AMPLIFIER

1. GENERAL

The key of the paramp design is the required overall maximum noise temperature specification of 30 K over most of the band from 2200 to 2300 MHz for an ambient temperature of up to +50°C. To attain this value, both single-ended and balanced parametric amplifier configurations were investigated. The single-ended approach has an inherently narrower bandwidth idler circuit, and a theoretical analysis indicated that it would give a slightly lower (16 K versus 18 K) noise temperature. A single-ended mount was built, and experimental evaluations indicated that the idler loading due to finite decoupling of the signal circuit chokes reduced the effective idler figure of merit. This actually would cause greater degradation in noise performance than the reduction in sum-frequency current occasioned by the narrower bandwidth idler circuit. In addition, the greater degree of double tuning required would also degrade the signal circuit figure of merit, which would again degrade the noise performance. The only solution to the problem would be a dual set of signal circuit chokes. These would, however, produce more narrowbanding in the signal circuit.

During this period, a balanced mount was successfully developed as an alternate approach. Further pursuit of the single-ended approach was therefore halted, and the remainder of the effort concentrated on the balanced mount.

The following other amplifier parameters and circuit configurations were used:

- Pump frequency of about 50 GHz which is the highest frequency commercially available fundamental low-noise Gunn oscillator source
- A four-port special low-loss circulator
- A balanced high idler mount with a tuning short located one wavelength from the varactors to minimize sum frequency noise by using a relatively narrowband idler circuit with high cutoff-frequency chip varactors

- Minimization of signal circuit losses by using a large diameter coaxial signal circuit connected directly, without a connector, to the amplifier port of the circulator
- Minimization of idler circuit losses by using an electroformed waveguide cavity
- Minimization of signal circuit losses by use of a minimum amount of double tuning, low loss in the circulator, and absence of explicit filtering of the idler or pump frequencies in the signal circuit. Thus, a balanced configuration is proposed (AIL patent no. 3105941) that is also capable of meeting the gain, bandwidth, and ripple specifications even with the use of a single stage having a minimum amount of double tuning in the signal circuit. These points are discussed in greater detail as follows.

A schematic diagram of the proposed parametric amplifier is shown in Figure 2-4. A greatly enlarged cross-sectional view of the varactors mounted in the reduced height waveguide is shown in Figure 2-5. The series resonant frequency of the varactors, slightly modified by the reactance of the approximate one-wavelength reduced height waveguide, provides the idler resonance. The balanced configuration serves to isolate the signal circuit from both the idler and pump without additional filtering, resulting in lower noise temperature and larger bandwidth than for the conventional single-ended configuration. The quarter-wave transformer shown in the signal circuit is the means of integrating the circulator and the amplifier. Typically, only a small transformation is needed between the ferrite disc of the circulator and the signal tuning inductor, resulting in a wideband, low-loss transformation.

The physical realization of the paramount is shown in Figure 2-6. A pair of high-quality AIL-developed varactors is mounted across a reduced-height electroformed waveguide. The waveguide propagates the pump frequency, the idler frequency, and the sum frequency sideband. The idler circuit is completed by positioning a short circuit approximately one wavelength behind the varactors, and pump energy is introduced through a properly spaced single-section waveguide filter which provides high rejection (greater than 20 dB) at the idler frequency and sum frequency sidebands.

The signal circuit is resonated by a short length of high impedance coaxial line, L1. A linear taper is provided in the coaxial line to reduce the magnitude of the discontinuity capacitance at the transition of the varactor contact from stripline (in the waveguide) to coax. Signal circuit loading as well as n-pole tuning is accomplished by signal transformer T1, which is an n-step quarter-wavelength coaxial transformer ($n = 2$, in this case). Relatively large diameter lines (0.275 inch) are used to minimize signal circuit losses. The paramount signal circuit is connected to the 4-port circulator by means of a type APC-7 precision connector. This permits ready field replacement of the amplifier mount only, reducing sparring costs.

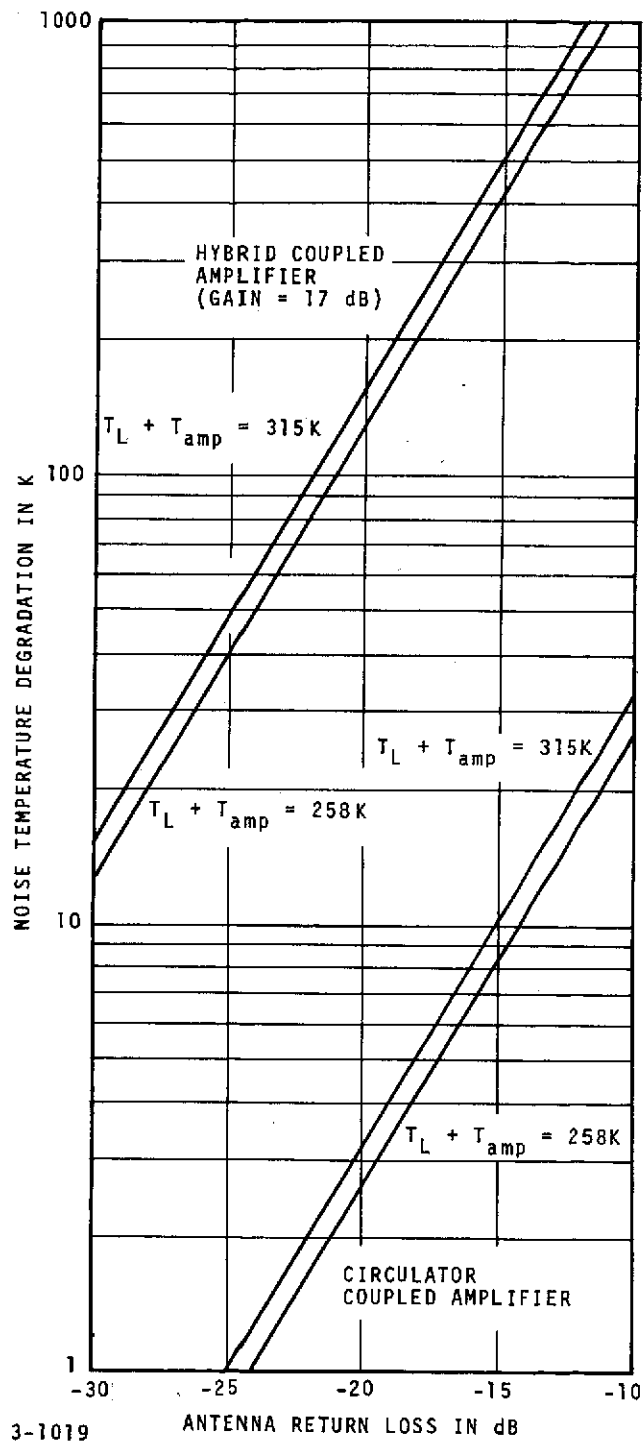
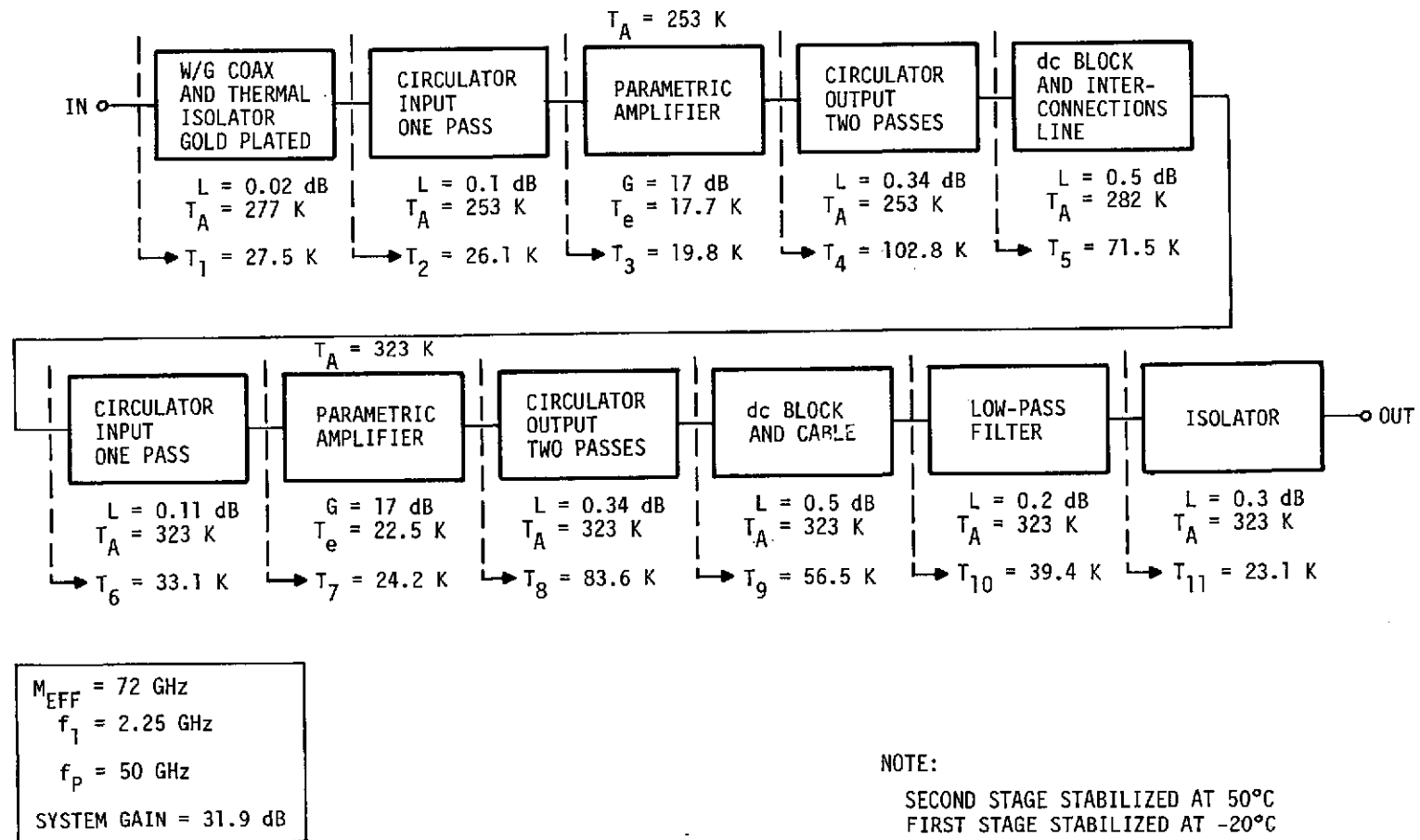


Figure 2-2. Noise Degradation Versus Antenna Return Loss



4-1925

Figure 2-3. Final System Gain/Noise Temperature Budget

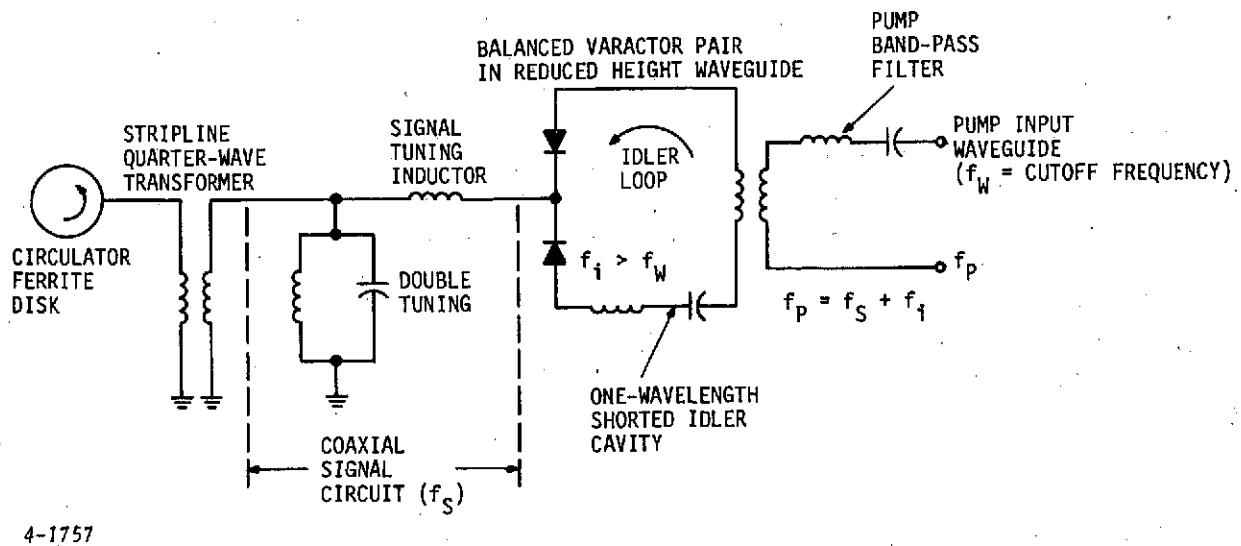


Figure 2-4. Schematic Diagram of Balanced Parametric Amplifier With Propagating Idler

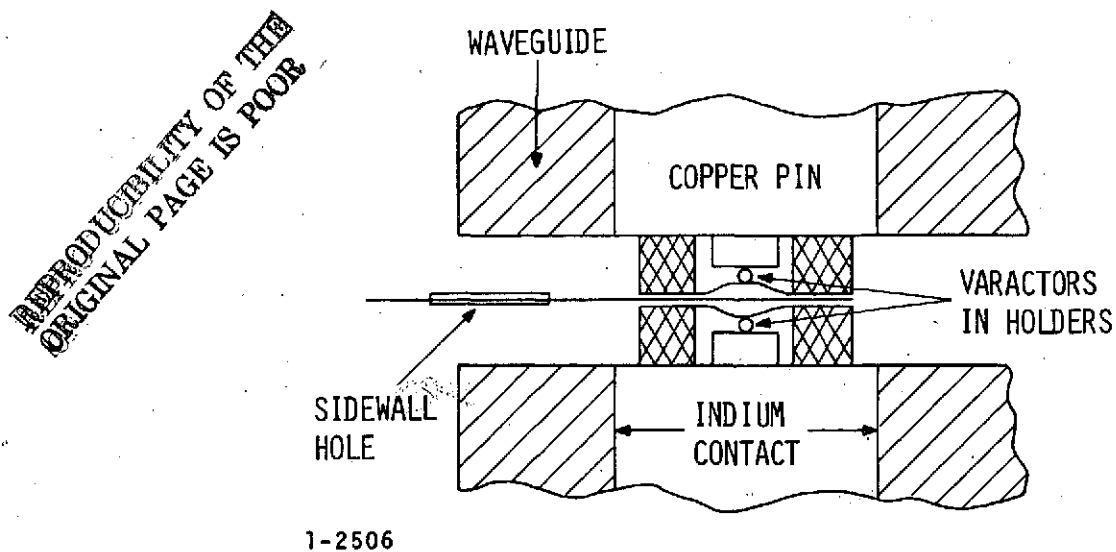


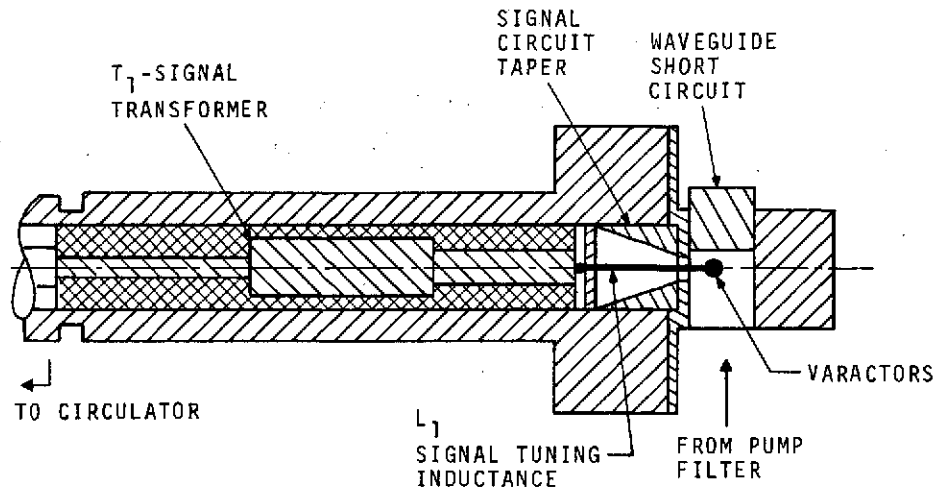
Figure 2-5. Varactors in Waveguide

2. GAIN/BANDWIDTH PERFORMANCE

During the past several years, many paramp development programs involved the design of high performance wideband amplifiers with gain/bandwidth requirements greater than those required for this program. It was found that many of the simplifying assumptions which were made in earlier theoretical analyses of amplifier performance did not hold for broad-band paramps, or for ultra low-noise paramps such as those required to meet the design goal specifications for this program, and led to overly optimistic predictions. As a result, a very complete theoretical model has been evolved which provides the most accurate representation of a wideband ultra low-noise paramp available (Appendix A). In order to perform the necessary calculation to obtain a gain/bandwidth analysis within a reasonable period of time, a computer program was developed using this mode. Among the factors considered in this analysis are:

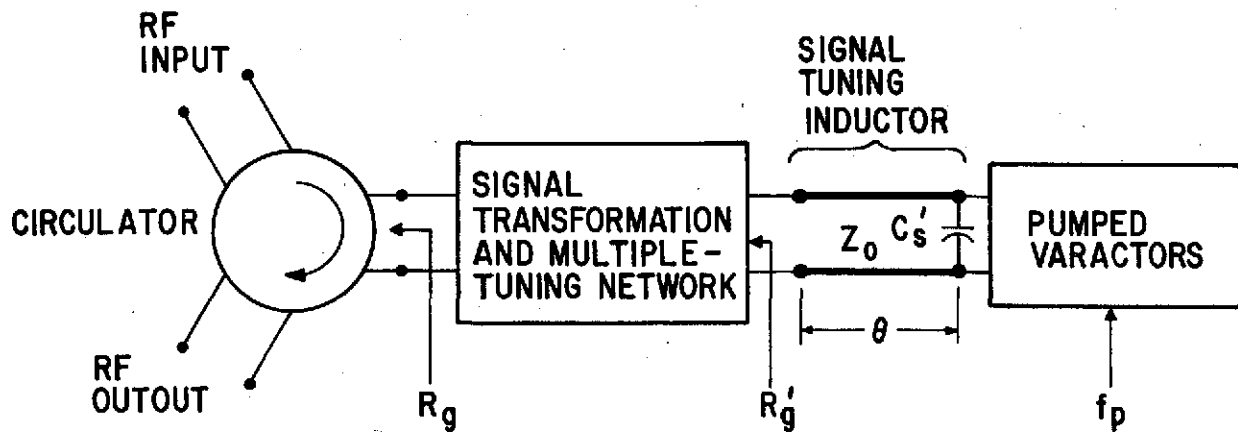
- Effect of sum frequency varactor current
- Actual idler terminating circuit consisting of a short-circuited length of waveguide
- Distributed nature of the signal tuning inductance, consisting of a short length of high-impedance coaxial line
- Distributed nature of the signal circuit multiple tuning network and transformation network
- Effect of discontinuity capacitances at steps in the coaxial signal transformer
- Effect of loss in the coaxial signal tuning inductor and multiple tuning/transformer elements

A block diagram of the theoretical model used is shown in Figure 2-7. A derivation of the input impedance of the pumped varactors which includes sum frequency effects is presented in Appendix A. Capacitance C_s in Figure 2-7 is the extra stray capacitance added across the varactors by the paramp mount. The short length (θ), of high-impedance coaxial line, Z_0 , is the signal tuning inductor. The signal transformation network consists of two quarter-wavelength sections of coaxial line for a double-tuned signal circuit and three sections for a triple-tuned signal circuit. This network provides the required signal circuit impedance transformation as well as the desired degree of multiple-pole tuning.



3-2649

Figure 2-6. Parametric Amplifier Configuration



3-2648

Figure 2-7. Block Diagram of Broadband Parametric Amplifier Theoretical Model

This complete model has been used to obtain the theoretical gain/frequency plot that is presented in this section. The varactor and mount parameters that were used in this analysis are listed in Table 2-1. C_o represents the varactor operating junction capacitance and f_{co} represents the varactor operating cutoff frequency at the idler frequency.

3. NOISE TEMPERATURE

The normalized noise temperature (T) of a high-gain parametric amplifier (exclusive of circulator losses) is given by (reference 1, equation 6.103):

$$\frac{T}{T_d} = \frac{\frac{f_s}{f_i} + \frac{f_s f_i}{M^2}}{1 - \frac{f_s f_i}{M^2}} \quad (2-4)$$

where

f_s = signal frequency

f_i = idler frequency

M = varactor figure of merit

T_d = physical temperature of varactor in K

A convenient way to include the effect of signal circuit losses is to recognize that the term M^2 in equation 2-4 arises from signal and idler circuit loss contribution that are generally different. Thus, M can be replaced by an effective value:

$$M = M_{\text{eff}} = \sqrt{M_s M_i} \quad (2-5)$$

where

M_s = effective M at the signal frequency, including signal circuit and varactor losses

M_i = effective M at the idler frequency, including idler circuit and varactor losses

TABLE 2-1. ASSUMED PARAMETERS FOR GAIN-
BANDWIDTH CALCULATION

f_p (pump frequency)	50.7 GHz
C_o	0.094 pF
C'_S	0.07 pF
C_p (varactor package capacitance)	0.03 pF
R_{S1}	8.45 ohms
R_{S2}	3.38 ohms
L_S	0.1 nH
C_1/C_o	0.25
C_2/C_o	0.0625
f_{co}	500 GHz
M_{eff}	79 GHz
Pump waveguide width	0.224 inch
Pump waveguide height	0.011 inch
Distance from varactor centerline to short	0.3224 inch
Distance from varactor centerline to side wall	0.036 inch
Signal tuning impedance	157 ohms
Signal tuning length	0.795 inch
First quarter-wave transformer impedance	17.0 ohms
Second quarter-wave transformer impedance	21.0 ohms

Referring to the overall system gain/noise temperature budget (Figure 2-3), the predicted overall noise temperature was calculated for various values of M and pump frequency ($f_p = f_s + f_i$, $f_s = 2.25$ GHz). In making the calculations, the effects of various losses at various physical temperatures were calculated as indicated in paragraph A, equation 2-4, and the standard formula for the overall noise temperature of a series of cascaded networks was used. The results are shown in Figure 2-8, and indicate that the overall maximum noise temperature of 30 K is more than compatible with a pump frequency of 50 GHz and $M_{\text{eff}} = 75$ GHz. Based on experience with the varactors, described in Section II. C, a value of M_i of about 125 GHz, corresponding to a cutoff frequency ≈ 500 GHz and a capacitance nonlinearity of about 0.25, was readily attainable for slight biasing of the varactor. With careful design of the signal circuit along the lines previously discussed, a value of M_s of about 50 GHz was readily obtained. The resultant value of M_{eff} of about 79 GHz¹ then meets the noise temperature specification using the readily attainable idler resonance of about 48 GHz.

Inspection of Figure 2-8 indicates that a negligibly greater margin in system noise temperature may be obtained by pumping at a frequency considerably higher than 50 GHz. For this reason, and also because of the availability of a commercial high reliability 50-GHz Gunn source, a pump frequency of about 50 GHz was chosen for this program.

4. GAIN, BANDWIDTH, AND GAIN RIPPLE

As mentioned previously, a double-tuned signal circuit was used. However, for a more linear phase characteristic, a response shape close to monotonic maximally flat, rather than an equiripple, gain response was employed. A midband stage gain of greater than 20 dB with a 1/2 dB down bandwidth of 130 MHz is theoretically possible. By slight double-tuning, the response can be broadened to 150 kHz (at 17 dB gain) making the overall response for two stages 135 kHz at the 1-dB points. This makes the response less critical to changes in GDO frequency and pump level (due to temperature deviations of $\pm 1^\circ\text{C}$ encountered in the stabilizing system).

¹ A value of M_{eff} of 125 GHz has been measured recently on an X-band non-cryogenic paramp which uses AIL chip varactors. The measurement of M_{eff} is based upon noise temperature measurements made using a calibrated hot and cold termination test system.

Appendix A summarizes the derivation of the paramp gain as a function of frequency. Using the computer program and the parameters of Table 2-1, the gain response of Figure 2-3 was obtained for a stage gain level of 20 dB, which exceeds the minimum of 17 dB used in the gain-noise temperature budget of Figure 2-9.

5. PUMP POWER AND DYNAMIC RANGE

An approximate formula for the pump power dissipated in the varactor is derived as follows. Assuming a sinusoidal pump voltage of peak amplitude V_p across the varactor junction, the peak amplitude of pump current is:

$$|I_p| \approx \omega_p C_0 V_p \quad (2-6)$$

where

C_0 = average junction capacitance

ω_p = pump angular frequency

The resultant power dissipated in a varactor having series resistance R_s is the minimum pump power per balanced parametric amplifier stage:

$$P_p = \frac{2 |I_p|^2 R_s}{2} \approx 2\pi \left(\frac{f_p^2}{f_{c0}} \right) C_0 V_p^2 \quad (2-7)$$

where the cutoff frequency, $f_{c0} = 1/(2\pi R_s C_0)$.

As can be seen from equation 2-7, the pump amplitude V_p is a key parameter in determining the pump power. The nominal value of V_p for hard pumping is $V_p \approx V_b + \phi$, where the applied dc varactor bias = $-V_b$, and ϕ = contact potential. Since the junction capacitance tends to vary as $(V_b + \phi)^{-1/2}$, P_p tends to be proportional to V_p rather than V_p^2 as apparently

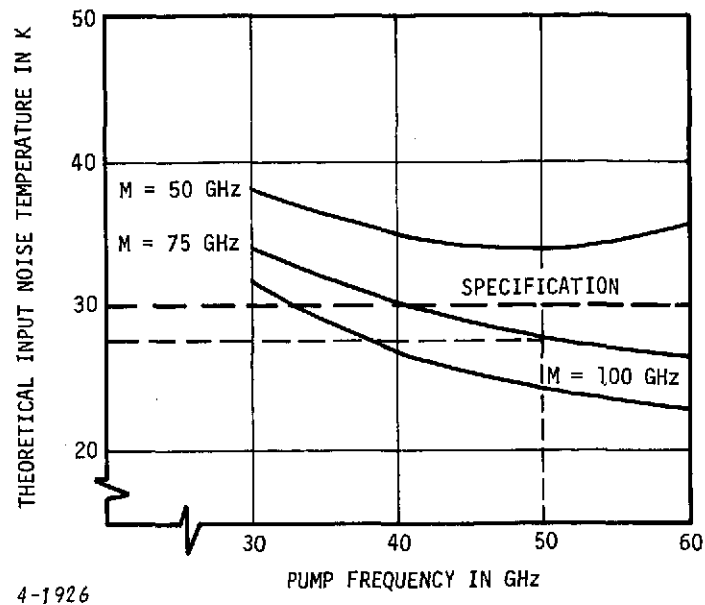


Figure 2-8. Noise Temperature as a Function of Pump Frequency and M

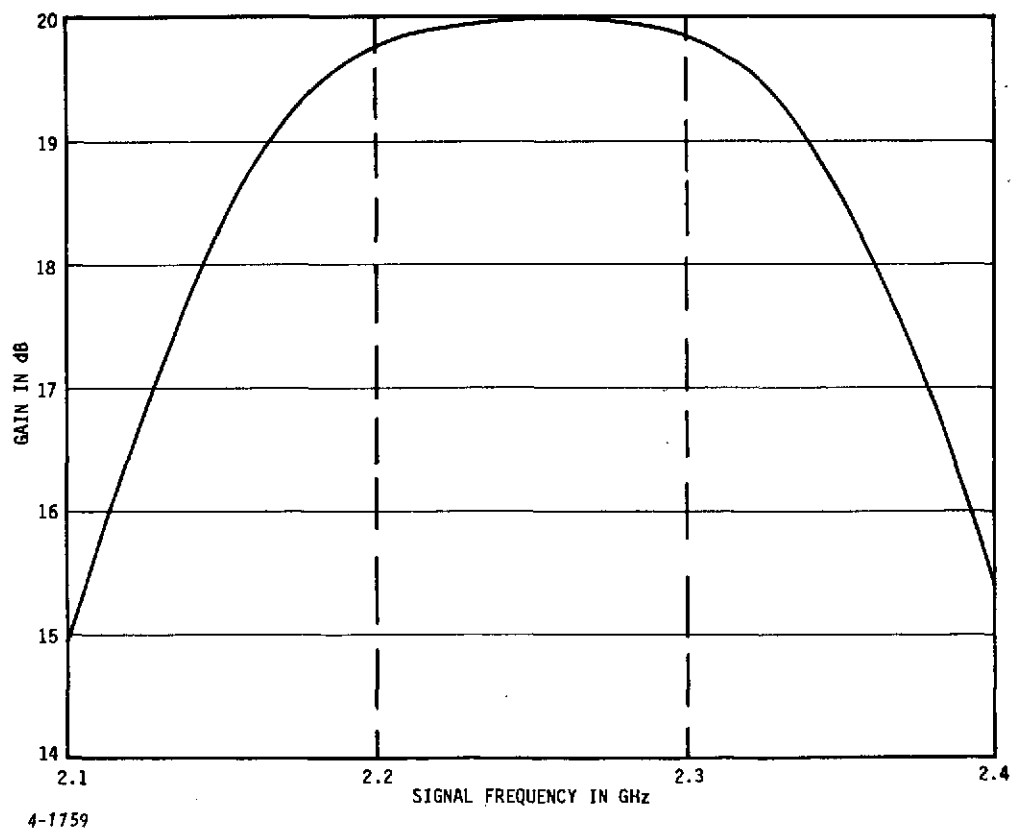


Figure 2-9. Theoretical Single Stage Gain for Proposed Balanced Parametric Amplifier with Ideal Circulator

indicated by equation 2-7. Nevertheless, there is still a tradeoff to be considered between pump power (or V_p) and varactor figure of merit (M). Increasing the bias and hence V_p and the pump power for hard pumping will also increase both the cutoff frequency and nonlinearity ratio to increase M. In our experience, a bias of about -2.0 V is more than necessary to achieve an M_i of about 125 GHz. Thus, the pump power is calculated for $V_p \approx 3.0$ V ($\phi \approx 1$ V) yielding a value of $P_p \approx 27.4$ mW for $f_p = 50.7$ GHz, $f_{c0} = 500$ GHz, and $C_0 = 0.094$ pF. In paragraph E it is shown that over 33 mW of pump power is attainable which provides a good margin of safety, even for hard pumping.

Reference 1, equation 10.65, gives the following simple relation between dissipated pump power and input signal power level to cause a fractional change in gain ($\Delta K/K$):

$$P_{in} = P_p K^{-3/2} \left(\frac{f_s}{f_p} \right) \left| \frac{\Delta K}{K} \right| \quad (2-8)$$

Using this value of $P_p = 27.4$ mW, $K = 20$ dB (conservative), $f_s = 2.25$ GHz, $f_p = 50.7$ GHz, and $|\Delta K/K| = 0.206$ (corresponding to -1.0 dB gain compression) yields $P_{in} = -46.0$ dBm at the input to the amplifier, which meets the dynamic range specification.

6. MEASURED SINGLE-STAGE PERFORMANCE

The following typical single-stage performance has been measured on the prototype mounts:

Prototype Mount Serial No.	B13	B15
Gain, dB	15.0	15.0
Center frequency, GHz	2.25	2.25
1 dB down bandwidth, MHz	130	120
Response shape	Monotonic	
Ripple	Less than 0.2 dB	
Bias, Volts	-1.9	-2.8
Pump frequency, GHz	51.0	50.8

The measured pump power for all mounts was under 20 mW making the average pump power margin 4 dB. As can be seen from the data, the prototype amplifier mounts meet bandwidth requirements. Figure 2-10 shows a prototype mount.

7. GAIN STABILITY

Gain instability versus temperature can arise from two principal causes:

- The effect of temperature on pump power
- The effect of temperature on the SWR at the amplifier port of the circulator

A third possibility, namely the effect of temperature on pump frequency is significant only insofar as such changes are reflected in corresponding changes in pump power occurring due to the limited bandwidth of the pump circuitry. Discussion of the two main effects follow.

Reference 1, equation 10.40, gives the approximate fractional gain change resulting from a fractional pump power change:

$$\frac{\Delta K}{K} \approx K^{1/2} \left(\frac{\Delta P_p}{P_p} \right) \quad (2-9)$$

Thus, for $K = 17$ dB, to meet the overall specification of ± 0.1 dB gain change requires less than ± 0.014 dB pump-power change over the temperature controlled range of $\pm 1^\circ\text{C}$. The predicted pump power change over this temperature range (paragraph II-E) is about ± 0.04 dB. This change in pump power can lead to ± 0.2 dB gain change as the temperature stabilizing elements turn on and off. This does not include thermal overshoot effects and two stages so that a firm specification of ± 0.3 dB is considered realistic for a two-stage system.

The effect of changes in the amplifier port SWR or, alternatively, changes in the nominal isolation of the circulator on the amplifier gain are

REPRODUCIBILITY OF THE
ORIGINAL PAGE IS POOR

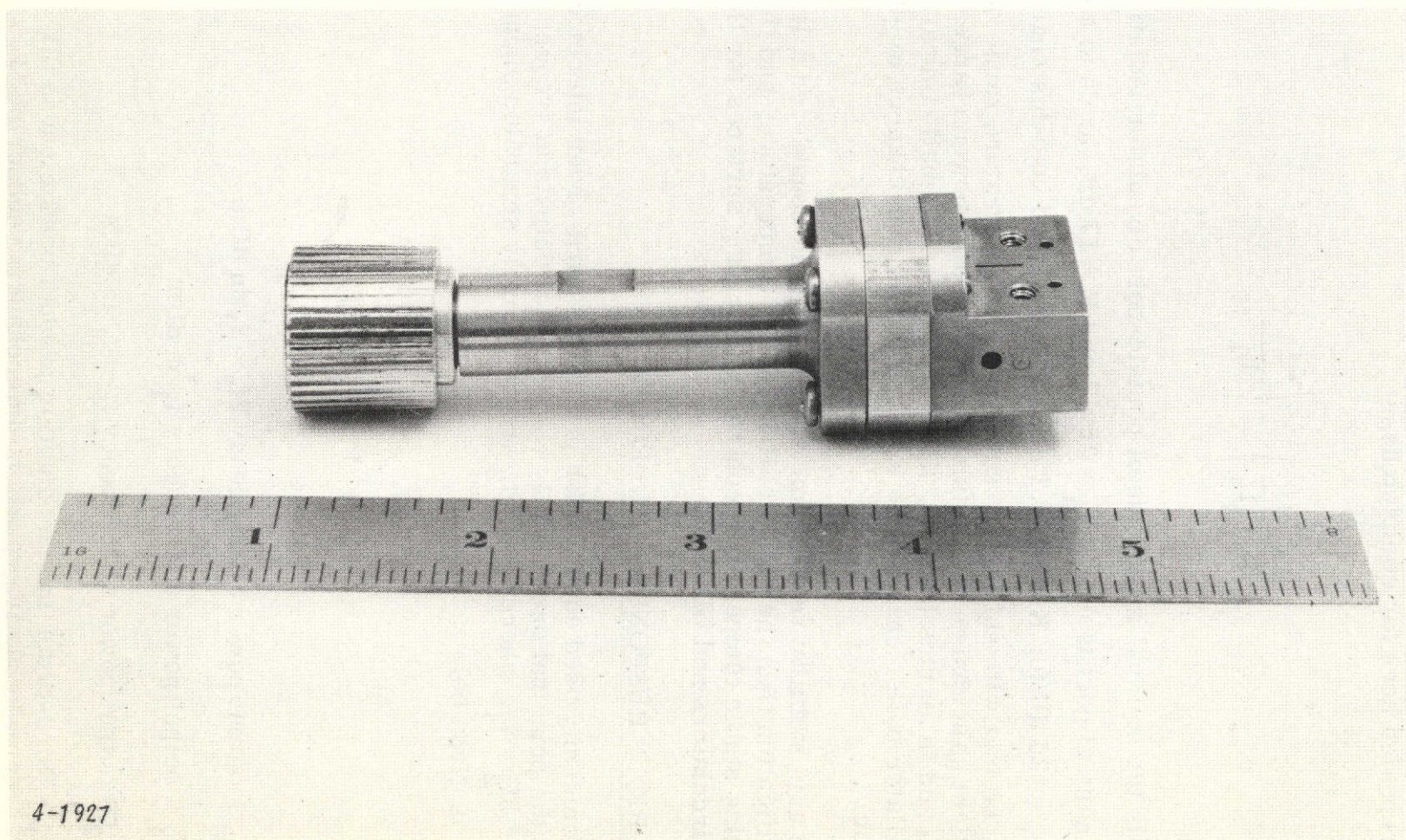


Figure 2-10. Parametric Amplifier Mount

derived in Appendix B. The relevant formula is equation B-5 in Appendix B, which is repeated here for completeness:

$$\frac{\Delta K}{K} \approx \left(\frac{K}{L_i} \right)^{1/2} \left(\frac{\Delta L_i}{L_i} \right) \quad (2-10)$$

where L_i is the nominal magnitude of port-to-port circulator isolation. Assuming a normal port isolation $L_i \approx 25$ dB and $K = 17$ dB, leads to an allowable $L_i/L_i = \pm 25$ dB for $K/K = \pm 0.1$ dB. It is believed that this change in L_i can easily be met with sufficient margin over a temperature range of $\pm 1^\circ\text{C}$. The resultant gain change due to this cause and pump power changes, considered to add in an rms fashion. Since this effect is small compared to Gunn oscillator power changes the total maximum gain changes to ± 0.3 dB is realistic.

The gain stability versus time specification is considered a less stringent specification than the gain stability versus temperature, and this was met by using stable temperature controlled mounting surfaces for the paramp circulators and GDO's.

8. SPURIOUS RESPONSES, IM PRODUCTS

A commonly used equation for predicting third-order intermodulation products (the principal ones usually consisting of outputs at frequencies $2f_1 - f_2$ or $2f_2 - f_1$, where f_1 and f_2 are two closely separated signal frequencies) is given below:

$$P_{IM} = P_1 + 2P_2 + K_{21}$$

where

P_{IM} = output power at frequency $2f_2 - f_1$ in dBm

P_1 = output power at frequency f_1 in dBm

P_2 = output power at frequency $f_2 \approx f_1$ in dBm

K_{21} = third-order intermodulation product coefficient in dB
(an alternative equation, interchanging subscripts 1 and 2 could also be written)

The key parameter in predicting IM performance is thus K_{21} . Previous experience at AIL for similar amplifiers employing chip varactors yielded $K_{21} = +8$ dB. Using a developed gain at midband of 33 dB in the specifications, two -65 dBm signals in the 2200 to 2300 MHz band result in a predicted IM level of -88.0 dBm which is 53.0 dB below the output of either in-band signal output level. This, therefore, meets the 50 dB down requirement and agrees reasonably well with the measured -51 dB value.

A filter has been incorporated to ensure that the pump leakage is at least -100 dBm at the output of the system. This filter must pass the signal band near 2.25 GHz with low loss and greatly attenuate the pump at about 50 GHz.

The form of this filter is a dual pair of radial chokes, each pair spaced one-quarter wavelength at 50 GHz. The measured signal frequency insertion loss of the filter is less than 0.2 dB while the VSWR is better than 1.15. The two pairs are separated by one-quarter wavelength at the signal circuit frequency. The measured performance of this filter shows greater than 60-dB rejection at the 50.7-GHz pump frequency. The minimum rejection of the pump frequency due to the balanced paramp configuration, coaxial links, circulator, and isolator is greater than 50 dB. Compliance with the spurious output requirement of greater than a 60 dB below the desired response with a -65 dBm input signal is possible for the calculated pump level of +14.3 dBm (27.4 mW in paragraph II-B-5). The actual spurious level could not be measured because of limited sensitivity of the spectrum analyzer. No spurious could be detected at -85 dBm which was the limit of the analyzer sensitivity.

9. PHASE STABILITY

As for gain, phase instabilities arise from pump-power changes. Pump frequency changes, however, are even more important and the situation is complicated by the passband characteristics (single or double tuned). Actually, the gain instability calculations in paragraph II-B-7 previously were done for midband, without regard to the passband shape. Extensive theoretical

analyses have been made at AIL of both gain and phase changes for single, double, and triple tuned maximally flat responses as a function of pump-power and frequency changes. However, correlation with experiment has not been attempted and it was not deemed worthwhile to include these analyses here. Suffice it to say that the long-term phase stability specification of ± 5 degrees across the passband was met when the temperature controlled enclosure is constant enough in temperature to minimize pump-power and frequency changes.

10. PHASE LINEARITY AND VARIATION OF PHASE LINEARITY

The theoretical predictions of phase linearity and variation of phase linearity used for the prototype will be given here. Note that these calculations should be conservative since they are for a single-ended parametric amplifier that has less bandwidth capability and phase linearity than the balanced parametric amplifier actually used for the prototype system.

A prediction of phase linearity requires a knowledge of the theoretical amplifier phase characteristic. This can be approached in one of two ways. First, use of a low frequency-lumped prototype analysis, or second, computer simulation of the complete parametric amplifier performance with printout of the phase response. The latter approach was chosen here as being more meaningful because it includes such important effects as distributed signal and idler circuits and the variation of negative resistance over the band, all of which would be ignored in the first approach.

Figure 2-11 shows the results of a least squares error fit to a third-order polynomial of the amplifier phase* in degrees versus the frequency deviation from midband in GHz. The columns headed X-ACTUAL and Y-ACTUAL are the frequency deviation and phase, respectively, and are derived from a computer simulation of a double-tuned almost maximally flat single-ended paramp stage with 17-dB midband (2.25 GHz) gain and 0.5-dB gain fall off at the band edges (2.2 and 2.3 GHz). The equation of the fit is as follows:

$$\phi = A_0 + A_1 (\Delta f) + A_2 (\Delta f)^2 + A_3 (\Delta f)^3 \quad (2-11)$$

* 180-degree nominal midband phase is subtracted out.

where, from Figure 2-11:

$$A_0 = 0.06$$

$$A_1 = 952.2$$

$$A_2 = 577.4$$

$$A_3 = -10150$$

From equation 2-11, the deviation from a linear phase characteristic is:

$$\phi - A_0 - A_1 (\Delta f) = A_2 (\Delta f)^2 + A_3 (\Delta f)^3 \quad (2-12)$$

Considering the signs of A_2 and A_3 , the maximum positive deviation from linear phase will occur for the largest negative value of Δf . Thus, for the center 60-MHz specification, the worst case is $\Delta f = -0.03$ GHz, and for the band-edge specification, the worst case is $\Delta f = -0.05$ GHz. Substituting numerical values in equation 2-12 yields corresponding maximum phase deviations of +0.8 and +2.7 degrees, respectively. Furthermore, since the deviation from linear phase is still positive at the upper band edge ($\Delta f = +0.05$ GHz), the maximum "negative" deviation from linear phase occurs at midband ($\Delta f = 0$) and equals 0.* The total greatest phase deviations from linearity for two identical stages, therefore, calculates to be 1.6 and 5.4 degrees for the center and band-edge frequency regions, respectively, compared to the specifications of 10 and 15 degrees.

Differentiating, equation 2-11 yields the rate of change of phase with frequency:

$$\frac{d\phi}{df} = A_1 + 2A_2 (\Delta f) + 3A_3 (\Delta f)^2 \quad (2-13)$$

* For the ideal symmetrical parabolic envelope delay characteristic, $A_2 = 0$ and the maximum positive and negative deviations from linear phase would be equal and occur at the band edges.

POLYFIT OF DEGREE 3
INDEX OF DETERMINATION = 0.999998
WHAT NEXT? 2

TERM	COEFFICIENT
0	0.060611
1	-952.245
2	577.376
3	-10147.2

X-ACTUAL	Y-ACTUAL	Y-CALC	DIFF	PCT-DIFF
-0.06	61.36	61.4656	-0.105648	-0.171881
-0.055	55.85	55.8689	-1.88775E-2	-3.37889E-2
-0.05	50.42	50.3847	3.53107E-2	7.00823E-2
-0.045	45.07	45.0055	6.45247E-2	0.143371
-0.04	39.79	39.7236	6.63762E-2	0.167095
-0.035	34.59	34.5315	0.058476	0.169341
-0.03	29.46	29.4216	0.038434	0.130632
-0.025	24.41	24.3861	2.38607E-2	9.78453E-2
-0.02	19.42	19.4176	2.3663E-3	1.21864E-2
-0.015	14.48	14.5084	-2.84383E-2	-0.196012
-0.01	9.61	9.65094	-0.040943	-0.424239
-0.005	4.78	4.83754	-5.75374E-2	-1.1894
0	0	0.060611	-0.060611	-100
0.005	-4.75	-4.68745	-6.25533E-2	1.33449
0.01	-9.46	-9.41425	-4.57542E-2	0.48601
0.015	-14.16	-14.1274	-0.032603	0.230779
0.02	-18.84	-18.8345	-5.48935E-3	2.91452E-2
0.025	-23.53	-23.5432	1.31969E-2	-5.60542E-2
0.03	-28.22	-28.2611	4.10666E-2	-0.145312
0.035	-32.93	-32.9957	6.57301E-2	-0.199208
0.04	-37.68	-37.7548	7.47976E-2	-0.198114
0.045	-42.48	-42.5459	6.58789E-2	-0.154842
0.05	-47.34	-47.3766	3.65853E-2	-7.72224E-2
0.055	-52.27	-52.2545	-1.54719E-2	2.96088E-2
0.06	-57.3	-57.1873	-0.112685	0.197045

STD ERROR OF ESTIMATE FOR Y = 5.92676E-2

3-1021

Figure 2-11. Least Squares Error Fit of Theoretical Paramp Phase Characteristic to Third-Order Polynomial

It is understood that the specification of maximum rate of change of phase with frequency of 0.5-degree/MHz refers to the maximum rate of change with frequency of the deviation of phase from a linear phase characteristic. This latter quantity is given by the derivative of equation 2-12 which is equation 2-13 minus the constant term A_1 .

The worst case is for $\Delta f = 0.05$ GHz, which yields a value of 0.13 degree/MHz. Doubling this value for two identical stages yields 0.27 degree/MHz compared to the specification of 0.5 degree/MHz.

C. VARACTOR

1. GENERAL

Over the past 10 years the Central Research Group of AIL has been engaged in varactor research. The goal has been to make varactors which have very high cutoff frequencies and at the same time have very low parasitic elements. This work was supported by AIL using internal research and development funds.

Both Schottky barrier (metal semiconductor) and P-N junction varactors having zero-bias cutoff frequencies in excess of 600 GHz with typical zero-bias capacities of 0.15 pF have been successfully fabricated during this period. The major development effort has been concentrated on Schottky barrier varactors since they offer advantages in ease of fabrication (fewer steps) and inherently lower series resistance.

Figure 2-5 shows the varactor configuration used on various parametric amplifier programs from 2 to above 50 GHz. Figure 2-12 shows the basic varactor holder before mounting the semiconductor chip. The advantage of this configuration is that all processing (etching, contacting, and so on) and low-frequency measurements (C versus V and I versus V) on the varactor chip can be made before it is inserted in the waveguide. Furthermore, the stray capacitance associated with the quartz is small (0.03 pF) and the configuration permits attainment of very small series inductance. The quartz piece, which is now routinely fabricated and metallized, is soldered to the copper pin. A processed varactor chip is also attached to the copper pin and then a conducting ribbon is bounded to the lands of the quartz. The varactor to date has gone through three stages of development as far as choice of ribbon material, ribbon to semiconductor mesa contact, and passivation of the semiconductor are concerned. A brief description of each stage follows.

a. FEASIBILITY VARACTOR

This type of varactor was developed for use in cryogenic systems and did not employ passivation since under these conditions they were impervious to deterioration over long periods of time (because of low operating temperatures and operation in a vacuum environment). A diode of this type was fabricated in June 1961. This unit was stored in an open lab environment and at approximately yearly intervals its I versus V characteristics were checked. During the most recent test, no changes were observed in its characteristics. This varactor used gold ribbon with an indium sphere acting as a contact between the ribbon and the semiconductor mesa.

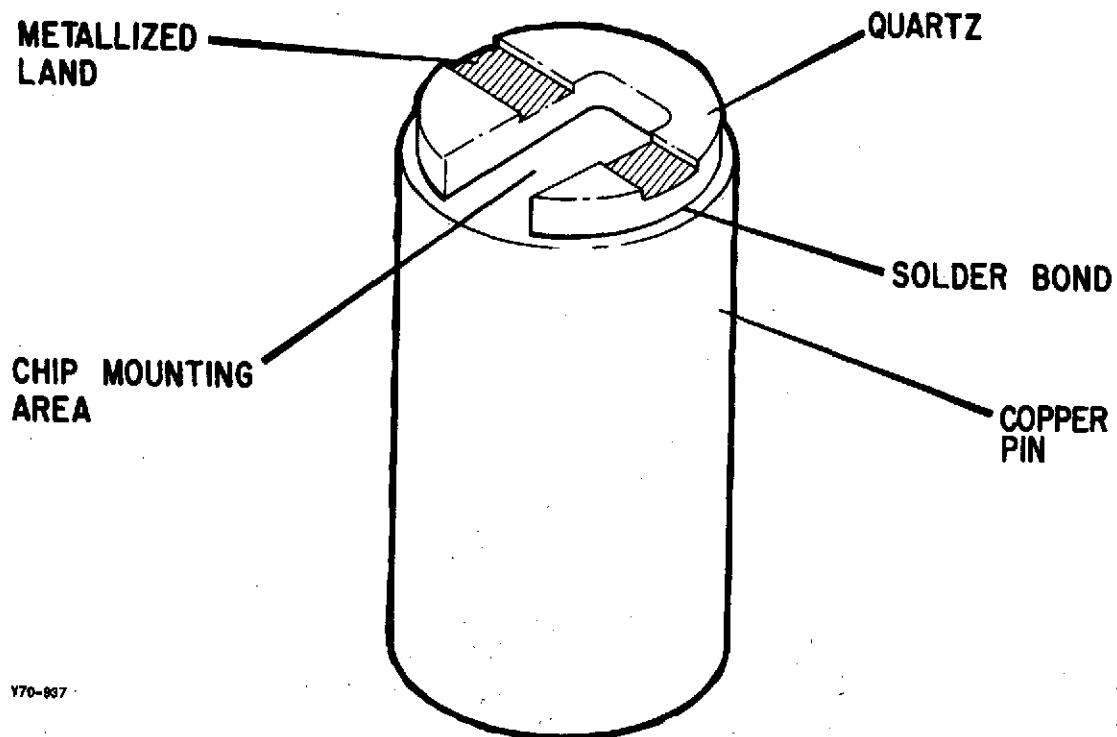


Figure 2-12. Varactor Holder

b. PROTOTYPE VARACTOR

This varactor was developed to allow use in paramps that had to be stabilized at temperatures up to 50°C. The indium-gold contact of the feasibility varactor was found to gradually diffuse at these temperatures. A platinum ribbon was substituted for the gold to overcome this problem. Like a feasibility varactor, this was not passivated.

c. QUANAR VARACTOR

Further developments by AIL's Central Research Group evolved the passivated quasiplanar (QUANAR) varactor which is used in present AIL paramps. This used a quasiplanar construction with a passivating layer to prevent deterioration when stored for prolonged periods at 100°C. The major failure mechanisms are understood and are under control during fabrication and screening procedures. The gold ribbon is thermal compression bonded to the mesa thereby eliminating the indium contact material. A scanning electron-microscope photo of a thermal compression bonded QUANAR varactor is shown in Figure 2-13.



REPRODUCIBILITY OF THE
ORIGINAL PAGE IS POOR

Figure 2-13. Assembled Quanar Varactor

2. CHARACTERIZATION MEASUREMENTS OF VARACTORS

Two low-frequency measurements are made on the varactor before it is inserted into a mount; namely, current versus voltage (I versus V) and capacitance versus voltage (C versus V). The I versus V data for a typical varactor is shown in Figure 2-14. This measurement is made on a Tektronix Type 575 Transistor Curve Tracer. Both the reverse breakdown voltages (V_b) at 1 and 10 μ A and the forward voltage (V_f) for 0.1 and 10 μ A are noted. Since the current between these forward and reverse conduction voltages can be as small as 10^{-12} A, the curve tracer shows no current except near the conduction points. However, a General Radio Type 1230A electrometer, which is capable of measuring 10^{-13} A, is employed to make I versus V measurements on selected units.

A Boonton Model 75D Capacitance Bridge is used to make C versus V measurements. The maximum ac voltage across the varactor during the measurement is 15 mV. A direct reading of C versus V is obtained from the bridge and this data is then computer processed as shown in Figure 2-15. The extraneous capacitance across the varactor, the built-in (contact) potential of the varactor, and the actual C versus V of the varactor are all calculated by the computer.

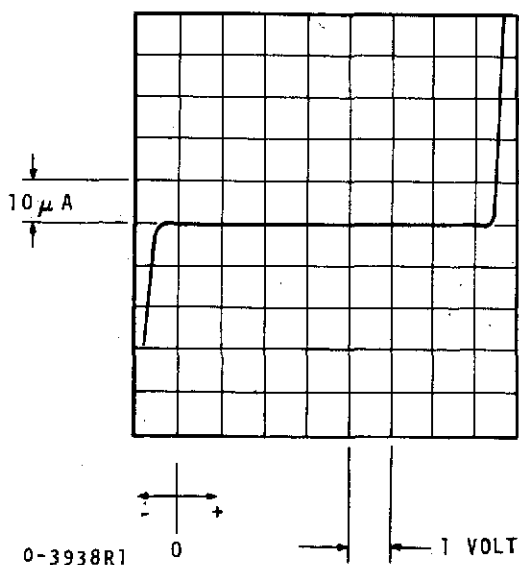
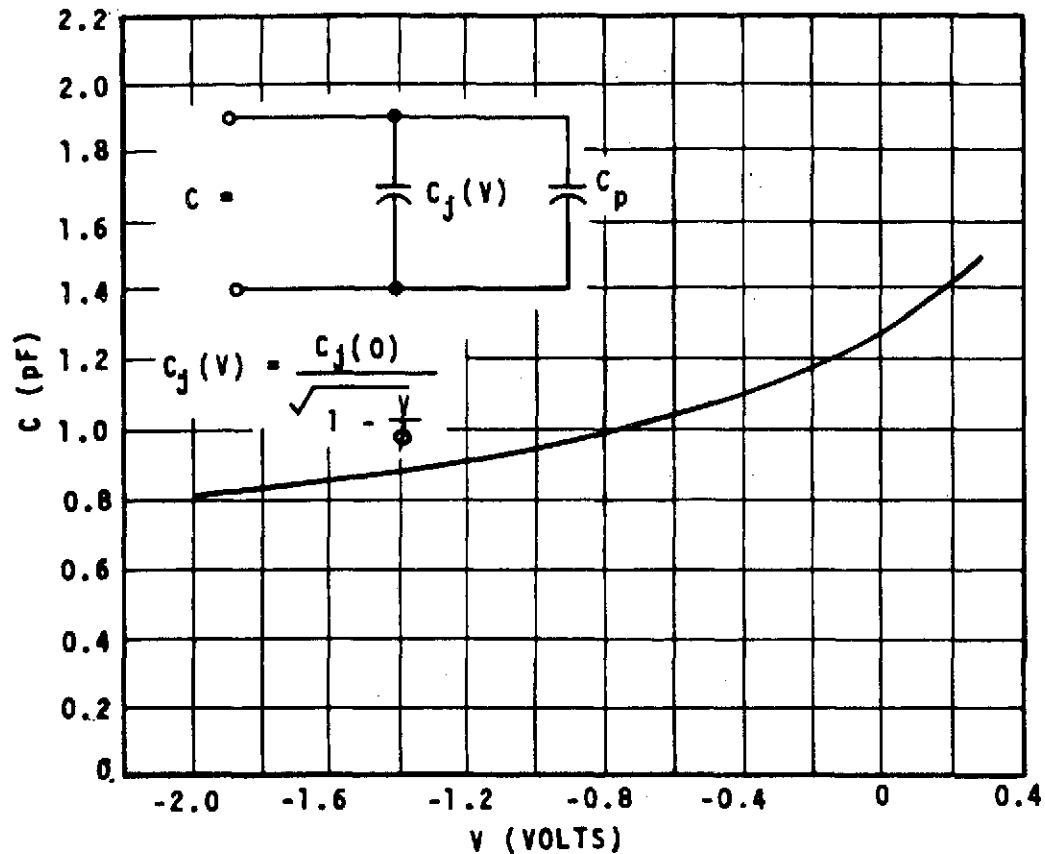


Figure 2-14. Typical Varactor I Versus V Trace



THE STD OF THE COMPUTED FIT IS 1.94132 E-4

CASE CAPACITY = 3.03217 E-2 + OR - 2.44128 E-4
 C(V=0) = 9.67221 E-2 + OR - 3.04691 E-4
 [1/C(V-0)]SQ. = 106.893 + OR - .673461
 PHI = .857477 + OR - 3.41106 E-2

VOLTS	MEAS.	Z1/C1SQ	+OR-	DIFF.
-0.3	0.15	69.8183	0.657445	-2.78156 E-4
-0.2	0.141	81.6348	0.831225	2.20393 E-4
-0.1	0.1335	93.9342	1.02598	2.69537 E-4
0	0.127	106.99	1.24715	-4.38276 E-5
0.25	0.1155	137.83	1.82356	7.04298 E-5
0.5	0.107	170.081	2.4997	-1.94172 E-4
0.75	0.101	200.183	3.19189	3.60197 E-5
1.0	0.096	231.823	3.97778	-3.83446 E-5
2.0	0.083	360.36	7.70923	-3.05826 E-4
3.0	0.076	479.271	11.8243	7.61296 E-5
4.0	0.071	604.331	16.7424	4.03449 E-5
5.0	0.0675	723.472	21.93	1.71463 E-4
6.0	0.0645	856.052	28.2264	-2.39842 E-5

0-3939

Figure 2-15. Varactor C Versus V

Cutoff frequency has been measured on balanced pairs of varactors at 70 GHz in a mount which was designed to minimize loss and also permit the microwave measurements of parasitic capacitance and inductance.

Figure 2-16 is a Smith Chart plot of a representative set of data for a pair of Schottky-barrier varactors. The zero-bias cutoff frequency is calculated from the equation:

$$f_c = \frac{1}{2\pi R_s C_j(0)} = -\frac{f_m}{R} \left[\frac{X(V_2) - X(V_1)}{\left(\frac{V_2 + \phi}{\phi}\right)^{1/2} - \left(\frac{V_1 + \phi}{\phi}\right)^{1/2}} \right] \quad (2-14)$$

where

f_c = zero-bias cutoff frequency

f_m = frequency at which the measurement is made

$X(V_2), X(V_1)$ = measured reactances at bias voltages
 V_2 and V_1

ϕ = contact potential

R = resistive component of the circle plot

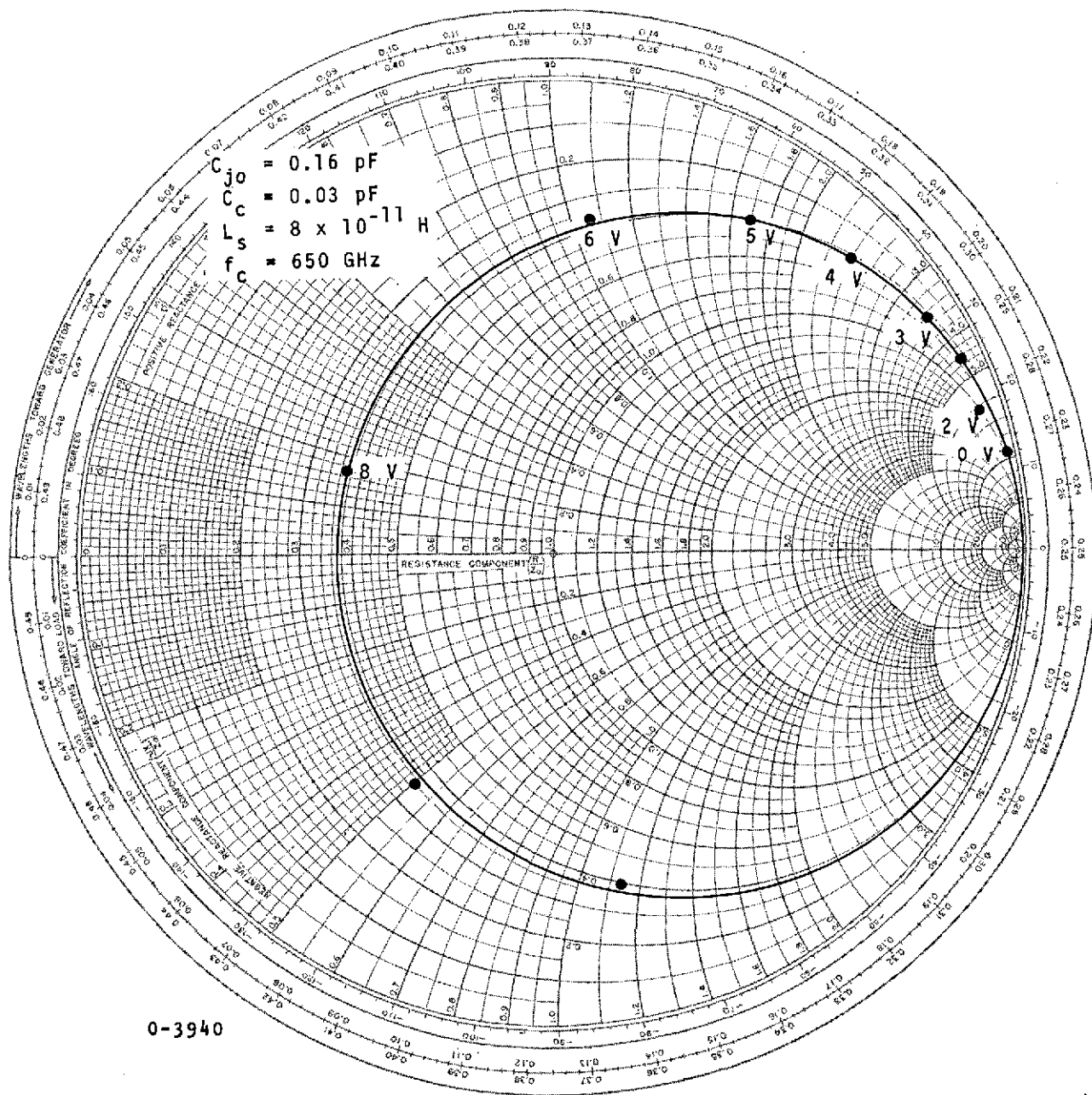
Equation 2-13 assumes that the capacitance of the varactor follows a square-root law with voltage. The cutoff frequency derived from Figure 2-16 is 650 GHz.

A representative equivalent circuit for the varactor is shown in Figure 2-17. The values of cutoff frequency obtained experimentally compare well with the theoretical calculations. Representative values for the elements of the circuit are:

$$L_s = 10^{-10} \text{ H}$$

$$C_p = 0.03 \text{ pF}$$

$$f_{c0} = \geq 600 \text{ GHz}$$

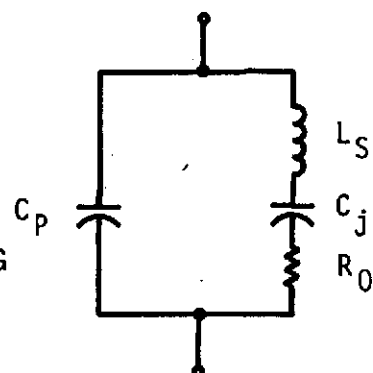


REPRODUCIBILITY OF THE
 ORIGINAL PAGE IS POOR

Figure 2-16. Impedance Plot of M-S Junction

WHERE:

C_j = JUNCTION CAPACITANCE
 L_s = STRAY INDUCTANCE
 R_0 = SERIES RESISTANCE
 C_p = STRAY CAPACITANCE RESULTING FROM METALLIZED LAND



3-1022

Figure 2-17. Equivalent Circuit of Chip Varactor and Holder

Typically, the reverse breakdown voltage of the varactors is greater than 10 V. The fabrication techniques permit making varactors with a zero-bias junction capacitance greater than 0.07 pF and a capacitance versus voltage law that is square root, with contact potential of:

$$\phi = 0.9 \text{ V}$$

Based on these considerations, the nominal electrical specifications of the paramp varactor is as follows:

- Operating junction capacitance $0.12 \pm 0.005 \text{ pF}$
- Operating cutoff frequency $\geq 600 \text{ GHz}$
- Reverse breakdown (at $1 \mu\text{A}$) $\geq 10 \text{ V}$
- Stray capacitance $0.03 \pm 0.01 \text{ pF}$
- Lead inductance $10^{-10} \text{ H (nominal)}$
- Nonlinearity Square law
- Maximum power dissipation 50 mW

3. EVALUATION OF UNPASSIVATED VARACTORS

The results of evaluation tests on the unpassivated feasibility and prototype varactors are described in this paragraph. These varactors were subject to the evaluation test procedure given in Appendix D. A summary of the test results follows.

a. FEASIBILITY VARACTORS

Evaluation of the feasibility varactors indicated that the gold-ribbon and indium sphere used to contact the junction reacted with each other at a storage temperature of 100°C, causing open-circuiting of the varactor as shown in A and B of Figure 2-18. A close examination of part B shows that the indium contact to the junction became open circuited. This indicated that a change in ribbon material was desirable for varactors used in equipment stabilized at temperatures above normal ambients. This resulted in the development of the prototype varactor described next.

b. PROTOTYPE VARACTOR

The gold ribbon used in the feasibility varactor was replaced with a platinum ribbon in this modification of the varactor. Tests of the combination of a platinum ribbon and indium spheres showed no reaction when heated to 100°C for 209 hours. This can be seen in parts C and D of Figure 2-18, where no physical deterioration is evident.

The prototype paramp varactors, using the above platinum ribbon construction, successfully passed the following evaluation tests given in the procedures of Appendix D:

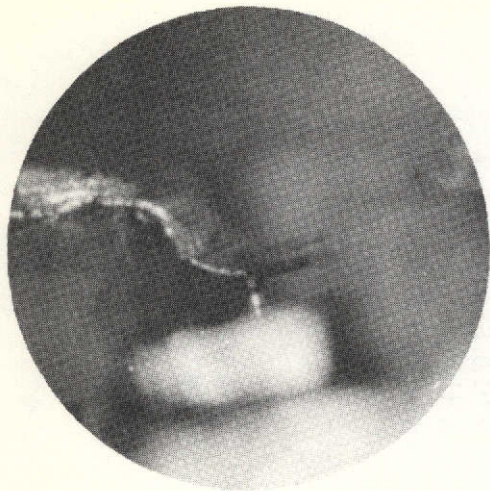
- Temperature cycling as per MIL-STD-202, Method 107 (-65 to 100°C, five cycles)
- High-temperature reverse bias (100°C, 96 hours at 80 percent of reverse breakdown voltage)
- Operating burn-in (96 hours, at 50 mW dc dissipation in the junction under forward bias)

The varactors were then divided into two equal groups for storage tests as follows:

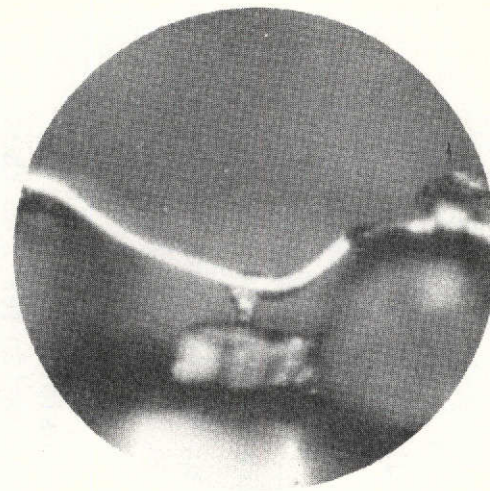
Group I: 960 hours, storage, nonoperating at 100°C

Group II: 960 hours operating life at 25°C with 50 mW dc power dissipation applied for 50 minutes out of every hour

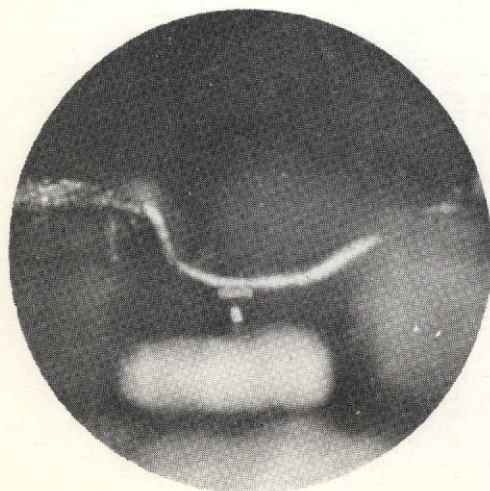
At the end of the 960-hour test on Group I, all the varactors had deteriorated in their forward and reverse characteristics to a point where they were unusable in a paramp application. In Group II, four out of the ten varactors remained usable after the 960-hour test was completed.



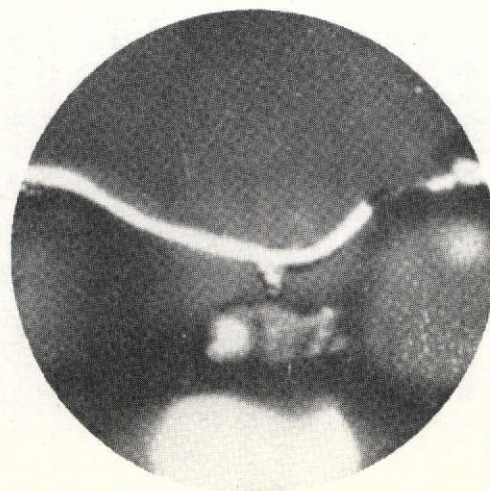
A. PRIOR TO BAKE FEASIBILITY
VARACTOR (GOLD RIBBON)



C. PRIOR TO BAKE ETM VARACTOR
(PLATINUM RIBBON)



B. AFTER 150 HOURS AT 101° C
FEASIBILITY VARACTOR (GOLD RIBBON)



D. AFTER 209 HOURS AT 101° C ETM
VARACTOR (PLATINUM RIBBON)

The results of an intensive study of these tests by AIL's Central Research Group indicated that the basic problem was surface diffusion of the indium contact material at 100°C which caused a gradual increase in forward conduction, eventually shorting out the junction. This was confirmed by etching away the indium, which restored the original varactor characteristics.

In order to overcome the temperature limitations, a quasiplanar varactor was developed with SiO₂ passivation which greatly reduces the diffusion rate at 100°C. In these varactors, the indium used to contact the mesa to the ribbon has been replaced by a thermal-compression bond of the gold ribbon to the mesa, thereby eliminating one potential source of failure.

A set of 20 of the thermal-compression bonded quasiplanar varactors were fabricated. These were subjected to the same evaluation tests as the prototype varactor. The results of these tests are given in detail in the next part of the report.

A check of the cutoff frequency of the quasiplanar varactors at 70 GHz showed that there was no degradation in cutoff frequency over the prototype varactors.

4. EVALUATION TEST RESULTS--QUANAR VARACTORS

The results of evaluation tests performed on the AIL "QUANAR" passivated, thermal-compression bonded varactor, described previously, will be presented in this paragraph. The evaluation procedure used for these tests is given in Appendix D along with sample data sheets. Initially, a total of 28 QUANAR thermal-compression bonded varactors was fabricated for evaluation purposes. Initially, the V versus I and C versus V characteristics of the varactors were measured. As a screening test they were subject to a 24-hour nonoperating bake at 150°C. The varactors were then thermally shocked from -65 to 100°C (five cycles). Upon measurement of the V versus I and C versus V characteristics, no deterioration was observed in any of the varactors with the exception of three units which were open due to defective thermal-compression bonds.

Twenty of these varactors were then subjected to the evaluation procedure given in Appendix D. A summary of the results of these tests is given in Table 2-2 with copies of the data given for each varactor in Appendix E.

**TABLE 2-2. SUMMARY OF QUANAR THERMAL-COMPRESSION
BONDED VARACTOR**

Evaluation Tests - V Versus I Characteristic

Varactor No.	Five Cycles Thermal Shock	96 Hours		Operating (50 mW at 25°C) Life Test		
		100°C 80% Rev. Bias	25°C 50 mW Dissipation	168 hrs	480 hrs	960 hrs
3-1	NC	NC	NC	NC-A	R-NC	R-NC
3-2	NC	NC	NC	NC-A	R-NC	R-NC
3-3	NC	NC	NC	NC-A	R-NC	R-NC
3-4	NC	NC	NC	NC-A	R-NC	R-NC
3-5	NC	NC	NC	NC-A	R-NC	R-NC
3-6	NC	NC	NC	NC	NC	NC
3-7	NC	NC	NC	NC	NC	NC
3-8	NC	NC	NC	NC	NC	NC
3-9	NC	NC	NC	NC	NC	NC
3-10	NC	NC	NC	NC	NC	NC

Storage Life at 100°C

1-1	NC	S	-	-	-	-
1-2	NC	NC	NC	NC	NC	D
1-3	NC	NC	NC	NC	NC	NC
1-4	NC	NC	NC	NC	NC	NC
1-5	NC	NC	NC	NC	NC	NC
1-6	NC	NC	NC	NC	NC	NC
1-7	NC	NC	NC	NC	NC	NC
1-8	NC	NC	NC	O	-	-
1-9	NC	NC	NC	NC	NC	NC
1-10	NC	NC	NC	NC	NC	NC

NC - No change in characteristics

A - Accidentally destroyed by instrument
malfunction

R-NC - Replacement units which showed
no change

S - Soft

O - Open

D - Decrease of 1.3 V in reverse
characteristic

Of the 20 varactors tested, it was observed that:

- Twelve varactors showed no signs of deterioration
- Five varactors showed no change until at the end of the 168-hour test they were accidentally destroyed by an instrumentation malfunction. These were replaced by five varactors which had been thermally shocked. After 790 hours of 50-mW of operation, these replacements showed no deterioration
- One varactor showed a slight decrease in reverse breakdown of 0.54 V at 10 μ A. Past RF tests have shown that this would not impair cutoff frequency or paramp performance since the capacity did not change (within experimental measurement accuracy). This was probably due to contamination of the passivating layer and would be obviated by improved cleaning techniques recently instituted
- One varactor open-circuited. This was traced to a poor thermal-compression bond which could probably have been discovered by more cycles of thermal shock
- One varactor soft. This was probably due to a crack in the semiconductor mesa which caused diffusion of contact materials into the depletion layer causing an effective change in doping. This would have been uncovered by a longer screening period. Presently 48 hours at 150°C screening is being considered to detect such failures during the screening phase

These tests indicated no basic failure mechanism was operative in the QUANAR varactors at elevated (100°C) temperatures as had been observed in the unpassivated varactors described earlier. Improvements in process control and screening presently being implemented should further improve the reliability of these units.

During the past year over 500 of this type varactor have been fabricated. At least 100 have gone through acceptance testing which consisted of:

- Thermal cycling, air to air, -55 to 100°C for five cycles
- High temperature storage--150°C for 48 hours

- High temperature reverse bias--a reverse bias of 8 V is applied at 150°C for 48 hours in accordance with MIL-STD-750 Method 1038 Condition A
- Thermal shock--liquid to liquid 0 to 100°C for 15 cycles in accordance with MIL-STD-750 Method 1056
- Mechanical shock--five shocks in both directions of each axis at 1500G for 0.5 ms in accordance with MIL-STD-750 Method 2016
- Power burn-in varactors are subjected alternately at a 60-Hz rate to 100-mW power dissipation in the forward direction then 8 V reverse bias for 168 hours

Only one failure occurred during the above testing. This unit became soft in the reverse direction and a SEM examination showed a cracked mesa due to the TC bond being made on the edge of the mesa. Ten varactors are being given additional testing as follows:

- Thermal shock as above for an additional 20 cycles
- Mechanical shock as above
- Operating life test--the power burn-in described above

These varactors were tested after 250 hours and have since undergone thousands of additional hours of testing. Another group of five varactors have been subjected to the Moisture Resistance Test, Method 1021 of MIL-STD-750 with no changes occurring.

5. JUNCTION TEMPERATURE

The AIL Central Research Group has developed varactors having over 600 GHz cutoff frequency and low parasitic reactances for application in high performance parametric amplifiers. The QUANAR varactors have reached a stage of development where they have been passivated to make them impervious to most contaminants. Evaluation tests reported herein indicate that the varactors are capable of operation at 150°C junction temperature for prolonged periods without significant deterioration in characteristics. Thermal resistance measurements have shown the thermal resistance to be an average of 0.8 mW/°C. Based on this, the maximum safe power dissipation for the maximum stabilization temperatures of 160°F and pump power level of 18 mW per varactor, the junction operating temperature of the paramp varactors would be 80°C or about 55 percent of the maximum rating. This is considered safe for long-term unattended operation. The previous series of tests show the direct applicability of the varactor to successfully meet all of the requirements of the program.

D. CIRCULATOR

1. GENERAL

One of the key parameters in the design of parametric amplifiers is the circulator. In noncryogenic system operation, the circulator is responsible for a severe degradation of the basic amplifier's low-noise properties. For this reason, considerable effort has been directed toward improving the circulator loss characteristic during the last few years.

Since most of the losses are inherent to the physical properties of the ferrite material, only limited improvements are to be expected in the near future. The loss of the breadboard prototype circulator covering the 2.20 to 2.30 GHz band is 0.1-dB per pass. This loss is assumed in the gain/noise temperature budget discussed earlier.

2. CIRCULATOR DESIGN

The basic circulator configurations are shown in Figure 2-19.

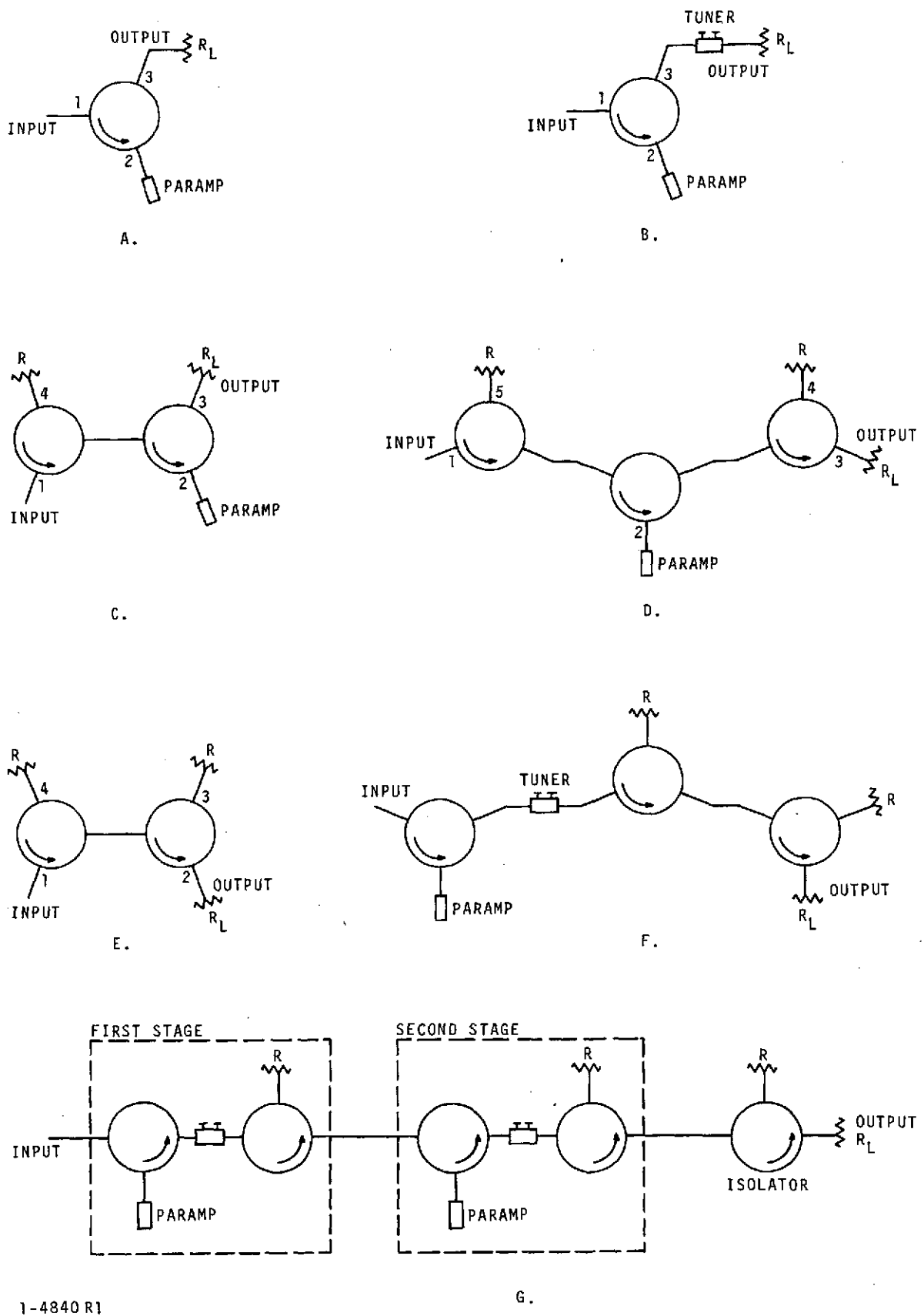
Let the circulator isolation per pass and the gain of the amplifier as a ratio or in decibels be indicated as L_i or $L_i(\text{dB})$ and K or $K(\text{dB})$, respectively.

If $L_{i(n+1)}$ is the isolation between the n^{th} and the $(n+2)^{\text{th}}$ port of a circulator (circulating in the direction of increasing n) with the $(n+1)^{\text{th}}$ port terminated in a load R , the VSWR (S) of the terminated port with respect to R is very closely given by:

$$S_{(n+1)} = \frac{1 + \left[L_{i(n+1)} \right]^{-1/2}}{1 - \left[L_{i(n+1)} \right]^{-1/2}} \quad (2-15)$$

In the configuration of Figure 2-19, the maximum possible effective input VSWR is then given by:

$$S_{1_{\text{max}}} \approx S_1 \cdot \frac{1 + \sqrt{\frac{K}{L_{i_3}}}}{1 - \sqrt{\frac{K}{L_{i_3}}}} \quad (2-16)$$



1-4840 R1

G.

Figure 2-19. Various Circulator Paramp Configurations

For $S_{\max} \leq 1.5$ and $S_1 < 1.25$ the following approximate relation is valid:

$$L_{i_3} \approx \frac{4K}{\left(S_{1\max}^{-1} - \sqrt{\frac{2}{L_{i_1}}} \right)^2} \quad (2-17)$$

A realistic number for a well designed circulator is $L_{i_n} \geq 23$ dB or $L_{i_n} \geq 200$. Using this number and assuming $K \approx 50$ and $S_{\max} \leq 1.5$ (as required by the specifications), the required L_{i_3} is:

$$L_{i_3} \geq 1540 \text{ or } L_{i_3} \geq 32 \text{ dB} \quad (2-18)$$

This is an unrealistic requirement for any one circulator port.

In principle, it is possible to separately tune the load R_L to an almost perfect match with the circulator output port giving the required $L_{i_3} > 32$ dB (Figure 2-19B). A very slight variation in R_L , however, would destroy this condition.

For the method of Figure 2-19 to be a practical solution, the return loss of the mismatch corresponding to a $VSWR = (1 + \Delta R_L / R_L)$ would have to be at least 42 dB (one order of magnitude $>$ required L_{i_3}) or $\Delta R_L / R_L < 1.6 \times 10^{-2}$.

In view of this, it is customary to use two circulator passes at the input of the parametric amplifier, accepting a further degradation in noise performance (Figure 2-19C). The required L_i is now, under normal circumstances, easily satisfied. However, the addition of an extra isolator on the output (Figure 2-19D) opens the possibility for another interesting solution.

Consider the four-port circulator of Figure 2-19E. The internal return loss for a signal after entering the input port is two orders of magnitude greater than the required 42 dB to make the method of Figure 2-19B practical. Thus, a solution is offered by the configuration of Figure 2-19F.

The prime feature of this arrangement is that the noise degradation as a result of the second pass input isolation can be avoided. Therefore, AIL used the configuration of Figure 2-19G with full integration of the parametric amplifier, tuning element, and four-port circulator, so that all RF connectors, except at the input and output, are eliminated.

Under these circumstances, the return loss of the interjunction following the amplifier can easily be tuned to a value > 40 dB even under the specified mismatch conditions, thereby fully meeting the VSWR specifications and at the same time exploiting the low-noise advantage of operation with a single input pass of isolation.

By integrating the parametric amplifier and the circulator, thus eliminating the requirement to transform via a 50-ohm impedance level, the transformation can be kept as simple as possible, resulting in a minimum physical length between varactor diode and ferrite boundary.

These conditions are all favorable for attaining the lowest possible loss at the input of the parametric amplifier.

3. STABILITY OF CIRCULATOR CHARACTERISTICS WITH REGARD TO TEMPERATURE AND APPLIED FIELD

It is of utmost importance that the circulator characteristics will have the least possible temperature dependence. This is to minimize changes in the circulator characteristics if the first-stage thermoelectric would fail and emergency room temperature of operation is required.

- Temperature sensitivity of the input impedance
- Temperature sensitivity of the return loss of the interjunction

Moreover, the effect of small changes of the applied field on these parameters has to be minimized.

Let Figure 2-20A represent an ideal circulator with the indicated impedance matrix (Z) at a temperature $T = T_0$.

If the temperature changes from T_0 to $T_0 + \Delta T$, the circulator will generally change its impedance as well as its frequency response.

It can be shown that when $T = T_0 + \Delta T$ the representation given in Figure 2-20B is valid, so that the input impedance has changed from R to $R + \Delta R + j \Delta X$.

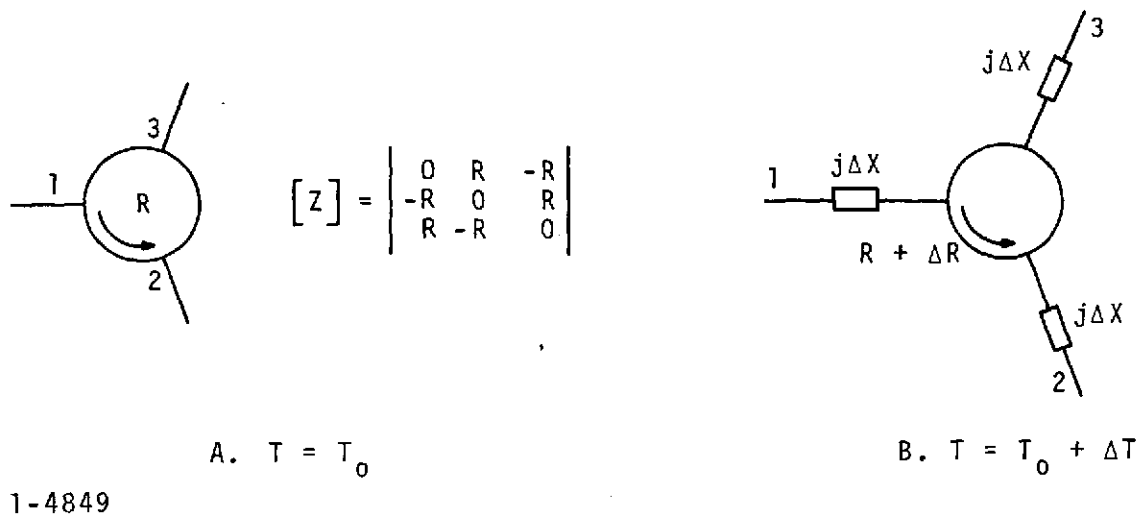


Figure 2-20. Circulator Representation at $T = T_0$ and $T = T_0 + \Delta T$

All the properties of a circulator of a certain geometry are completely dictated by the values μ and κ of the complex permeability matrix, which are in the first place determined by the magnetization (M) of the ferrite material and moreover a function of the dimensions of the finite ferrite sample.

The effect of the sample shape is accounted for by introducing the demagnetization factors N_x , N_y , and N_z for the X, Y, and Z direction of the sample, respectively.

For a circular ferrite disc, assuming the Z-direction parallel to the applied dc magnetic field, H_A , and perpendicular to the circular cross section of the disc, $N_x = N_y = N_t$.

The dc magnetic field inside the ferrite sample is given by:

$$H_i = H_A - N_z 4\pi M \quad (2-19)$$

The effective RF resonance field is shown to depend also on the value of N_t (Kittel) and is given by:

$$H_K = H_A + (N_t - N_z) 4 \pi M$$

or

(2-20)

$$H_K = H_i + N_t 4 \pi M$$

With these terms defined μ and κ are given by:

$$\mu = 1 + \frac{f_r \gamma 4 \pi M}{f_r^2 - f^2} \quad (2-21)$$

$$\kappa = \frac{f \gamma 4 \pi M}{f_r^2 - f^2}$$

where

$$f_r = \gamma H_K$$

$$\gamma = \text{gyromagnetic ratio} = 2.8 \text{ MHz/oersted}$$

As the circulator characteristics are completely determined by μ and κ and assuming $H_A = \text{constant}$, it follows that the only way of making the circulator independent of temperature is to keep M constant.

For a circulator biased in the region of magnetic saturation, $M = M_s$.

The saturation magnetization M_s , however, normally varies appreciably with temperature.

Although it is possible to make the magnetic circuit temperature dependent, and thus change H_A in such a way as to keep one of the parameters, such as H_K , constant, thereby changing some of the properties of the circulator less than others, it is impossible to keep the properties constant on all fronts.

However, there is a solution. From the internal dc magnetic field:

$$H_i = H_A - N_Z 4 \pi M$$

therefore,

(2-22)

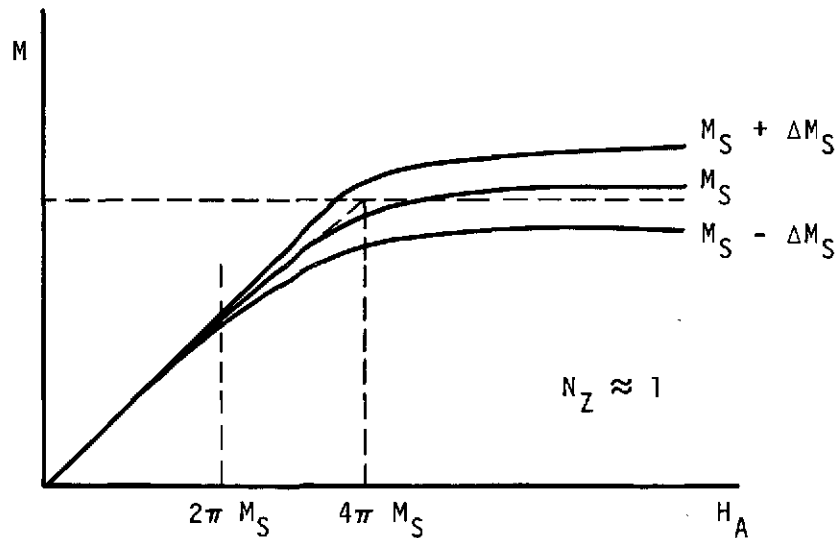
$$4 \pi M = \frac{H_A - H_i}{N_Z}$$

Below saturation $M \ll M_s$ the dc- μ of the material is very high. The result of this is $H_i \approx 0$, from which $4 \pi M = H_A / N_Z$ so that the value of M is independent of M_s but proportional to H_A instead:

$$M \propto H_A \text{ for } M \ll M_s$$

Graphically, this effect is shown in Figure 2-21, where M is given as a function of H_A with M_s as parameter.

From this graph, it can be seen that, for example at $H_A \approx 1/2 (4 \pi M_s)$, M is practically independent of moderate changes of M_s .



1-4848

Figure 2-21. Magnetization as Function of dc Field and M_s .

Because in the region $H_i \approx 0$ the Kittel-field $H_K = N_t 4\pi M$ is very small (order of magnitude of $N_t = 0.2$) it follows $f_r \ll f$. Moreover, to avoid low field losses, the condition of $\gamma 4\pi M_s < f$ has to be satisfied at all times.

Under these conditions, the expressions for μ and κ go over into

$$\mu \approx 1 \quad (2-23)$$

$$\kappa \approx \frac{-\gamma 4\pi M}{f}$$

It can be shown from circulator theory that the frequency determining parameter is $\mu_{\text{eff}} = (\mu^2 - \kappa^2)/\mu$, whereas the value of R is inversely proportional with M .

$$R \propto \frac{1}{M}$$

These relations in combination with the above conditions yield:

$$\begin{aligned} \mu_{\text{eff}} &\approx 1 \\ R &\propto \frac{1}{M} \propto H_A^{-1} \end{aligned} \quad (2-24)$$

Thus, for operation below saturation $M < M_s$, μ_{eff} the frequency dependent parameter is independent of temperature as well as of the dc applied field so that $j\Delta X = 0$ (Figure 3-21B). As the expected variation in H_A , as a result of temperature and/or elapsed time, is extremely small in case of the proper choice of magnetic material (for example, Alnico, Cobalt Samarium), the expected ΔR over the specified temperature range will be far within the limits allowed by the parametric amplifier as far as the input impedance is concerned.

However, at first sight, it might be questioned whether this slight change ΔR will be small enough not to destroy the critically tuned, high return loss condition of the interjunction that is necessary to make one-pass operation possible.

Surprisingly, an extra bonus is added in the form of self-regulating action of the interjunction, as far as a change in the real value, ΔR , is concerned.

As was pointed out, the input impedance, in case of a change of temperature or of applied field, is given by:

$$R + \Delta R + j \Delta X \quad (2-25)$$

Under the stated condition of bias field $M < M_s$, $j \Delta X = 0$ so that the input impedance is $R + \Delta R$.

This input impedance of the second circulator, however, constitutes the load impedance of the first circulator which also changed its characteristic impedance to $R + \Delta R$, so that, theoretically, a perfect interjunction match is maintained. Even in case slight asymmetries are present, it is, in view of the previous mechanism, fully justified to render their effects negligible.

4. CIRCULATOR MEASURED CHARACTERISTICS

The following are the measured characteristics of the stage 1 and 2 prototype circulators and the second-stage output isolator:

a. CIRCULATORS FOR STAGE 1 AND 2

	<u>S/N-001</u>	<u>S/N-002</u>
Insertion loss 1-2 (average)	0.10 dB	0.104 dB
Isolation 2-1 (2.2 GHz)	38 dB	40 dB
Isolation 2-1 (2.25 GHz)	40 dB	40 dB
Isolation 2-1 (2.3 GHz)	43 dB	40 dB
VSWR port 1	1.03	1.07
VSWR port 3	1.03	1.06
Isolation 3-1 (average)	37 dB	32 dB
Insertion loss 2-3 (average)	0.4	0.4 dB

b. OUTPUT ISOLATION (AVERAGE OVER BAND)

S/N-001

Isolation 2-1	23 dB
Insertion loss 1-2	0.25 dB
VSWR (input)	1.08
VSWR (output)	1.06

This indicates that the required high isolation, low forward loss techniques theoretically described in the previous section have been achieved in practice in the S-band system.

E. PUMP SOURCE

1. GENERAL

The design requirements for the S-band paramp system dictated the use of a millimeter-wave pump source at an operating frequency of ~ 50 GHz. Since a solid-state pump source was specified, the basic choice of oscillator type was limited to a Gunn-effect device or an IMPATT oscillator. The main advantage of a Gunn device is that it has a much lower inherent noise level, while the IMPATT oscillator has the advantage of higher output power levels as well as somewhat greater dc-to-RF conversion efficiency. The pump-power requirements of the amplifier are such that suitable Gunn and IMPATT devices are both commercially available at the present time.

2. PUMP NOISE CONSIDERATIONS

Since the noise of a pump source can be considered as a random fluctuation in instantaneous pump power, the varactor capacitance will fluctuate accordingly. Because of this, the pump noise is downconverted into the signal frequency domain, thereby degrading the tangential sensitivity of the amplifier.

In normal operation, even with a noisy pump, this degradation is often negligible. However, it has been observed that when a strong interfering signal is present in close proximity of the received frequency, a severe degradation in tangential sensitivity occurred. In this case the pump-derived noise sidebands of the strong interfering signal increase the input noise level at the received frequency. This phenomenon will be explained in some detail in Appendices C and F, where it will be derived that the degradation in tangential sensitivity at $f = f_s$ as a result of a strong interfering signal Δf away, is given by:

$$\frac{P_{T(f_s \Delta f)}}{P_{T(f_s)}} = 1 + \left[\frac{K}{T_{op}} F(\Delta f) \right] P_{s(\Delta f)}$$

where

$P_{T(f_s \Delta f)}$ = tangential sensitivity at $f = f_s$ in the presence
of an interfering signal Δf away

$P_{T(f_s)}$ = tangential sensitivity at $f = f_s$

K = power gain of amplifier

T_{op} = operational temperature $\left(T_{op} = T_{\text{amplifier}} + T_{\text{signal-source}} \right)$

$F_{(\Delta f)} = \frac{W_{(\Delta f)}}{K} = \text{figure of merit of pump source}$

$W_{(\Delta f)}$ = normalized spectral noise power density of pump oscillator Δf away from carrier

k = Boltzmann's constant = 1.38×10^{-23} joules/K

$P_{s(\Delta f)}$ = power of interfering signal Δf away from f_s

In Figure 2-22, this relation $P_{T(f_s \Delta f)} / P_{T(f_s)}$ is shown graphically as a function of $P_{s(\Delta f)}$ with $\left(K/T_{op} \right) F_{(\Delta f)}$ as parameter.

With the carrier power as 0-reference level, the noise of an oscillator is often specified by the manufacturer as the decibel-level, seen across a small bandwidth displaced a given distance from the carrier frequency. From this data, at least one value of $W_{(\Delta f)}$ can be obtained.

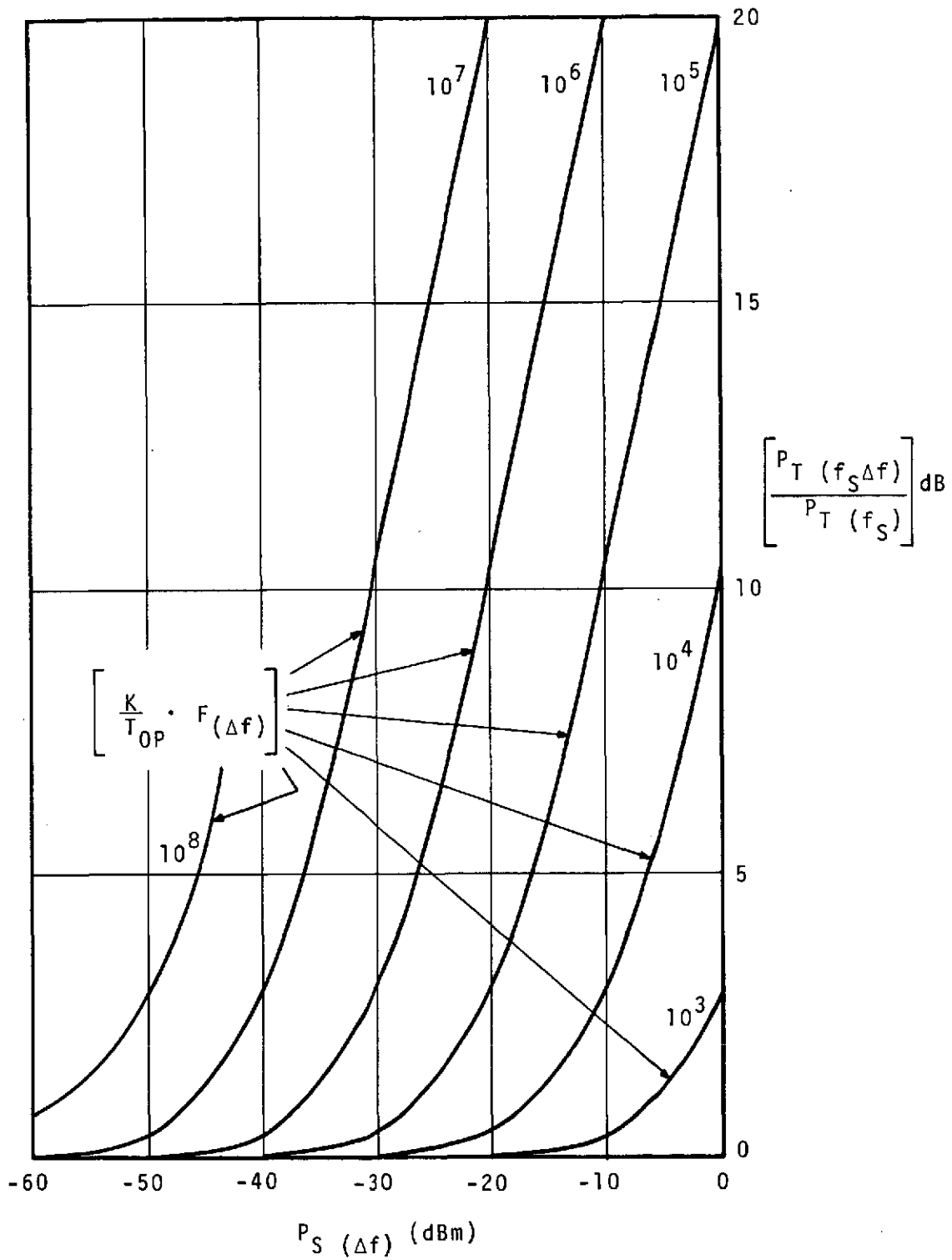
From reference 2, Figure 2, we derive, as typical numbers for these power levels at 100-kHz distance from the carrier in a 100-Hz bandwidth, -128 dB for an IMPATT, and -148 dB for a Gunn effect oscillator. Using these numbers we find:

$$\text{IMPATT: } W_{(10^5)} = 1.55 \times 10^{-13} \times 10^{-2} = 1.55 \times 10^{-15} \text{ (second)}$$

$$F_{(10^5)} = \frac{W_{(10^5)}}{k} = \frac{1.55 \times 10^{-15}}{1.38 \times 10^{-23}} = 1.12 \times 10^8 \frac{\text{(second K)}}{\text{(joule)}}$$

$$\text{Gunn: } W_{(10^5)} = 1.55 \times 10^{-17}$$

$$F_{(10^5)} = 1.12 \times 10^6$$



1-4846 R1

Figure 2-22. Degradation of Tangential Sensitivity as a Function of Absolute Power of Interfering Signal

For an amplifier operational temperature of 100 K and two stages with a gain of 17 dB per stage, it is found that for $(K/T_{op}) F_{(\Delta f)}$ the numbers are 1.2×10^6 and 1.12×10^8 for the Gunn and the IMPATT, respectively.

From Figure 2-22, we can derive that the degradation of the tangential sensitivity will be noticeable when a signal of -60 dBm is present at a distance of 100 kHz when an IMPATT pump source is used.

In the case of a Gunn effect oscillator, the same signal can go up to a level of -40 dBm before the same degradation is noticed.

The difference of 20 dB in this quite possible range of interfering signal power made AIL decide to choose a Gunn effect oscillator as the pump-power source for the S-band paramp system

3. 50-GHz GUNN OSCILLATOR

A Gunn oscillator was available from Varian Associates which was suitable for use as a pump source for this program. The pertinent specifications for the type VSQ-9021 Gunn oscillator are:

Frequency	50 GHz
Power output (minimum)	75 mW at a flange temperature of 50°C
Amplitude variation with temperature	0.040 dB/°C (maximum)
Bias voltage	4.0 volts (maximum)
Bias current	1.0 ampere (maximum)

Assuming a worst-case total loss of 2.5 dB for the pump isolator, pump filter, and waveguide sections, a power level of 33.7 mW would be available at the amplifier pump input port. As shown in paragraph II.B.5, the theoretical pump power required by the amplifier is 14.1 mW which leaves a 3.8-dB margin in available pump power. This margin is sufficient for the system. The final system operated with a good margin of pump power.

The basic unstabilized oscillator has an amplitude stability of 0.040 dB/°C by temperature stabilizing the GDO's at $50 \pm 1^\circ\text{C}$.

An isolator is necessary at the output of the Gunn oscillator to ensure amplitude and frequency stability of the Gunn source. A suitable 50-GHz isolator having a maximum insertion loss of 0.5 dB and a minimum isolation loss of 20 dB was developed by AIL and is employed in this system.

F. ENVIRONMENTAL CONSIDERATIONS

Compliance with the specifications for the mechanical and environmental conditions was achieved for the S-band paramp system in the following manner.

1. TEMPERATURE STABILIZATION

The system was temperature stabilized by means of thermoelectric modules, heaters, and proportional controllers, over the ambient temperature range of -15 to $+50^{\circ}\text{C}$. The first stage paramp/circulator was cooled and stabilized via thermoelectrics at -20°C when installed within its insulated enclosure.

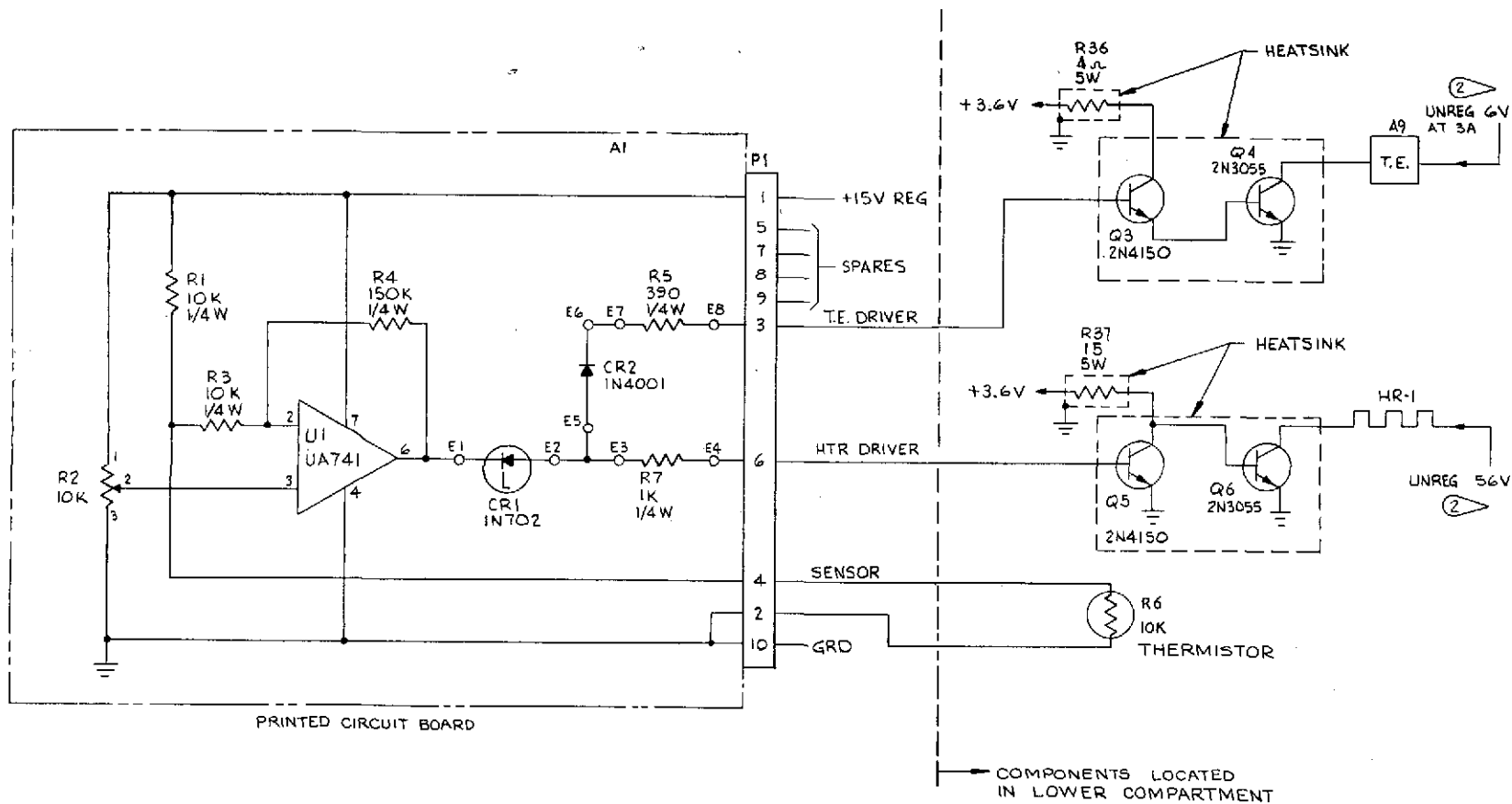
The second stage paramp/circulator Gunn oscillators and their associated components were installed in the second section of the system chassis and temperature controlled at an elevated temperature by means of heaters and proportional temperature controllers. Open-on-rise thermostats were used on all thermal circuits to assure maximum system protection.

The basic temperature controller circuit diagram is given in Figure 2-23. The components within the dashed lines are mounted on a printed-circuit board in the paramp module. The driver and output transistors are mounted in the lower compartment chassis (see Figure 2-27). The following is the function and type of circuit used for each of the three temperature controlled sections of the system.

<u>Controlled RF Component</u>	<u>Type</u>	<u>Stabilizes Components at ($^{\circ}\text{C}$)</u>
First stage Paramp (circulator)	Monopolar	-20
Second stage Paramp (circulator)	Bipolar	$+50$
Gunn Diode Oscillator	Bipolar	$+50$

a. TEMPERATURE STABILIZATION OF FIRST STAGE

The first stage paramp/circulator was thermally insulated from the rest of the system using thin-wall stainless steel transmission lines and polyurethane foam. The paramp/circulator was stabilized at $-20 \pm 2^{\circ}\text{C}$ (a ΔT of 70°C from maximum ambient) utilizing thermoelectric modules and a solid-state proportional temperature controller. The cold junction side of the module is bolted to the paramp/circulator. The hot side is fed through the insulation and chassis, and is exposed directly to ambient air. The heat to be pumped from the paramp/circulator, plus the conduction losses through the foam and the losses of the feedthrough components (that is, thin-wall stainless steel transmission lines), require the module to be

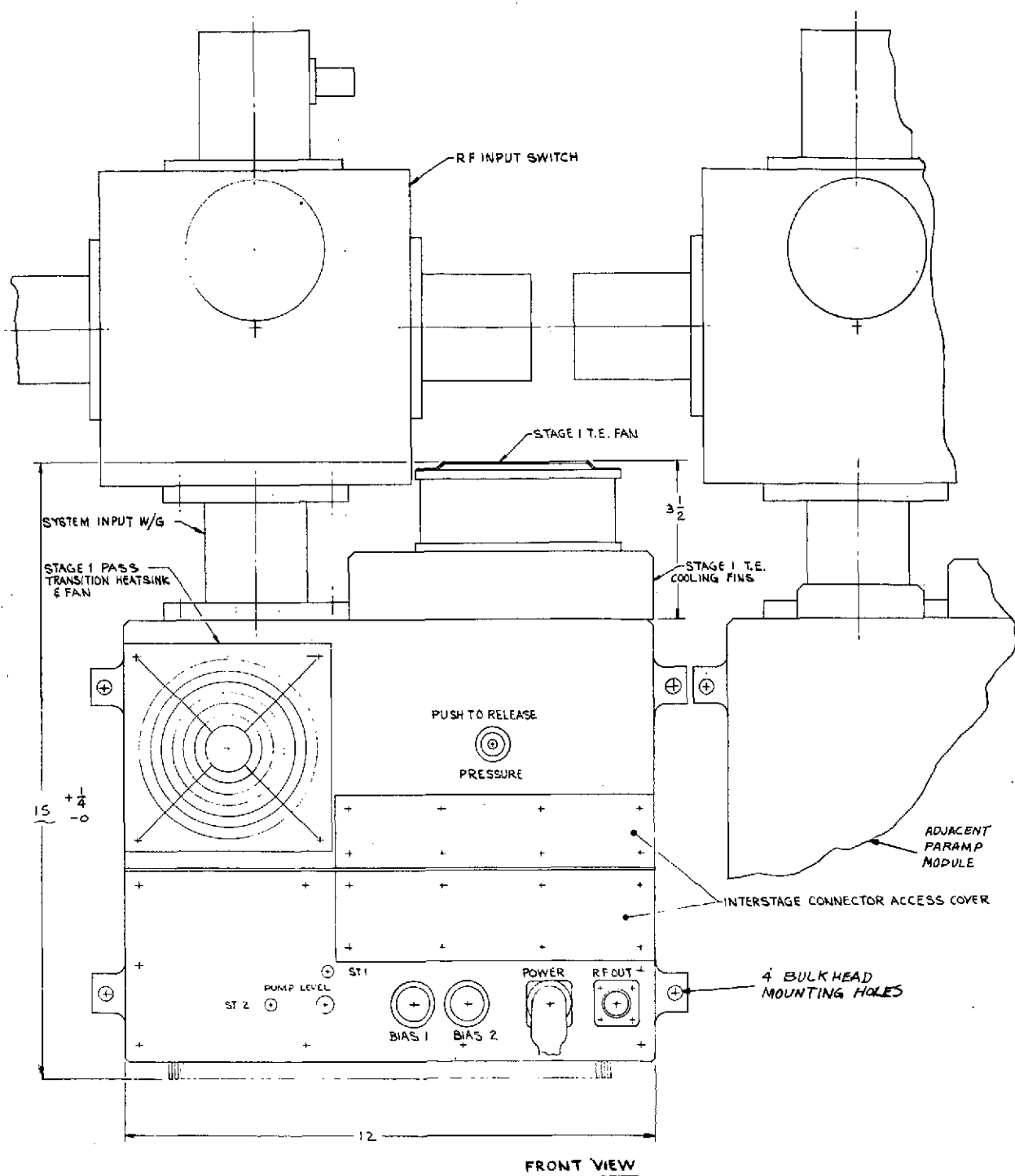


NOTES:

1. UNLESS OTHERWISE INDICATED:
ALL RESISTOR VALUES ARE IN OHMS.
- ② UNREGULATED VOLTAGES GIVEN AT FULL LOAD
MAY VARY UP TO 50% UPWARD.

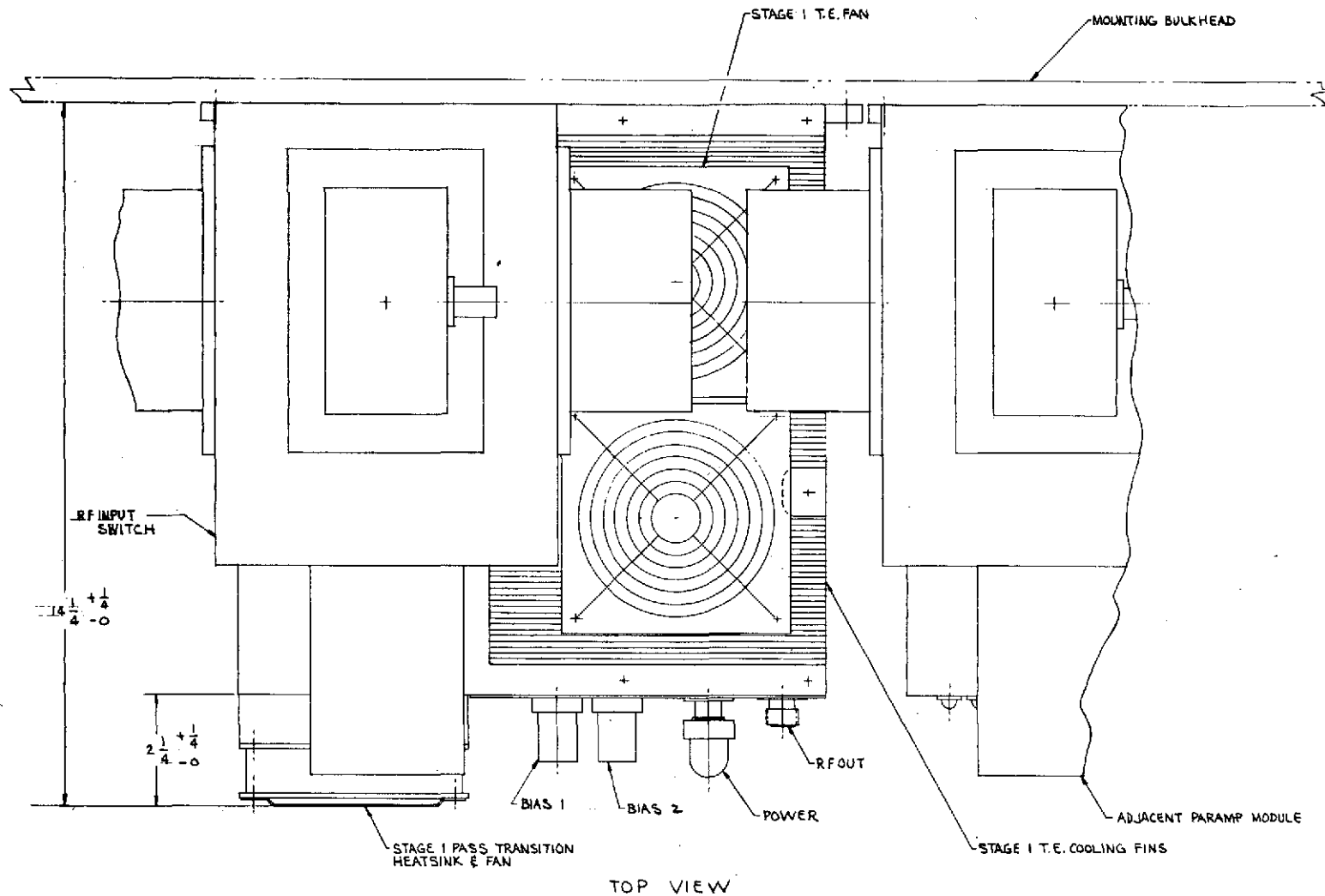
4-2591R1

Figure 2-23. Typical Bipolar Temperature Controllers



4-1929R1

Figure 2-24. Paramp Module, Site Interface Outline (Sheet 1 of 3)



4-1930

Figure 2-24. Paramp Module, Site Interface Outline (Sheet 2 of 3)

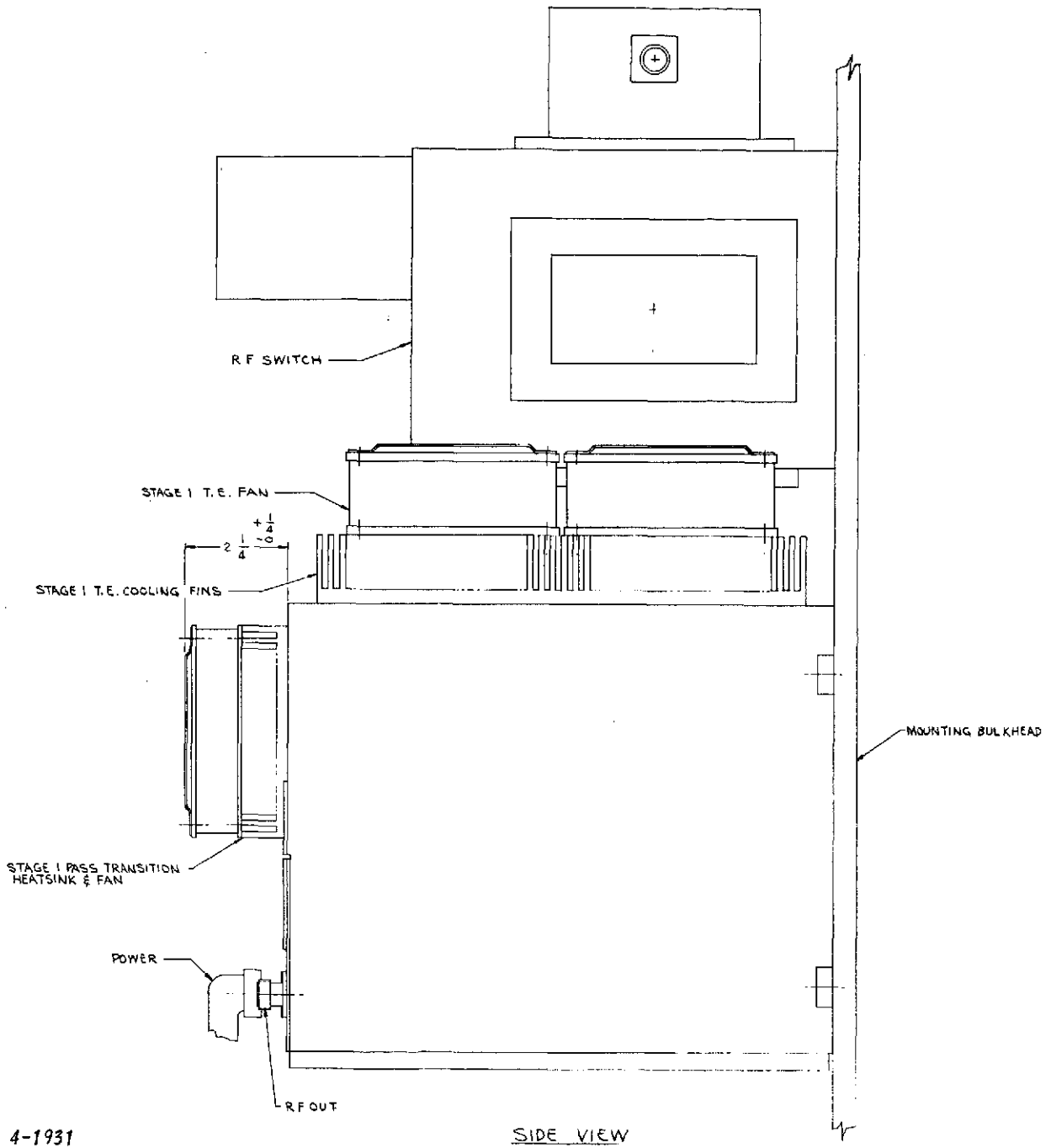


Figure 2-24. Paramp Module, Site Interface Outline (Sheet 3 of 3)

capable of pumping 14 watts for steady-stage operation for a ΔT of 70°C. The thermal budget for the first stage is as follows:

<u>Thermal Load due to</u>	<u>Estimated S-Band System (watts)</u>
Foam	10.2
Input waveguide	2.6
Radiation	1.0
Pump waveguide and coaxial	<u>0.5</u>
	14.3

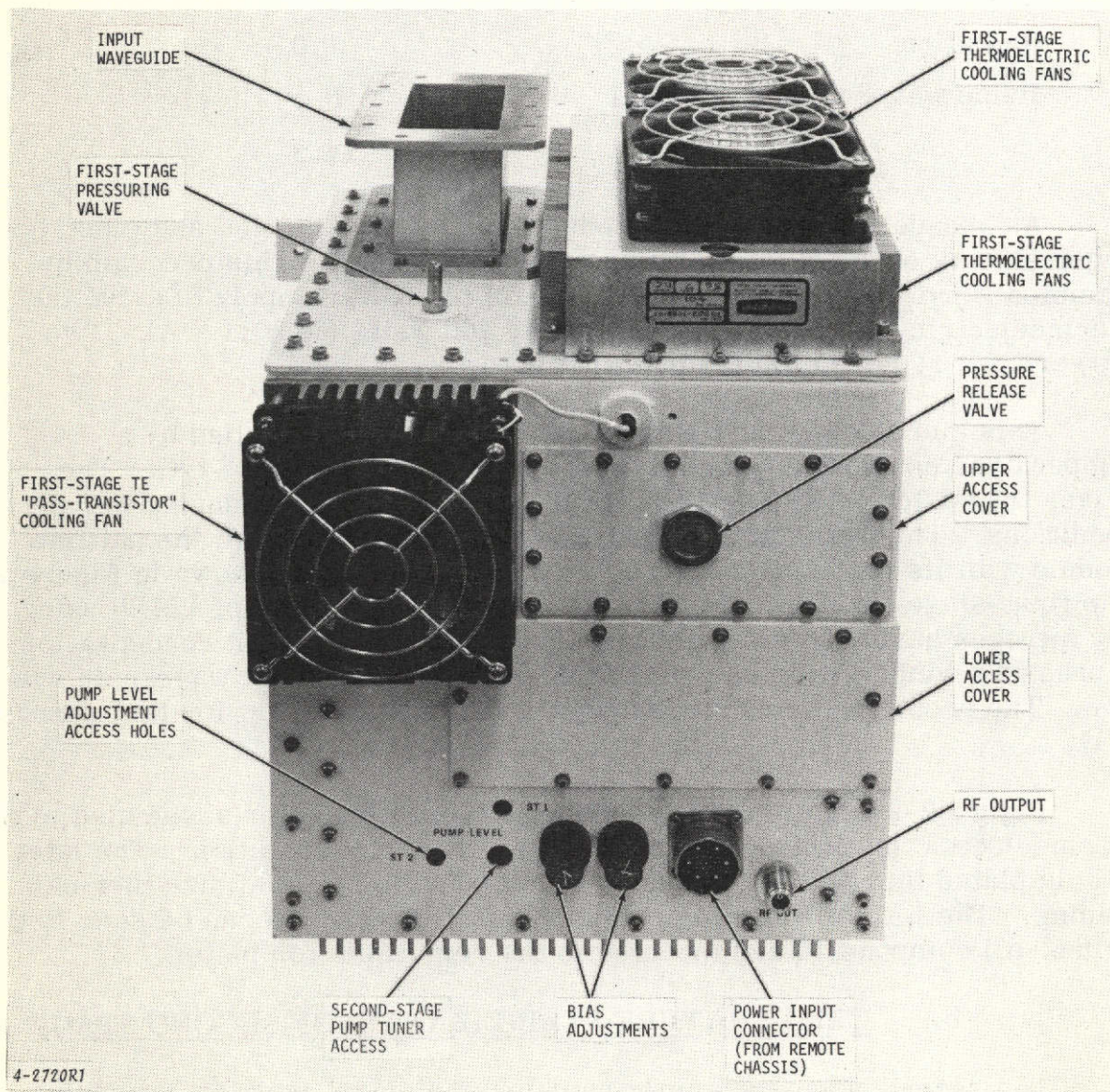
A cascade thermoelectric module meeting the thermal and electrical requirements of the system was custom designed for this program by Cambion Corp. The power requirement of the power supply to drive the thermoelectric modules is approximately 400 watts (38 V at 7 A). Two blowers are required to dissipate this power.

This thermoelectric module is proportionally controlled by a temperature controller to maintain the temperature within $\pm 1^\circ\text{C}$. The driver transistor must be capable of dissipating 100 watts during worst-case conditions. This transistor is mounted on the front-panel of the paramp module with its heat sink cooled by a separate blower as shown in Figure 2-25. The first-stage shall be maintained at a positive pressure of 1/4 lb using dry nitrogen having a dew-point of at least -30°C to prevent condensation. A pressure window is to be supplied elsewhere in the input waveguide system. The prototype system employs a 1 mil mylar window for test purposes only.

Figure 2-26 shows the first stage paramp/circulator assembled to the thermoelectric module and input waveguide-to-coax transition. The latter is of gold plated thin-wall stainless steel construction to minimize thermal loading. The loss of the transition is about 0.02 dB. As can be seen in the figure, all components are mounted to the removable top plate.

b. TEMPERATURE STABILIZATION OF SECOND STAGE

The second-stage paramp/circulator and output isolator are stabilized at maximum ambient ($+50^\circ\text{C} \pm 1^\circ\text{C}$) by means of heaters and thermoelectric modules controlled by a bipolar temperature controller. Up to 50 watts of power is required by the heaters and thermoelectrics. The heaters are 56 V cartridge-type embedded in the second-stage, temperature stabilized plate which sits on the two thermoelectrics connected in series (3 V at 5 A maximum input requirement). The 50°C stabilizing temperature prevents



REPRODUCIBILITY OF THE
ORIGINAL PAGE IS POOR

Figure 2-25. Paramp Module

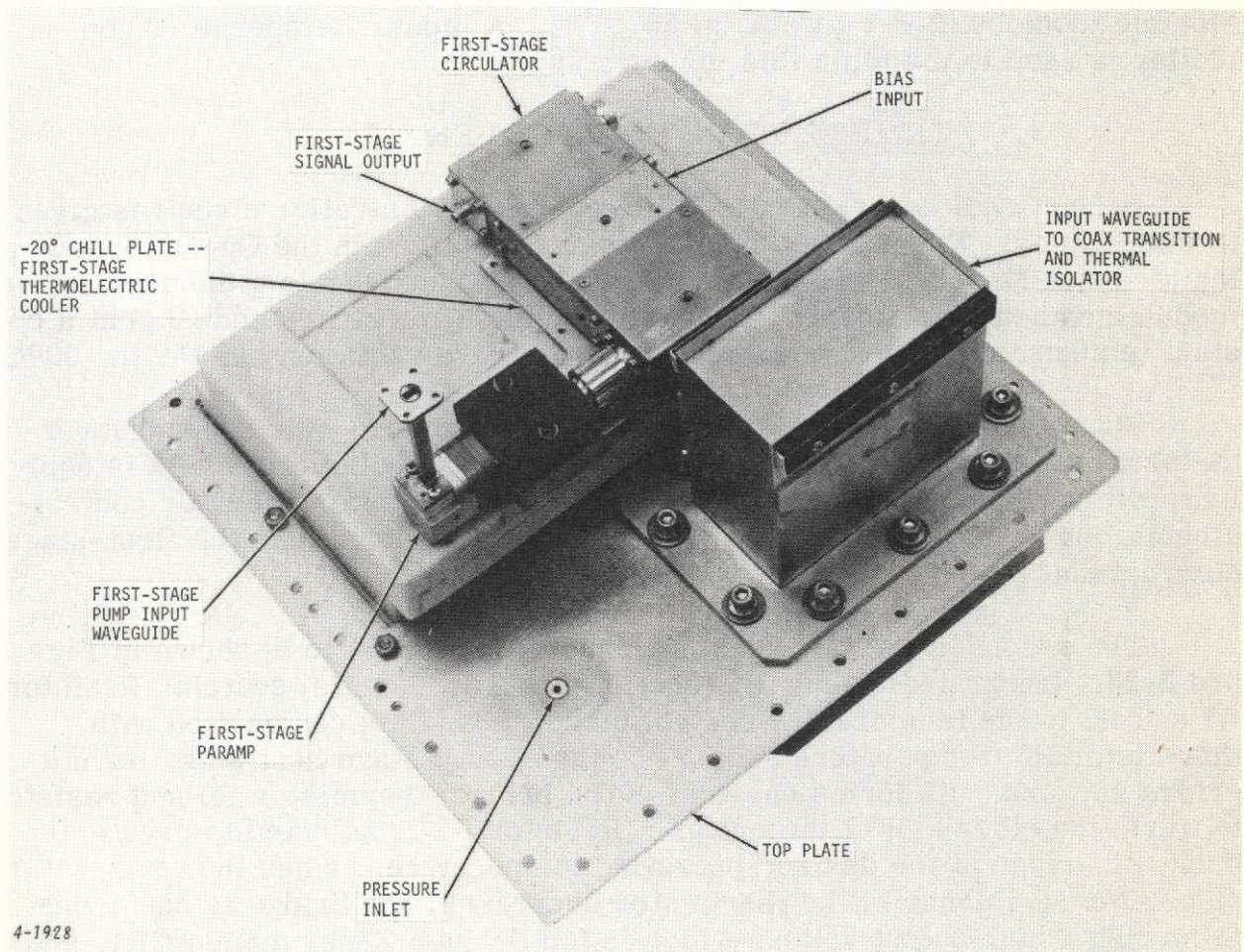


Figure 2-26. First-Stage Circulator-Paramp Assembled to Thermo-electric Chill Plate and Input Transition

condensation since it is equal or higher than maximum ambient. The prototype design does, however, allow for pressurization of the lower compartment for use in areas of very severe environmental conditions (humidity, dust, and so on).

c. TEMPERATURE STABILIZATION OF GUNN OSCILLATORS

Both first and second stage Gunn oscillators are mounted on a common heat sink and stabilized by means of a cartridge heater and two thermoelectric modules (2.6 V at 5 A) at $50 \pm 1^{\circ}\text{C}$. A bipolar temperature controller is used to maintain this temperature.

d. TEMPERATURE CONTROLLER

A functional description of the temperature controller circuit is given in this section. Exact details of the circuit are given in the Operations and Maintenance Manual. This circuit controls the dc power to a thermoelectric module and heater element to maintain the amplifier stages and GDO at a constant temperature over the baseplate temperature variation of -15° to $+50^{\circ}\text{C}$.

Since the operation of these circuits are similar, only second-stage temperature controller A1 is described. The monopolar circuit A2 is equivalent, with the exception that it does not include or require a heater control-circuit, since this is provided by the normal "heat-leak" into the first-stage compartment.

The second-stage temperature controller schematic is shown in Figure 2-23. Integrated circuit U1 functions as a differential switch. Resistors R1 and R2 in the temperature control circuit board, in conjunction with thermistor R6 (temperature sensor) on the second stage heat sink, form a bridge network. R2 forms one-half of the bridge; thermistor R6 and resistor R1 form the other half of the bridge. Resistor R2 is adjusted to create a balanced bridge at the desired operating temperature. When the temperature rises, the resistance of the thermistor decreases, the bridge is unbalanced, producing a high output voltage which is fed through Zener diodes CR1, and R5 to Q3 and Q4, the "Darlington" connected driver transistors, which supply power to the thermoelectric module (A9). When the circuit is cooled sufficiently, the thermistor resistance increases giving reduced output from 1 and 0 volts at terminal "E2" (due to the drop through Zener CR1). This turns off Q5. Consequently, the collector of Q3 is at high potential, turning on Q6 which actuates the heater to drive the temperature back up to the set-point value. Diode CR2 provides an "offset voltage" to separate the heater and thermoelectric turn-on points to prevent "hunting." This controller circuit can maintain the setpoint temperature to within 0.5°C .

Although initial thermal tests of these circuits indicated that proportional control was maintained at all points in the -15 to +50°C temperature range, final system tests show additional heater capacity is required in the GDO stability circuit. A larger heater would be used in the production units.

2. ENVIRONMENT CONSIDERATIONS (SHOCK AND VIBRATION)

The parametric amplifier system has been designed to operate satisfactorily within the dynamic environmental specification as encountered in typical ground base antenna system employing a hydraulic drive system.

Typical specifications for this type of system are vibration levels up to 2 g from 30 to 500 Hz, 0.05-inch maximum double amplitude displacement from 1.5 to 30 Hz.

Based upon previous experience with the vibration characteristics associated with ground-based antennas, no problem was expected in the dynamic environment as related to this system. The basic design approach for the structural and dynamic environment was to limit the amplitude of motion of the common baseplate below 500 Hz thereby isolating the system components from the dynamic environment.

G. PACKAGING REQUIREMENTS

The type A-471 prototype system has been packaged to meet the site interface requirements required for this program as follows.

1. PARAMP MODULE

The module has been designed to be installed against a bulkhead by means of four mounting tabs. Access for all tuning adjustment is from the front-only as required in a 26-meter antenna site where two units are mounted side by side and other components are installed on either side of these. These limitations have required careful layout and design to properly locate all components in the allotted space. Figure 2-24 is an outline drawing of the A-471 system connected to the 26-meter antenna site input RF switch. Sites using the 9-meter antennas have less stringent mounting requirements since the paramp module will be mounted in a standard rack enclosure.

The module is divided into an upper area which is pressurized and contains the first-stage paramp/circulator mounted on the thermoelectric cooler. These components are all mounted to the top plate which is gasketed to maintain a low leakage rate. After fastening the top plate to the module housing the connections to the second-stage, bias and power connections are made by removing the upper gasketed access cover which contains an overpressure relief and release valve.

The lower compartment components are mounted on a heat-sink which can be slid out of the housing after removing the front-panel screws and disconnecting the connections to the first stage. The latter are exposed by removing the lower access cover. The design of the lower compartment is such as to make it adaptable to pressurization as may be required at some sites. The following components are located in the lower compartment:

- First and second stage Gunn diode oscillators, isolators, test couplers and pump level set attenuators
- Second stage paramp/circulator
- Paramp and Gunn diode bias adjustment potentiometers
- Temperature controller boards
- Integrated regulator modules for paramp bias and GDO bias
- Pass transistors for all temperature stabilizing element except first stage thermoelectric module
- Bias divider and monitoring boards
- Output filter

Figure 2-27 shows the layout of the drawer in the prototype unit. The various components listed are identified in this figure. The detailed schematic diagrams are given in the Operations and Maintenance Manual for this program.

In the production units all terminal boards will be replaced with printed-circuit boards for ease of assembly and compactness. Terminal boards were used in some circuits of the prototype to facilitate design adjustments and testing. The paramp module with both access covers installed is shown in Figure 2-25.

The pump level and bias adjustment seen in this figure would be placed under a separate access cover in the proposed production units to meet EMI requirements. In addition, an EMI filter box would be incorporated at the power connector.

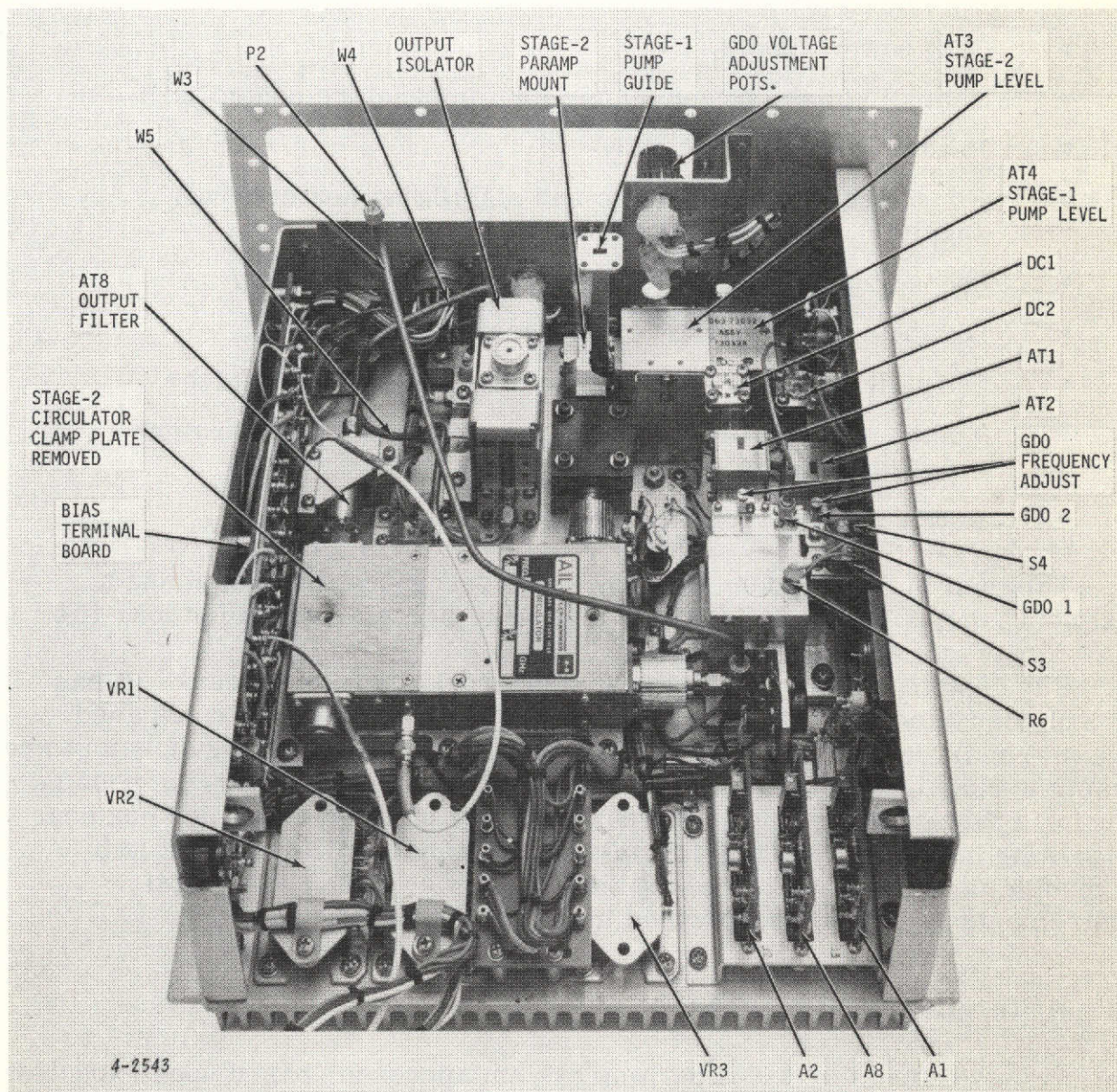


Figure 2-27. Lower Compartment Components Drawer (Partially Wired)

2. REMOTE CONTROL/POWER SUPPLY CHASSIS

Figure 2-28 shows the remote control/power supply chassis. This chassis houses the following major components:

- GDO power supply
- Control voltage power supply for temperature controllers
- Paramp bias power supply
- First stage thermoelectric and stabilizing heater power supply
- Second stage and GDO thermoelectric power supply
- Digital monitor voltmeter and selector switch
- Status lights showing presence of power supply voltage
- Temperature fault lights showing over/under temperature conditions
- Power switches with built-in circuit breakers

This unit operates from the 115-V ± 10 percent ac line requiring a maximum input power of 650 watts. LED pilot lights are used for long life.

The remote control unit fits in a standard 19-inch relay rack. It has a 7-inch high panel and is 21 inches deep. The prototype unit is designed for a maximum length interconnecting cable between the power supply unit and paramp module of 15 feet. Longer runs up to 100 feet will be accommodated by using a larger connector on the power supply unit and a junction box near the paramp module, since the size of connector mechanically possible in the module is limited. Filtering of the input power line to meet EMI requirements would be incorporated in the production units.

H. RELIABILITY PREDICTION

An assessment of AIL's paramp system approach, based upon expected parts complexity, indicated that the MTBF requirement is attainable predicted on the following:

- The use of the failure rates listed in MIL-HDBK-217A except in the case of the varactor diodes where the rates provided in RADC-TR-67-108 are deemed to be more appropriate to the application and the state of the art
- The use of EEE parts that are of MIL or JAN grade

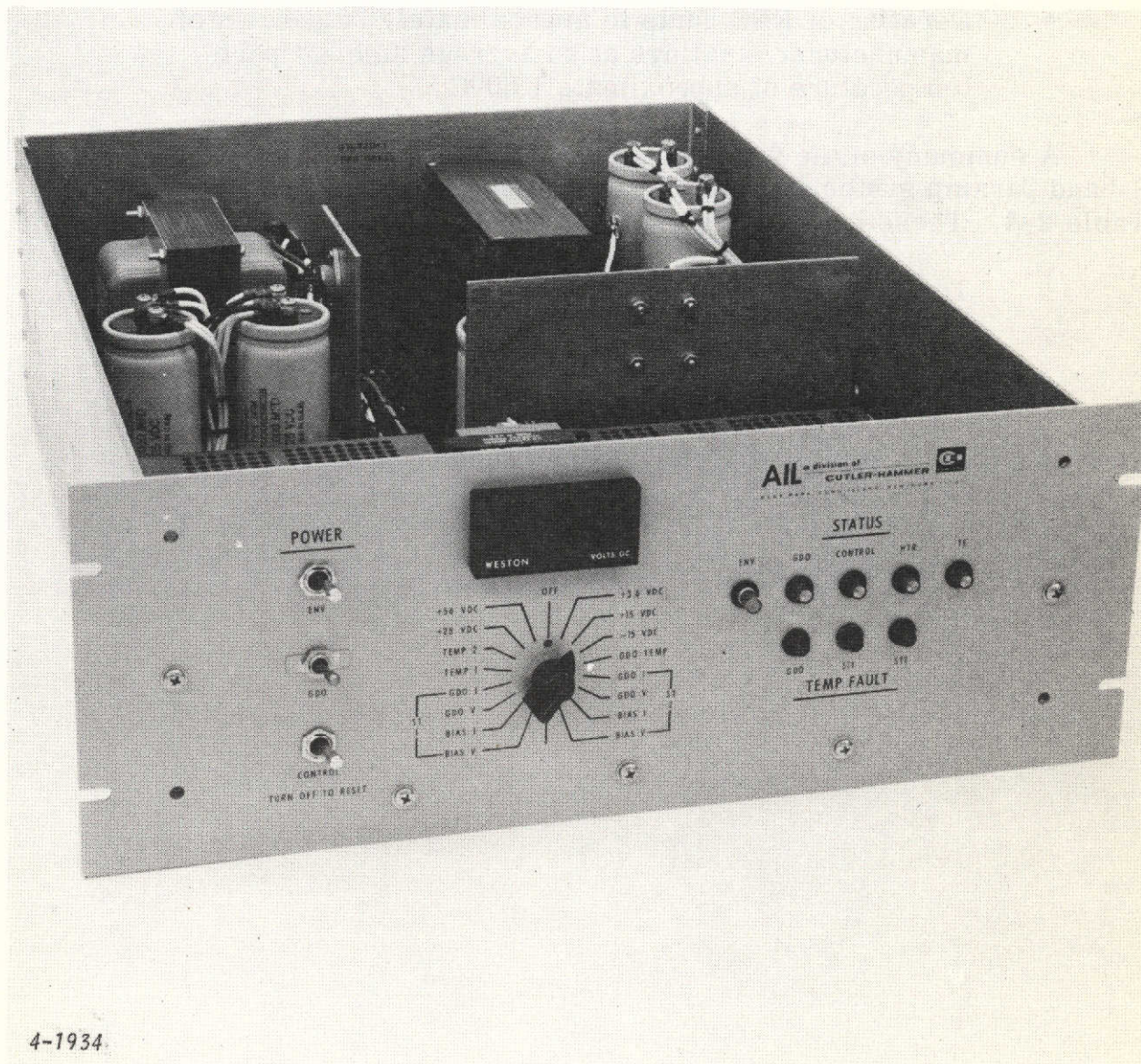


Figure 2-28. Remote Control/Power Supply Chassis

Note

The use of EEE parts of established reliability grade (ER or JANTX) would yield a predicted increase in MTBF by a factor of approximately 1.17.

- Derating of EEE parts to approximately 25 percent of manufacturer's ratings at an average ambient part temperature of approximately 60°C

A summary of the failure rate estimates for various units of the S-band paramp system (single varactor diode configuration) is given in Table 2-4. These estimates yield the following values of predicted MTBF:

<u>Total Failure Rate (fpMh)</u>	<u>MTBF (hours)</u>
55.51	18,015

This exceeds the minimum 10,000 hours required in the contract.

TABLE 2-3. FAILURE RATES FOR S-BAND CHIP VARACTOR PARAMP SYSTEM

Assembly/Unit/Part	Qty	Part Failure Rate (fpMh)	Total Unit Failure Rate (fpMh)	Remarks
<u>Bias-T Network</u>	<u>2</u>		<u>0.264</u>	
Coaxial Connectors	3	0.044	0.132	Fig. 7.9.8 (217A)
Deposited or Discrete Transmission Line Elements	Misc	Negligible	Negligible	
<u>4-Port Circulator</u>	<u>2</u>		<u>6.264</u>	
Coaxial Connectors	3	0.044	0.132	See Note 1
Ferrite Elements, Low Power (Pair)	3	1.000	3.00	
Magnets (Pair)	3	Negligible	Negligible	Permanent Magnets without pulsing coils
Deposited or Etched Terminations	2	Negligible	Negligible	
<u>Pump Circuits</u>	<u>2</u>		<u>16.92</u>	
Gunn-Diode Oscillator	1		6.000	Based on vendor life-test data
Ferrite Isolator	1			Equated to 10 percent of power ferrite (217A) Permanent Magnets without pulsing coils
Ferrite Elements, Low Pwr (Pr)	1	2.000	2.000	
Magnets (Pair)	1	Negligible	Negligible	
Variable Attenuator	1	0.100	0.100	Tables IV to IX (Avg. Rate 217A)
Directional Coupler	1	0.010	0.010	Tables IV to IX (Avg. Rate 217A)

TABLE 2-3. FAILURE RATES FOR S-BAND CHIP VARACTOR PARAMP SYSTEM (cont)

Assembly/Unit/Part	Qty	Part Failure Rate (fpMh)	Total Unit Failure Rate (fpMh)	Remarks
<u>Paramp</u>	<u>2</u>		<u>6.108</u>	See Note 2
Varactor Diode and Mount	1	3.0	3.0	
Coaxial Connector	1	0.044	0.044	
Waveguide Transition	1	0.010	0.010	
<u>Thermoelectric Cooler and Controller</u>	<u>1</u>		<u>2.412</u>	Tables IV to IX (Avg. Rate 217A)
Peltier Junction	Misc	Negligible	Negligible	
Resistors, Composition	2	0.021	0.042	
Linear IC's	2	0.400	0.800	
Resistors, Power Wirewound	1	0.500	0.500	
Capacitors, Ceramic	2	0.005	0.010	
Capacitors, Tantalum	2	0.030	0.060	
Resistor, Variable	1	1.000	1.000	
<u>Heater and Heater Controller</u>	<u>1</u>		<u>1.678</u>	Equated to resistor, fixed, power WW
Heater	1	0.500	0.500	
Thermistor	2	0.300	0.600	
Resistors, Composition	8	0.021	0.168	
Capacitors, Ceramic	2	0.005	0.010	
Linear IC	1	0.400	0.400	
<u>Thermoelectric Power Supply</u>	<u>1</u>		<u>1.7</u>	Tables IV to IX (Typical Rate, 217A)
Transformer	1	0.300	0.300	

TABLE 2-3. FAILURE RATES FOR S-BAND CHIP VARACTOR PARAMP SYSTEM (cont)

Assembly/Unit/Part	Qty	Part Failure Rate (fpMh)	Total Unit Failure Rate (fpMh)	Remarks
Bridge Rectifier	1	1.200	1.200	Tables IV to IX (Typical Motor Rate, 217A)
Capacitor, Electrolytic	1	0.200	0.200	
<u>Control Panel and Miscellaneous</u>	<u>1</u>		<u>8.836</u>	
Switches	2	0.200	0.400	
Resistor, Variable	2	1.000	2.000	
Fans	2	2.5	5.0	
Meter	1	0.500	0.500	
Linear IC	2	0.400	0.800	
Resistors, Composition	6	0.021	0.126	
Capacitors, Ceramic	2	0.005	0.010	
<u>Bias and Op. Amp. Power Supply</u>	<u>1</u>		<u>6.165</u>	
Transformer	1	0.300	0.300	
Linear IC	1	0.400	0.400	
Transistor, Power	1	0.850	0.850	
Resistor, Composition	10	0.021	0.210	
Capacitor, Ceramic	5	0.005	0.025	
Diodes	6	0.300	1.800	
Capacitors, Tantalum	6	0.030	0.180	
Diodes, Zener	4	0.600	2.400	

TABLE 2-3. FAILURE RATES FOR S-BAND CHIP VARACTOR PARAMP SYSTEM (cont)

Assembly/Unit/Part	Qty	Part Failure Rate (fpMh)	Total Unit Failure Rate (fpMh)	Remarks
<u>GDO Power Supply</u>	<u>1</u>		<u>5.166</u>	
Transformer	1	0.300	0.300	
Diodes	4	0.300	1.200	
Capacitor, Tantalum	4	0.030	0.120	
Linear IC	2	0.400	0.800	
Resistor, Wirewound	2	0.300	0.600	
Resistors, Composition	6	0.021	0.126	
Resistors, Variable	2	1.000	2.000	
Capacitors, Ceramic	4	0.005	0.020	

NOTES:

1. Equated to 1 percent of power ferrite (217A) based on field/service use-experience with AIL designs of a higher degree of complexity under similar environmental conditions (low temperature/power applications).
2. Based on RADC Reliability Notebook, RADC-TR-67-108; Section XI, Group VIII (Varactor and Step-Recovery Diodes).



III. MEASURED PERFORMANCE

A. GENERAL

The RF components of the system were assembled about midway through the program (February 1974) to evaluate performance with a room temperature first stage. The results of these tests are given in Section A. The results of the tests on the final packaged system, with the first stage cooled to -20°C are presented in Section B.

B. BREADBOARD SYSTEM

The Model A471 breadboard system microwave components were assembled and measured as a two-stage room temperature system during the February 1974 review meeting on the prototype development program. The tests were monitored by the NASA technical officer on this program. The summary of the measured performance is given in Table 3-1.

TABLE 3-1. MEASURED PERFORMANCE SUMMARY OF S-BAND
PARAMP MOUNT SYSTEM (ROOM TEMPERATURE STAGE 1)

Data Taken: February 14, 1974

A. System Performance

Center Frequency:	2265 MHz
Bandwidth (1 dB down):	145 MHz
1 dB Down Frequencies:	2185 and 2330 MHz
Gain (Port to Port):	31 dB
Input VSWR (Maximum Operating Over Band):	1.3
Compression Level (1 dB Down):	-47 dBm

TABLE 3-1. MEASURED PERFORMANCE SUMMARY OF S-BAND
PARAMP MOUNT SYSTEM (ROOM TEMPERATURE STAGE 1) (cont)

Noise Temperature:

	<u>At 26°C Ambient</u>	<u>Extrapolated Final System</u>
2190 MHz	37.4 K	29.5 K
2210 MHz	37.9 K	29.9 K
2230 MHz	37.1 K	29.2 K
2250 MHz	37.8 K	29.8 K
2270 MHz	35.8 K	28.2 K
2290 MHz	36.5 K	28.8 K
2310 MHz	35.3 K	27.7 K

Average Over Band: 36.8 K

Calculated average input noise
temperature with plate wave-
guide coax transition and first
stage cooled based on these
measurements:

29.0 K

B. Single Stage Measured Performance

	<u>Stage 1</u>	<u>Stage 2</u>
Gain:	15 dB	15 dB
Center Frequency:	2265 MHz	2265 MHz
Lower 1 dB Point:	2.190 GHz	2.340 GHz
Upper 1 dB Point:	2.190 GHz	2.340 GHz
Response Shape:	Monotonic double tuned	
Bias:	-2.6 V at 1 μ A	2.4 V at 0 μ A
Pump Frequency - GHz:	50.75 GHz	51 GHz
Pump Power	10 mW	16 mW

Figure 3-1A shows the two-stage pass-band taken during the February review meeting demonstration. The 136-MHz, 1-dB down bandwidth more than meets the 100-MHz, 1-dB down, minimum bandwidth requirement. The noise temperature data measured during the review meeting is given in Table 3-1 and is plotted in Figure 3-1B. The average noise temperature is 36.8 K for seven frequencies measured across the band. The equivalent average final system noise temperature was calculated to be 29 K based on a first stage stabilized at -20°C and a second stage stabilized at $+50^{\circ}\text{C}$. This is less than the 30 K maximum noise temperature specification. This has been borne out by subsequent measurements on the final system. Since to-date the prototype system has not been fully tested in the final cooled configuration, the 30 K noise temperature can only be taken as a design goal with 35 K as a firm specification. This is because changes in cooled circulator characteristics, and an additional length of input waveguide to mate with the input RF switch may slightly increase the input noise temperature.

The first stage circulator was adjusted for optimum performance at -20°C . Performance at room temperature will be possible by readjustment of the pump and bias levels of the paramp and GDO in case of failure of the first-stage thermoelectric module. Operation would be normal except the input noise temperature would increase about 6 K.

Figure 3-1C shows the measured active and inactive input VSWR across the band. This is less than the 1.5 to 1 required VSWR. Figure 3-2 gives the amplifier saturation characteristic. The measured 1-dB compression point is -47.4 dBm which is below the -50 dBm required. A photograph of the two-stage system RF components assembled for this test are shown in Figure 3-3.

C. MEASURED PERFORMANCE - PROTOTYPE SYSTEM

Final acceptance tests of the complete prototype system were performed at AIL during October and November 1974 using NASA approved "Acceptance Test Procedure" No. 376807. The tests were monitored by the NASA technical officer, DCAS, and Quality Assurance at AIL. Results of the tests as compared with the specifications are given in Table 3-2. As can be seen, the system met or exceeded all the electrical performance requirements. The only exception was that the gain variation with change in ambient temperature slightly exceeded specifications below 10°C . This problem can be readily solved in production units by using higher-power heater elements in the GDO and second-stage stabilizing circuits. The following figures show the major measured performance characteristics as plotted from the test data.

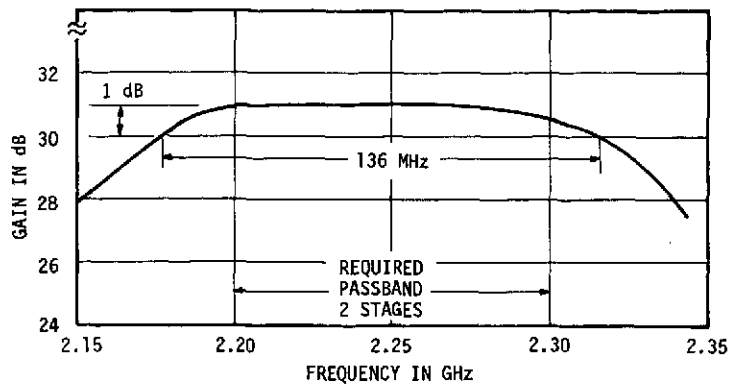
<u>Figure No.</u>	<u>Parameters Plotted</u>
3-4	Gain-Bandwidth Characteristics
3-5	Noise Temperature Versus Frequency
3-6	Input-Output VSWR Versus Frequency
3-7	Dynamic Range Versus Frequency
3-8	Phase Linearity Versus Frequency
3-9	Envelope Delay Distortion Versus Frequency
3-10	Gain Stability Versus Thermal Cycling

The plots are basically self-explanatory. It should be noted that the variation in the phase linearity versus frequency plot (Figure 3-8) near mid-band is possibly attributable to the waveguide-to-coax transition and coaxial bends since it also appears in the reference phase plot.

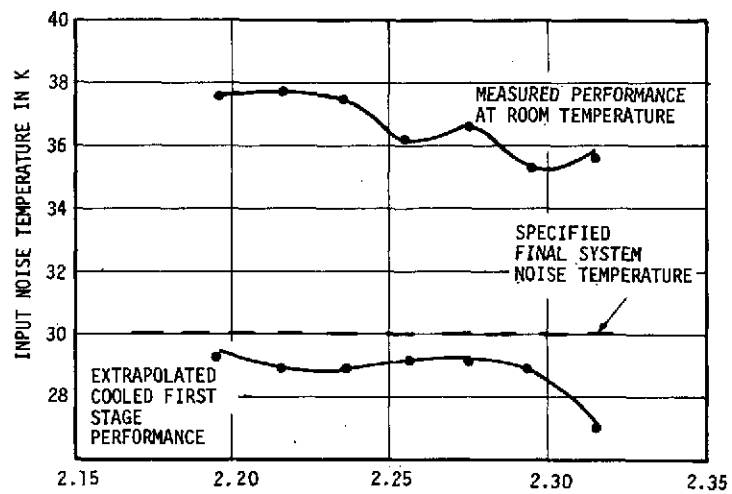
The level of pump frequency spurious output (Table 3-2) will meet specifications even though the specified level is below the range of sensitivity of available test equipment. This is based on the fact that the output filter has a pump-frequency rejection of better than 80 dB and the amplifier/circulator normally have rejection levels of 35 dB, giving a total rejection of greater than 115 dB. This is above the 100-dB minimum rejection required in the specifications.

TABLE 3-2. PERFORMANCE CHARACTERISTICS PROTOTYPE UNIT

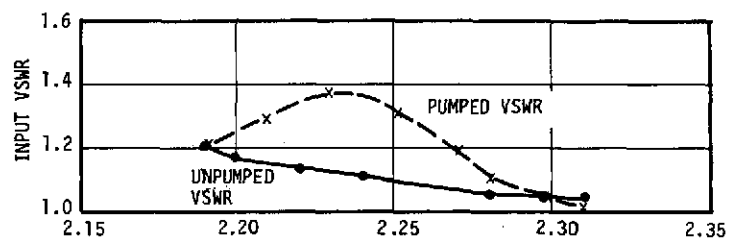
<u>Parameter</u>	<u>Specification</u>	<u>Measured Performance</u>
Frequency Range:	2.2 - 2.3 GHz	2.2 - 2.3 GHz
Bandwidth 1 dB down:	100 MHz min, 150 MHz max.	134 MHz
Gain:	30 dB min.	30 dB
Gain Ripple:	0.5 dB max. over bandpass	0.25 dB
	1.0 dB peak-to-peak at band edges	0.25 dB
Gain Compression (1 dB point)	-50 dBm min.	-46.5 dBm
Noise Temperature:		
2210 to 2290 MHz	29.2 K max.	30 K max.
2200 to 2300 MHz	35 K max.	32.5 K max.
Phase Linearity:		
2215 to 2285 MHz	±2 degrees	±1.5 degrees
2200 to 2215 and 2285 to 2300 MHz	±5 degrees	±1.5 degrees -2.0 degrees
Envelope Delay Distortion	5 ns	1.4 ns
Input VSWR	1.50	1.45
Output VSWR	1.50	1.30
Intermodulation Products (below input) (two -65 dBm input signals)	50 dB	51 dB
Gain Stability (8 hrs, midband)	±0.5 dB	+0.06 dB -0.08 dB
Phase Stability (12 hrs, midband)	±5 degrees	+0.6 -3.5 degrees
Gain Stability over -15 to +50°C Ambient at Midband		
Gain:	±1 dB	+0 -2 dB
Tilt (peak-to-peak):	1 dB	1.5 dB
Primary Power	115 Vac	115 Vac
Approximate Weight	No spec	LNA: 55 lbs RCPS: 70 lbs



A. MEASURED 2-STAGE PASSBAND



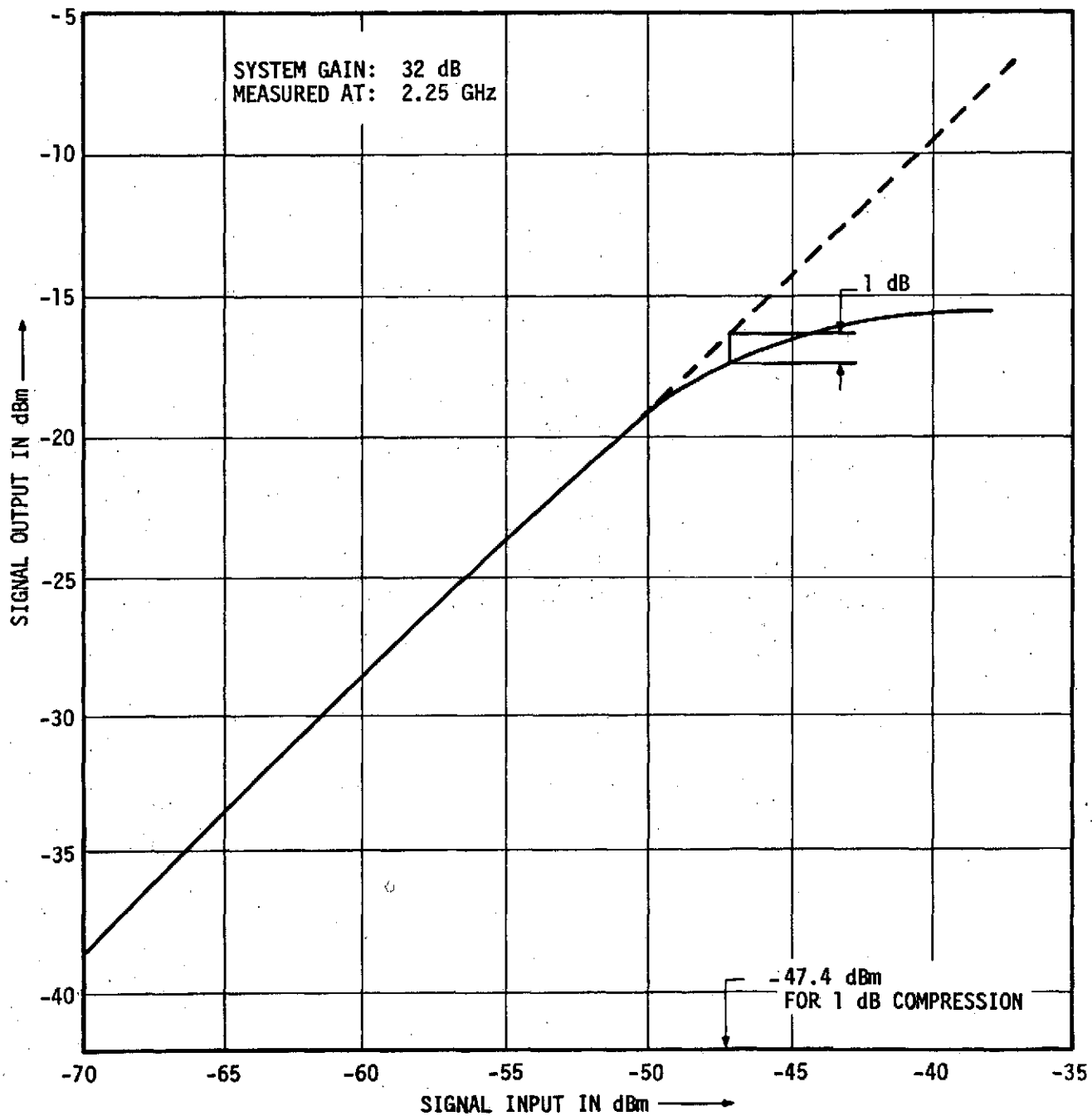
B. MEASURED NOISE TEMPERATURE VERSUS FREQUENCY



C. MEASURED INPUT VSWR VERSUS FREQUENCY

4-1923

Figure 3-1. Measured Breadboard Room Temperature Performance



4-1924

Figure 3-2. Measured Breadboard System Saturation Characteristics

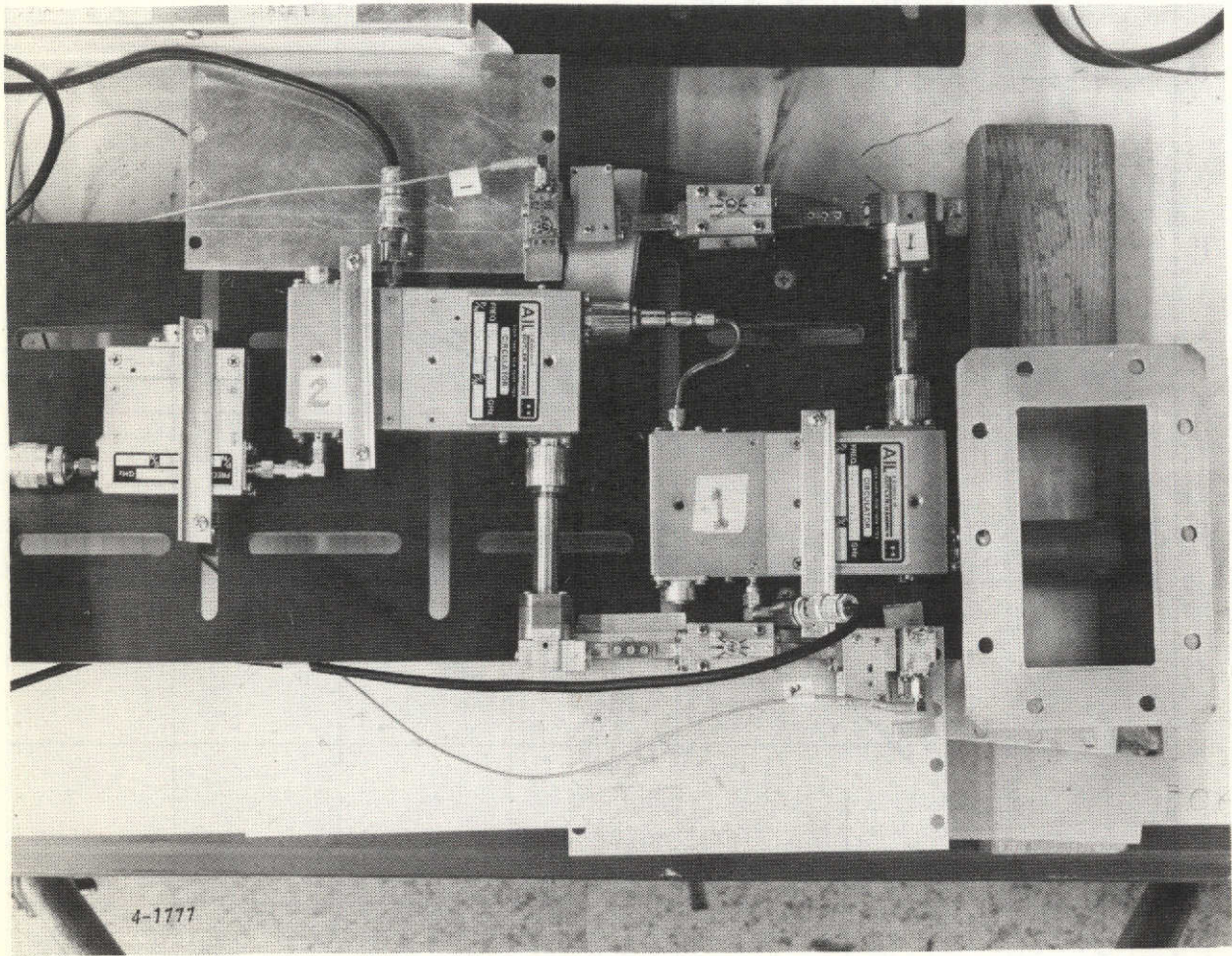


Figure 3-3. Prototype Components for S-Band Chip Varactor System - Breadboard Tests

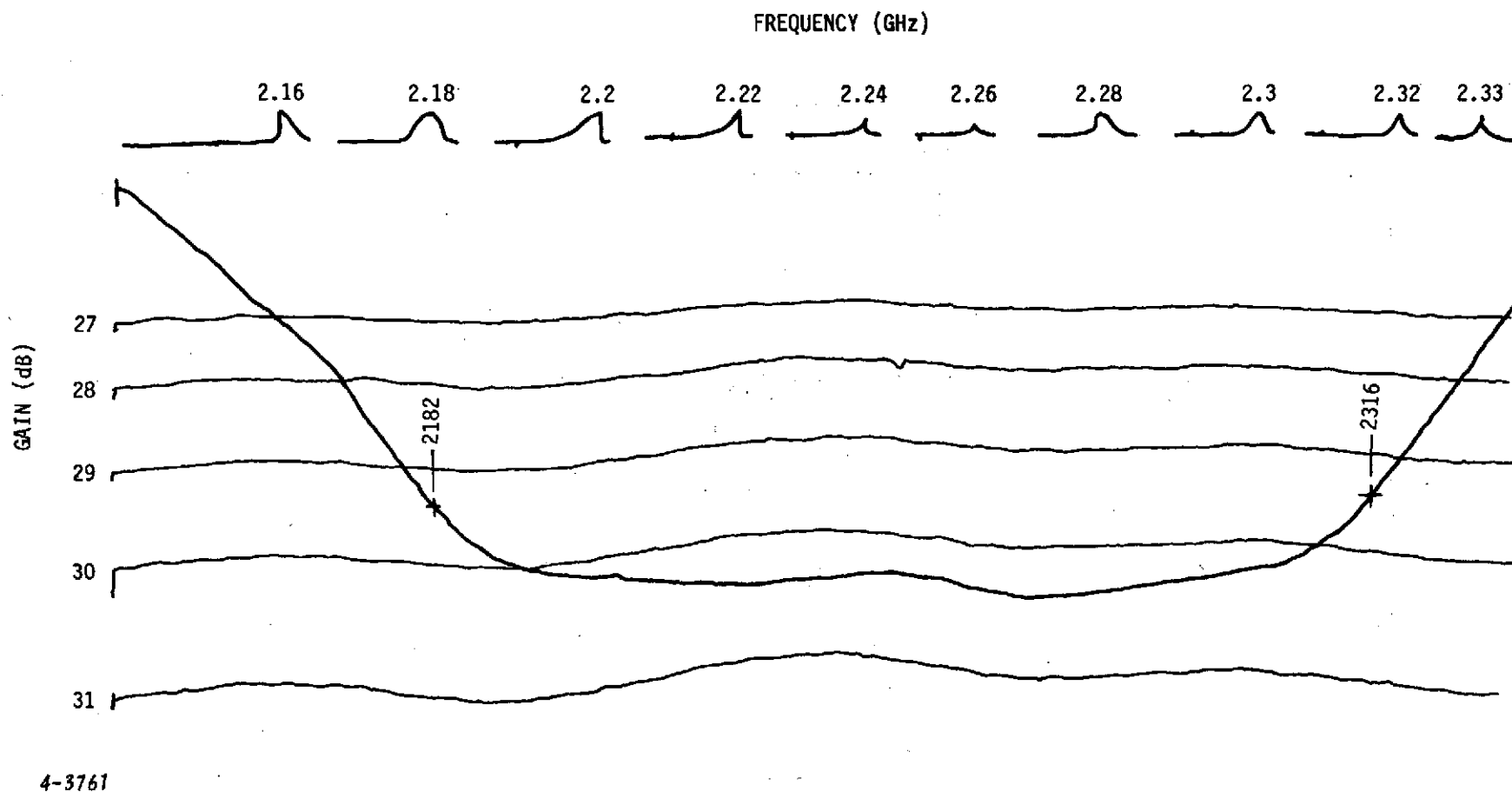


Figure 3-4. Gain-Bandwidth Characteristics

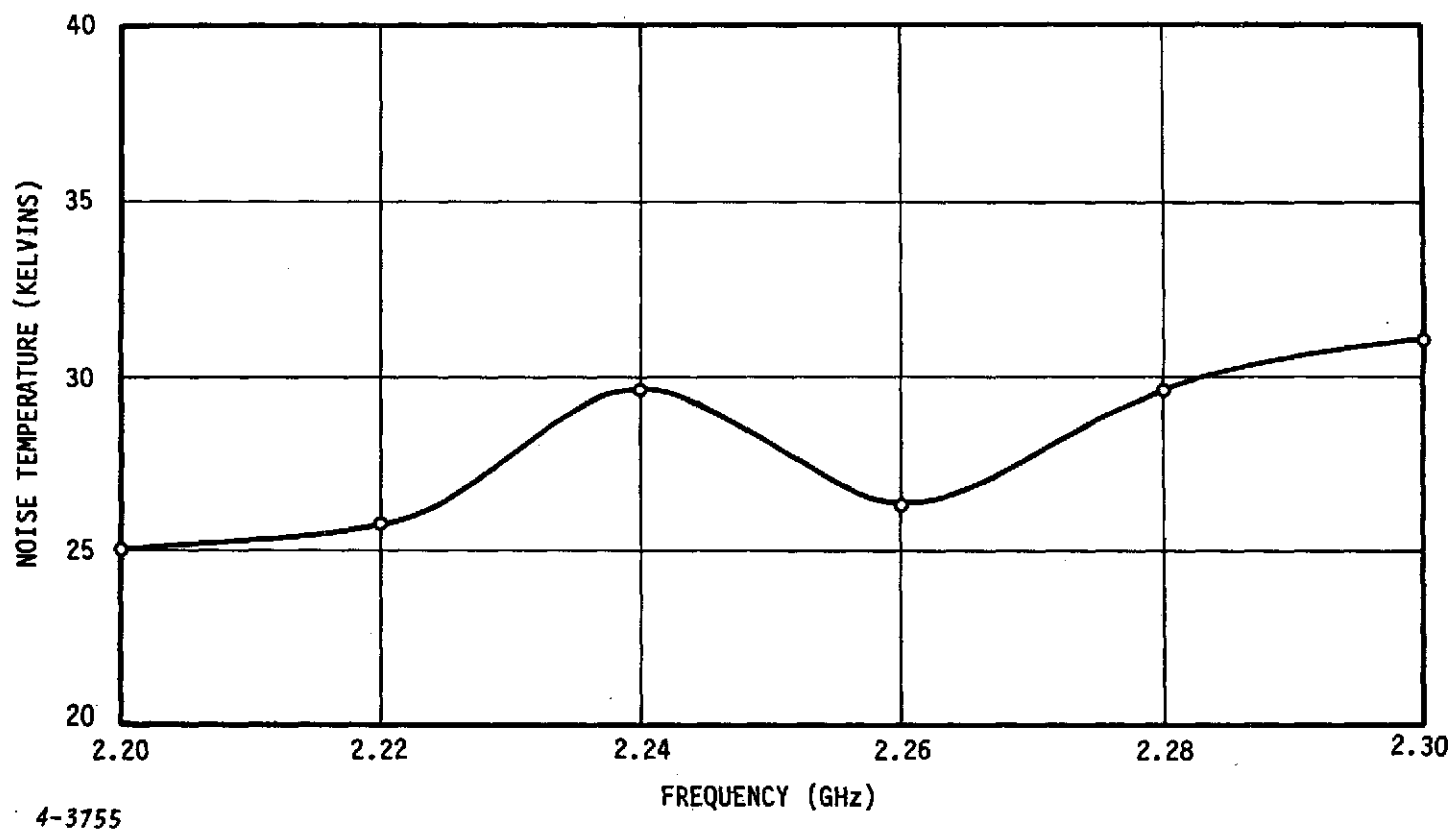


Figure 3-5. Noise Temperature Versus Frequency

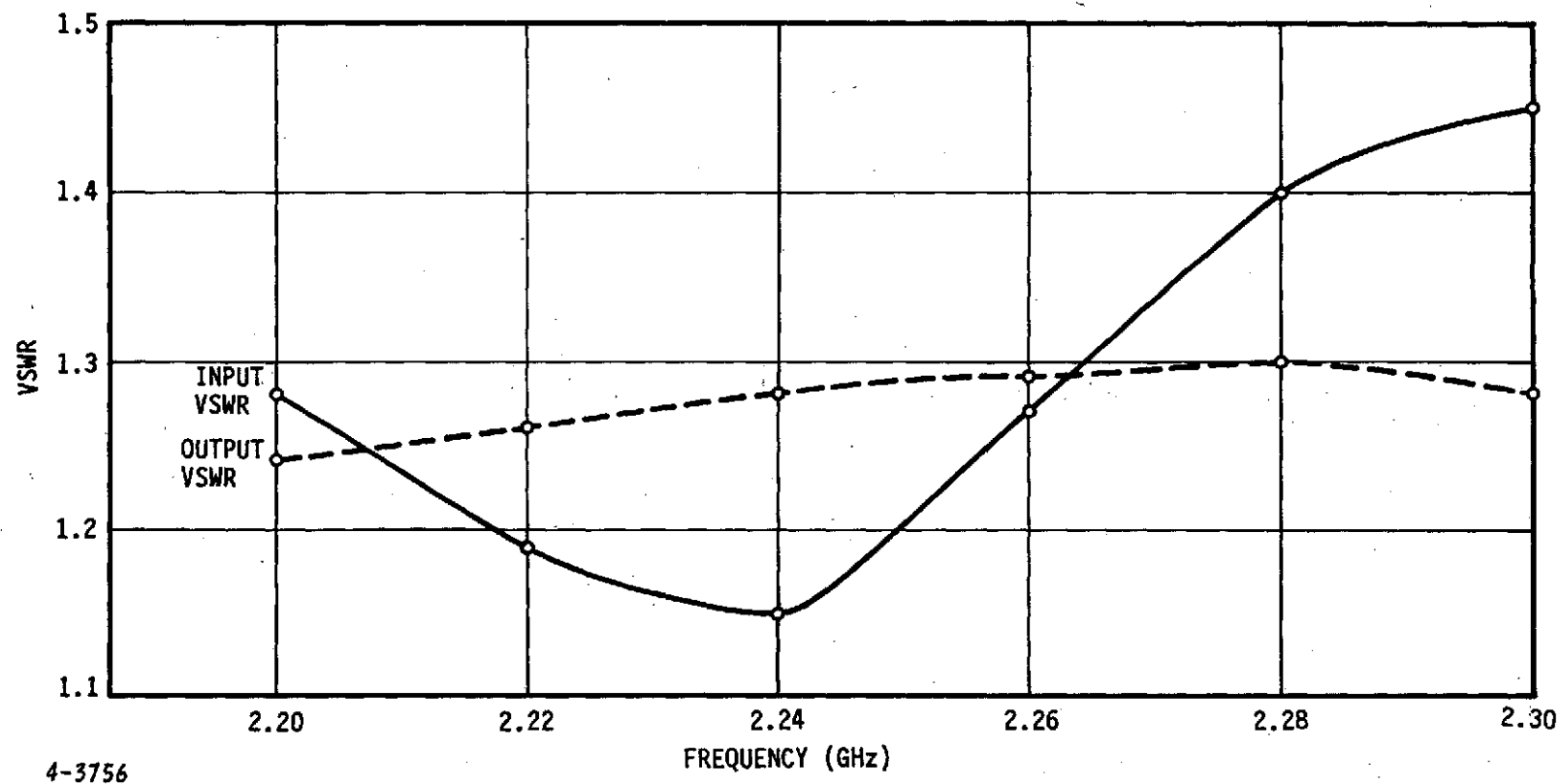


Figure 3-6. Input-Output VSWR Versus Frequency

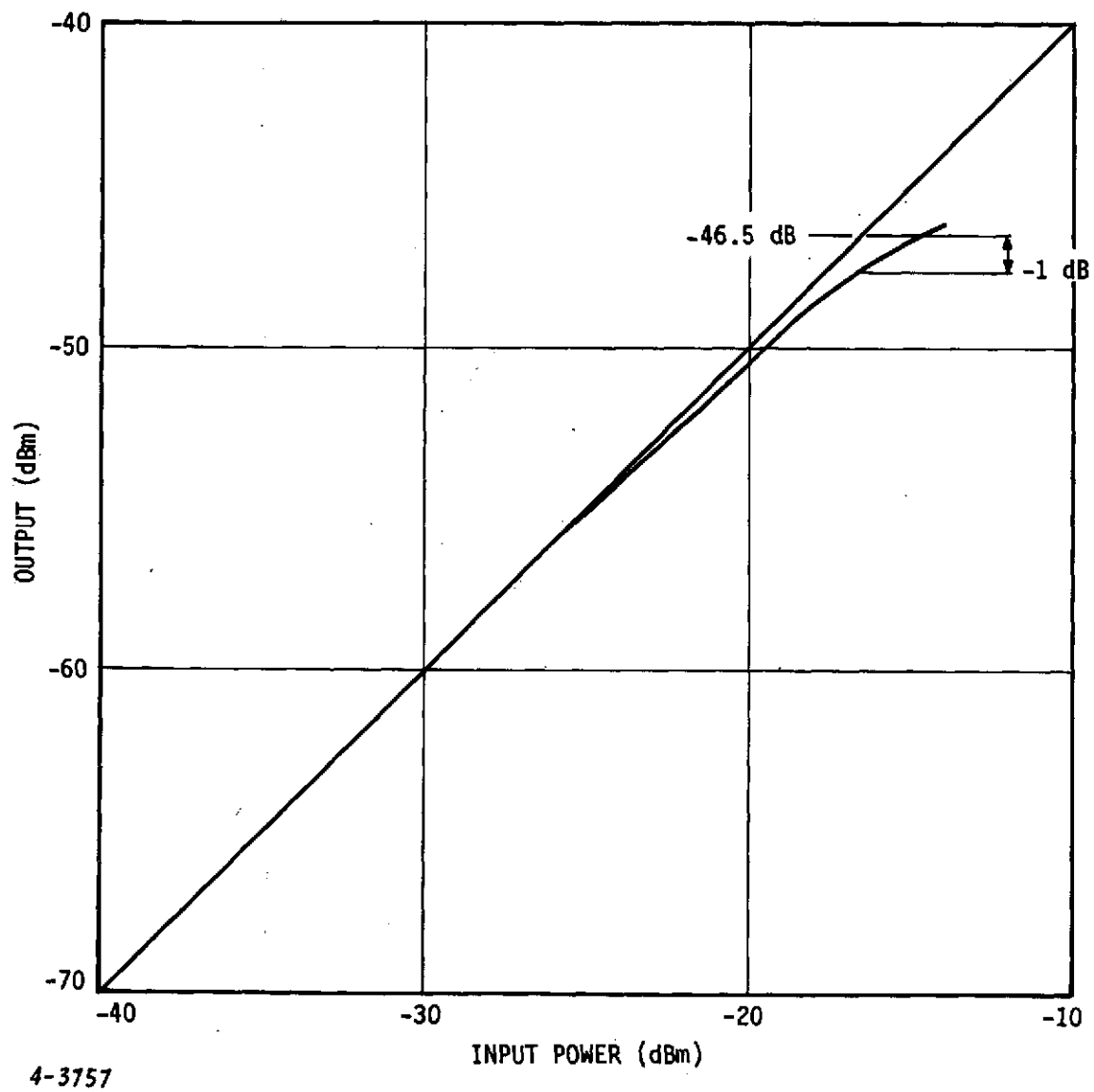


Figure 3-7. Dynamic Range Versus Frequency

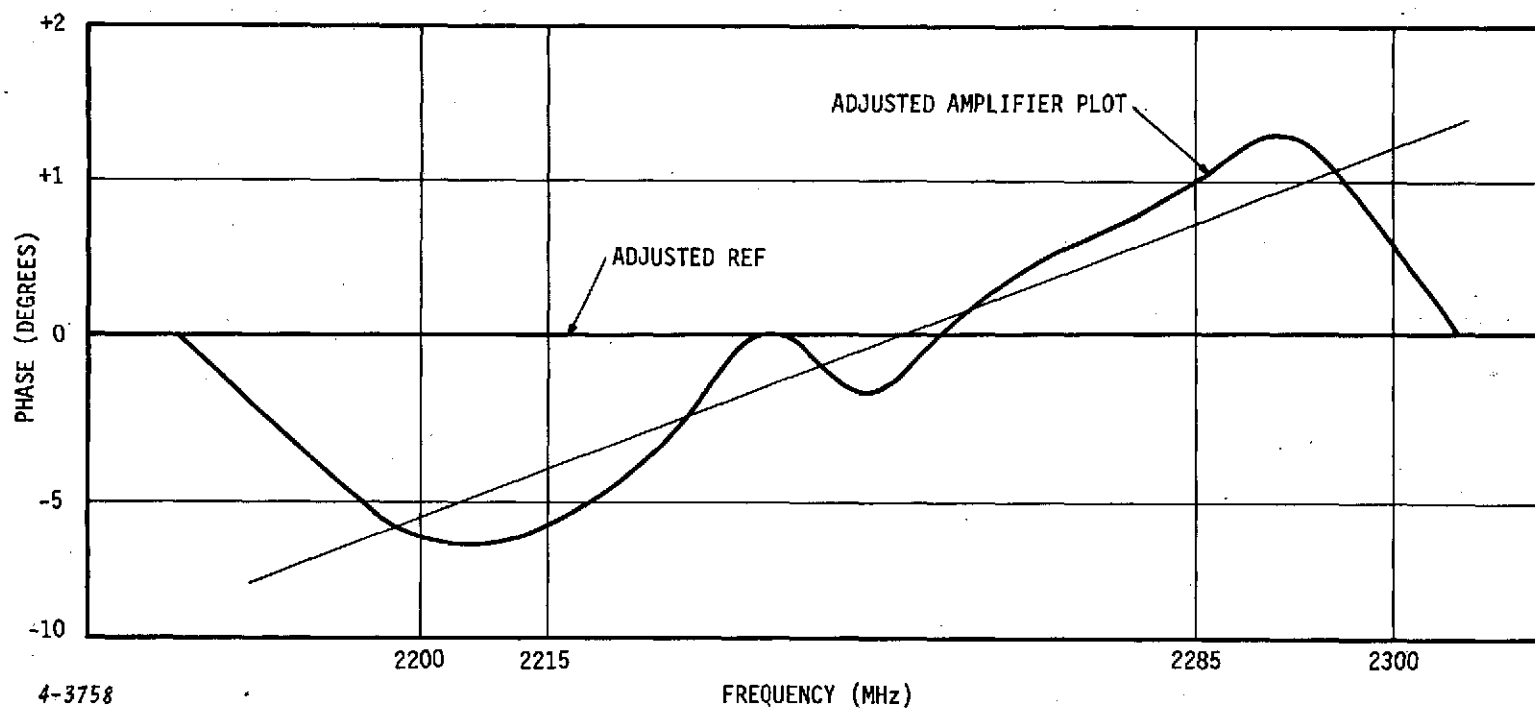
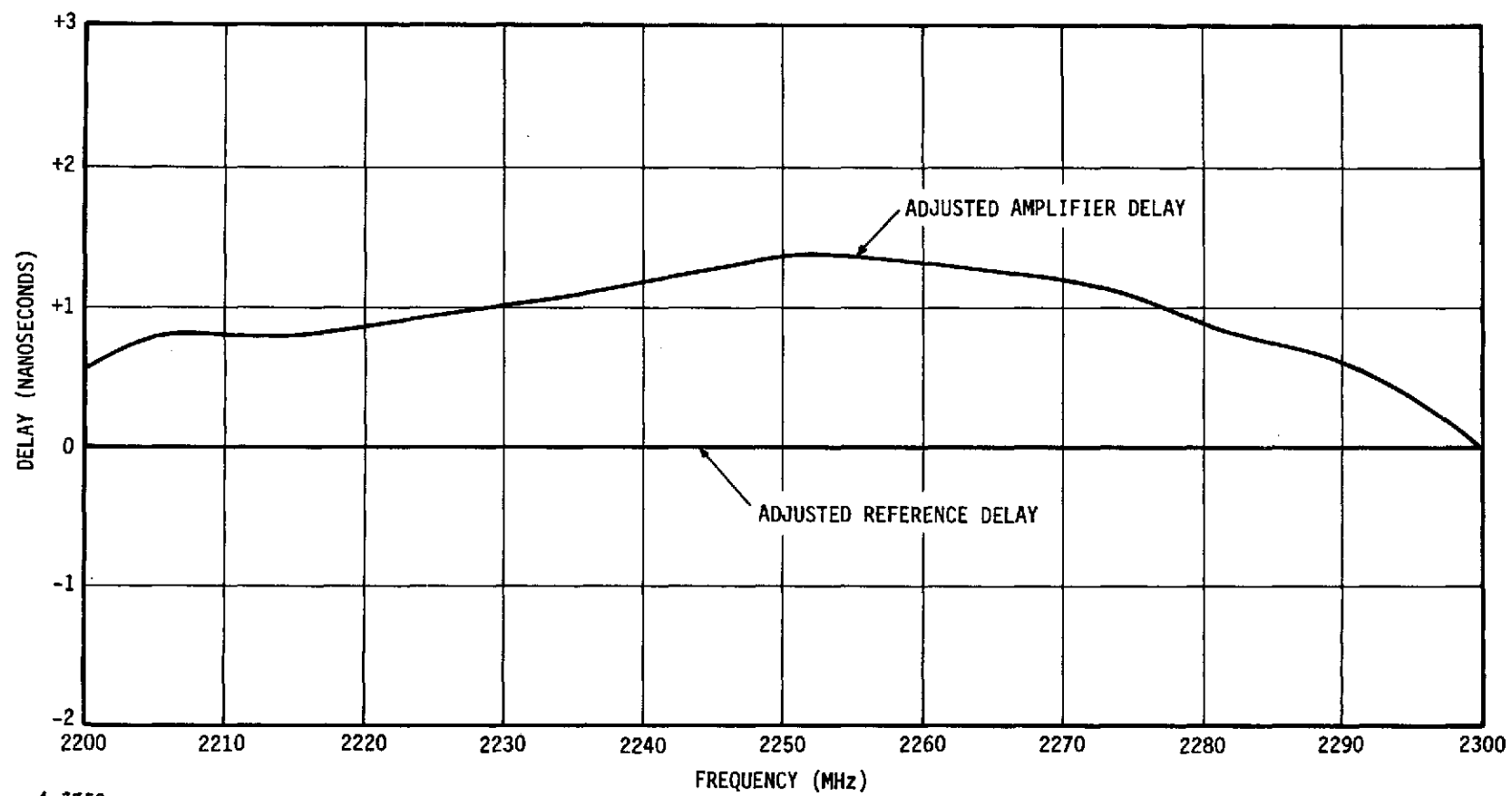


Figure 3-8. Phase Linearity Versus Frequency



4-3759

Figure 3-9. Envelope Delay Distortion Versus Frequency

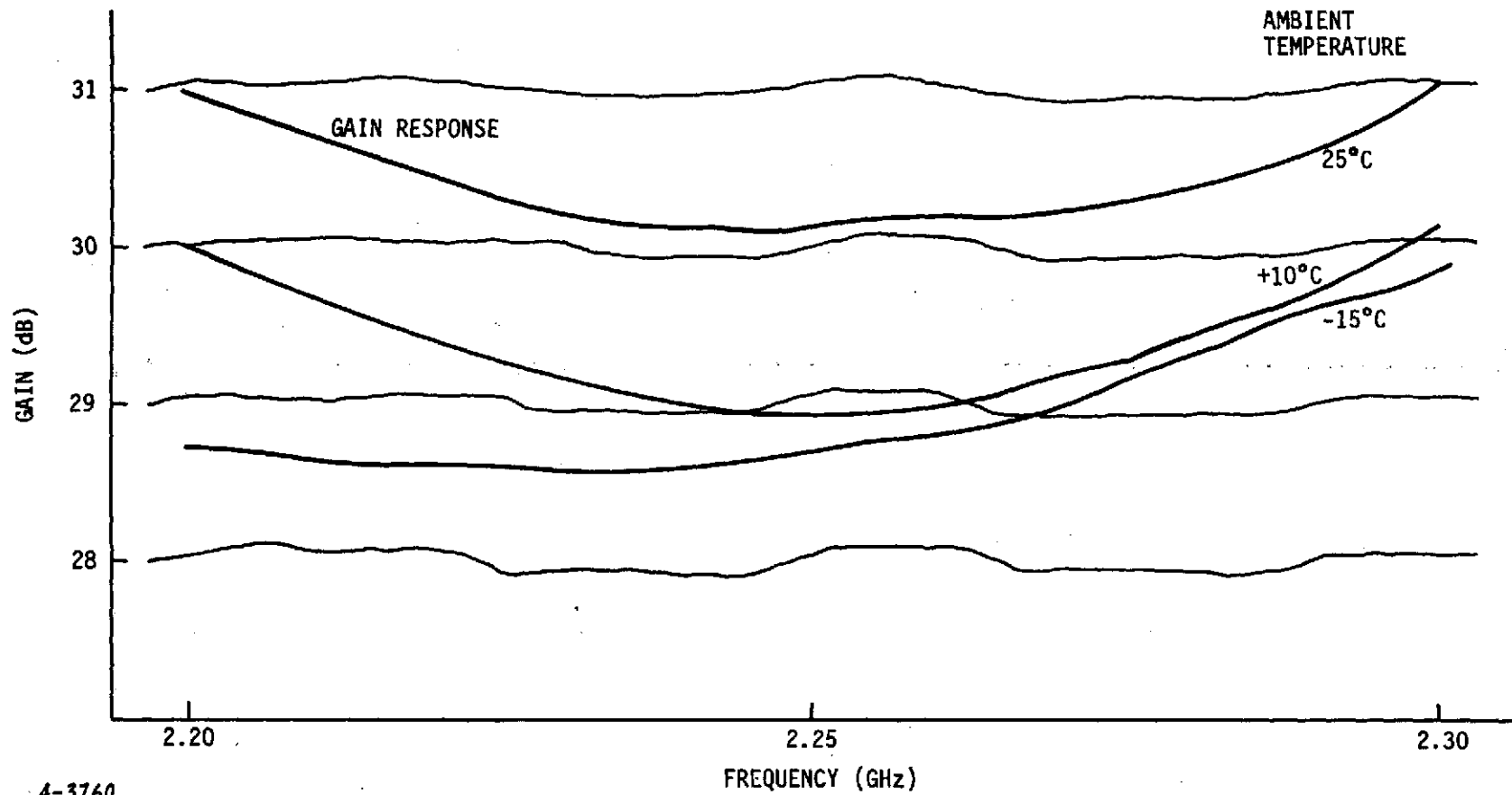


Figure 3-10. Gain Stability Under Thermal Cycling



IV. NEW TECHNOLOGY DEVELOPMENTS

No new technology was developed on this program.



V. CONCLUSIONS AND RECOMMENDATIONS

A. CONCLUSIONS

The S-Band Paramp System has successfully met all the major technical requirements of the program. The design is such as to allow transition to the production phase with a minimum of further engineering effort. The system represents a significant advance in low-noise amplifier technology in the following areas:

- Reduced Size, Weight and Power Consumption - Figure 5-1 shows a comparison of size to an equivalent cryogenic system. The reduction in size can readily be seen. The unit also requires less than one-third the power of a cryogenic system
- Solid-State Reliability - The unit has no moving mechanical parts, such as compressors, cross-heads, pumps, etc., which require periodic maintenance and have limited life. The only exceptions are four simple blowers which can readily be replaced in the event of failure and are of the sealed-bearing type requiring no maintenance
- Standby Performance in the Event of First Stage Cooler Failure - Unlike cryogenic systems, the system can be operated in the event of failure of the first-stage peltier cooler with slightly degraded noise temperature (30 to 37 K), increased input VSWR, and slightly greater passband ripple
- Lower Initial Costs - Since no expensive cryogenic refrigerator is required, the system will have lower initial and long-term operating costs

B. RECOMMENDATIONS

During the developmental effort and system testing, several areas of potential improvement were noted. These would be included in future

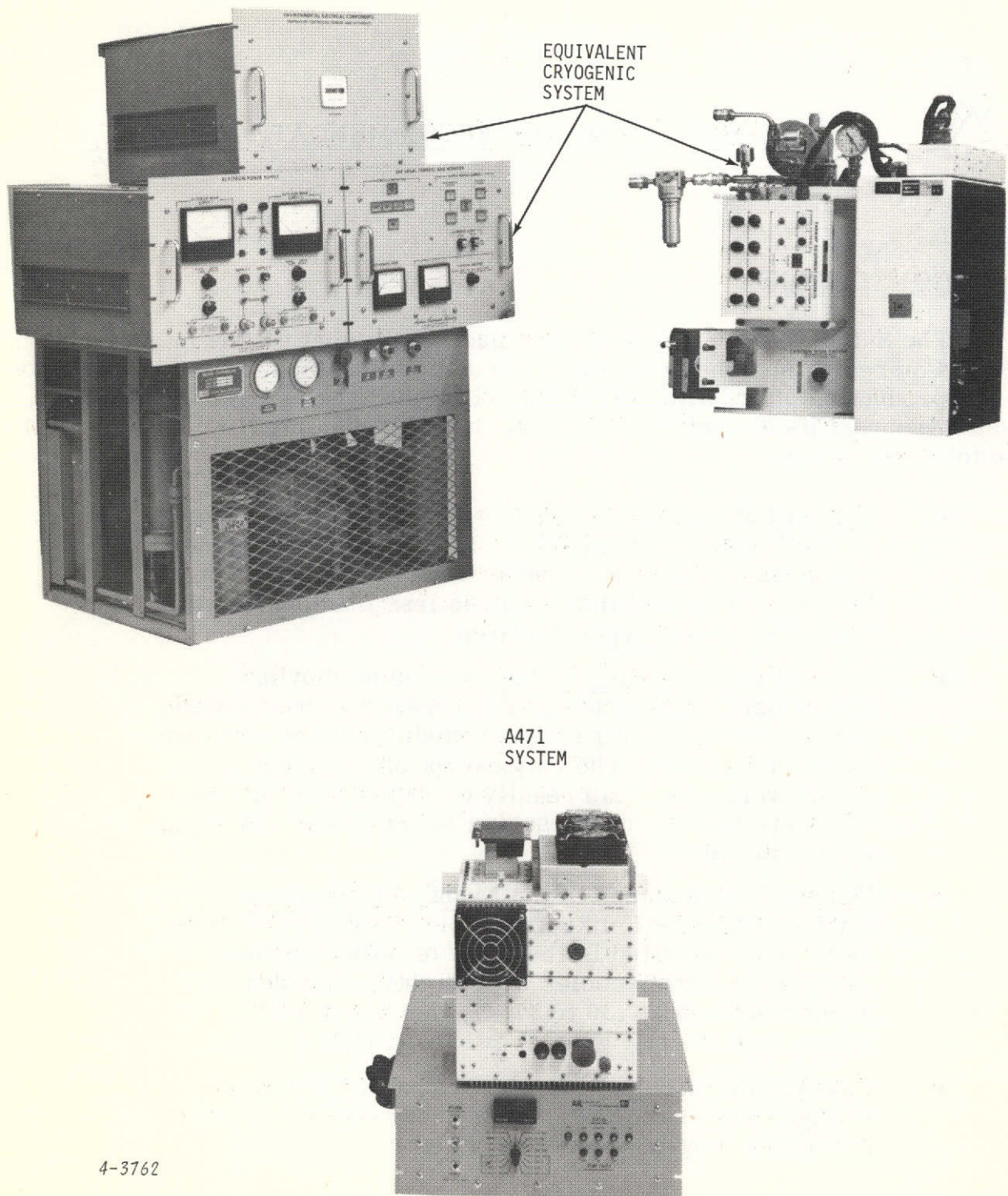


Figure 5-1. Comparison of the Prototype System with a Typical Equivalent Cryogenic Unit

production units to improve performance, maintainability, and reliability as indicated below:

1. LNA MODULE (Figures 5-2, 5-3, and 5-4)
 - Relocate Stage 1 GDO - This could be done by locating the stage 1 pump chain on the intercompartment bulk-heads as shown in Figure 5-3. This would allow use of a very short pump waveguide run. Changes in the pump waveguide ambient were found to be responsible for some thermal instabilities in the prototype model. By running the stage 1 pump line through a flexible insulating "pressure-tight" boot, the pump guide will tend to remain at a constant temperature over the ambient range, since the GDO end is stabilized at 50°C and the paramp end at -20°C. The waveguide would be made of stainless steel which is thermally isolating. This location and method of mounting would eliminate "tight" tolerances on location of the pump line relative to the GDO assembly, since the flexible boot could be made to accommodate up to $\pm 1/32$ misalignment. The shield over the GDO compartment would tend to minimize convection currents from changing thermal distributions along the pump chain.
 - Stabilize GDO's and Second-Stage at +60°C - This would eliminate the necessity of using thermoelectric modules and simplify the temperature controller circuits. In addition, it would reduce "breathing" of the response due to "crossover" between thermoelectric and heater cycles. This would be possible due to recent improvement in the GDO which would allow satisfactory operation to 60°C.

The revised packaging arrangement will greatly improve field maintainability since GDO replacement and adjustment is greatly simplified. In addition, installation and removal of the lower drawer does not involve mating of assemblies which require close tolerances in their location relative to each other.

- Desiccator - A desiccator could be added to absorb moisture in the first-stage compartment to eliminate the need for a continuous supply of dry nitrogen. Every 3 months, the desiccator cartridge would be replaced. This is presently being investigated further on other AIL programs.

- Mount Entire Second Stage on One Temperature Stabilized Plate (Figure 5-4) - The second stage GDO paramp chain components would be mounted on a common thermally isolated plate stabilized at 60°C. This would give much greater room in the lower compartment. In addition, this would improve maintainability since the entire section can be removed as a unit.
- Printed Circuit Boards Mounted on GDO and Bias Regulators (Figure 5-4) - Printed circuit boards mounted on the voltage regulator pins would make a more compact reliable arrangement than the terminal boards used in the prototype. The latter were used in the prototype to facilitate adjustments and design changes.
- Filter Box - All wiring coming into the LNA enclosure would be properly bypassed by use of a shielded filter box as shown in Figure 5-4. All gaskets would be made of conductive materials to eliminate potential EMI problems.
- Larger Lower Access Panel (Figure 5-2) - This would facilitate adjustments of the GDO frequencies and allow more ready access to interstage connections.
- High Power Darlington Heater Driver Transistors - The use of high-power "Darlington" transistors would reduce the number of discrete components in the temperature controller circuit, therefore, improving reliability.
- Revised Lower Drawer Gasketing - Since the lower compartment would probably be pressurized in the production units, an "L-shaped" frame as shown in Figure 5-2 would probably be used. This would make a simpler, more pressure-tight structure than the shelf arrangement used in the prototype. This construction is possible if 4 to 6 bolts can be employed on the bottom side of the unit to fasten the lower compartment assembly to the main frame.

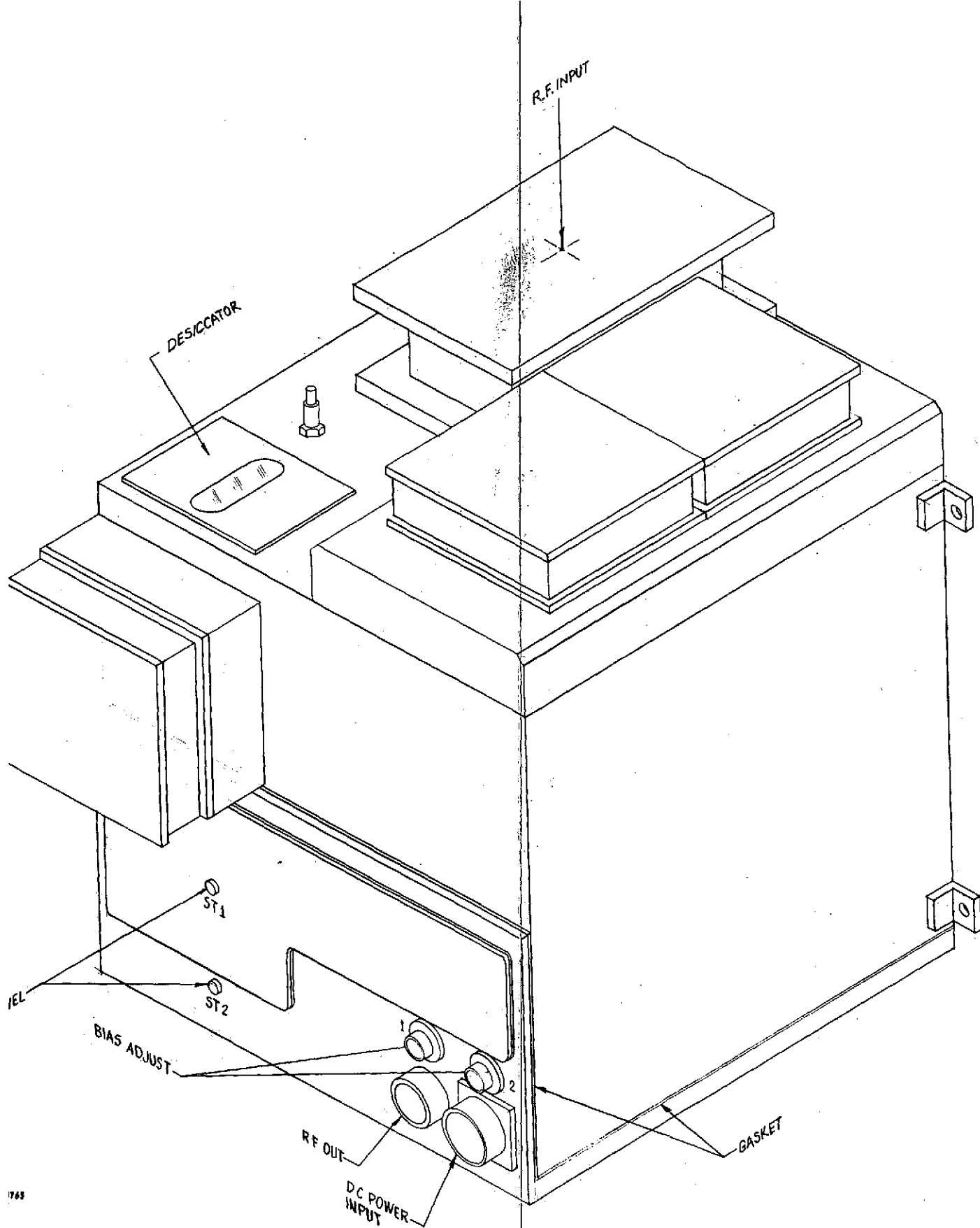


Figure 5-2. Proposed Production Model - LNA Configuration

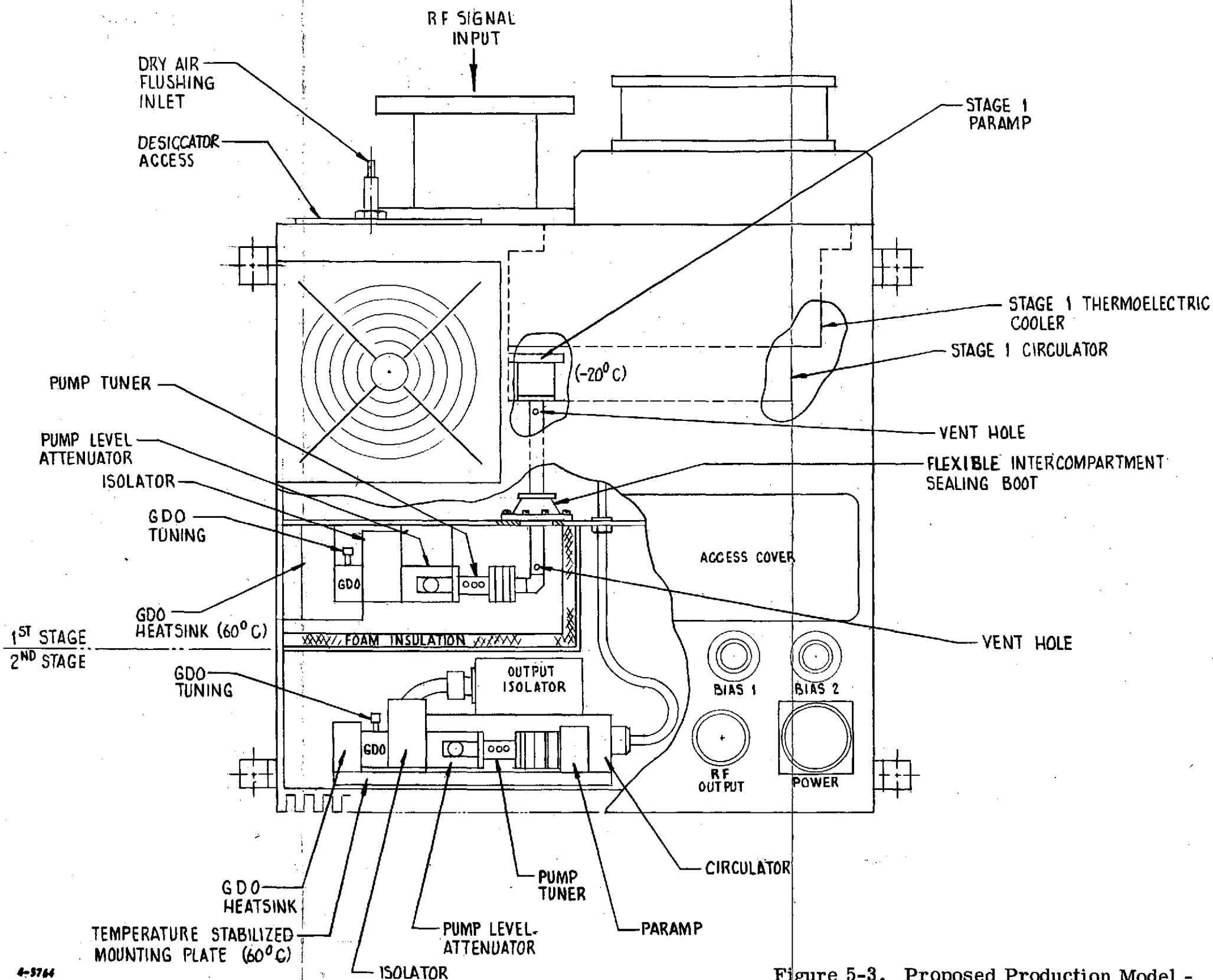


Figure 5-3. Proposed Production Model - Front View

FOLDOUT FRAME 7

FOLDOUT FRAME

5-7/(5-8 blank) 2

2. REMOTE CONTROL POWER SUPPLY (RCPS)

The following changes in the RCPS unit would be incorporated in production units:

- Low-Voltage Thermoelectric (+3.6V 20A) Power Supply - This supply could be eliminated if the GDO's and second stages are heater stabilized.
- Printed Circuit Boards - For use in meter multiplier circuits to make a more compact reliable assembly.

All of these changes can be made with a minimum of engineering effort since the prototype unit is close to the production unit proposed in many basic aspects.

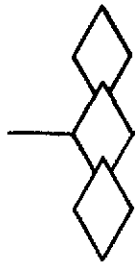


VI. REFERENCES

1. P. Penfield, Jr. and R. P. Rafuse, "Varactor Applications," MIT Press, Cambridge, Massachusetts, 1962.
2. J. R. Ashley and F. M. Polka, "Reduction of FM Noise in Microwave Diode Oscillators by Cavity and Injection Stabilization," 1971 GMTT International Microwave Symposium.



VII. APPENDIXES



APPENDIX A

COMPUTER MODEL OF PARAMETRIC AMPLIFIER CIRCUIT

Figure A-1 shows a three-port model for the pumped varactor. Port 1 is at the input frequency (f_1). Port 2 is at the idler or difference frequency ($f_2 = f_{\text{pump}} - f_1$). Port 3 is at the sum frequency ($f_3 = f_{\text{pump}} + f_1$). This model was derived by an extension of the two-port analysis given by Matthaei¹. The elements of the impedance matrix are given as follows:

$$Z_{11} = R_{s1} + j(\omega_1 L_s - X_{11}); Z_{12} = -jX_{12}; Z_{13} = jX_{13}$$

$$Z_{21} = jX_{21}; Z_{22} = R_{s2} + j(X_{22} - \omega_2 L_s); Z_{23} = -jX_{23}$$

$$Z_{31} = jX_{31}; Z_{32} = jX_{32}; Z_{33} = R_{s3} + j(\omega_3 L_s - X_{33})$$

where $\omega_1 = 2\pi f_1$; $\omega_2 = 2\pi f_2$; $\omega_3 = 2\pi f_3$

and L_s = series lead inductance

For generality different series resistances have been assumed at each frequency. Also

$$X_{11} = \frac{1 + \frac{C_2}{C_0}}{\omega_1 C_0 \left[1 + \frac{C_2}{C_0} - 2 \left(\frac{C_1}{C_0} \right)^2 \right]}$$

¹ G. L. Matthaei, "A Study of the Optimum Design of Wide Band Parametric Amplifiers and Up-Converters," IRE Trans on Microwave Theory and Techniques. January 1961.

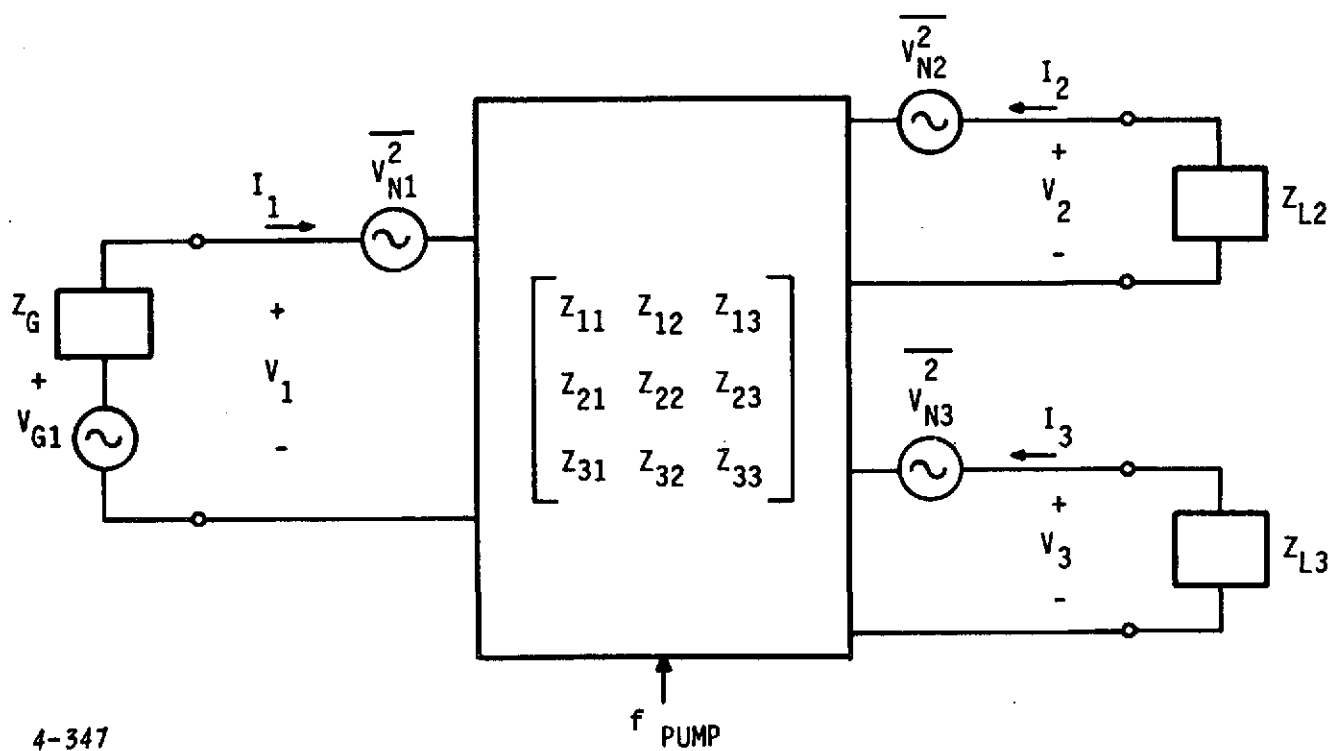


Figure A-1. Three-Port Model of Pumped Varactor

$$X_{12} = \frac{\frac{C_1}{C_0}}{\omega_2 C_0 \left[1 + \frac{C_2}{C_0} - 2 \left(\frac{C_1}{C_0} \right)^2 \right]}$$

$$X_{13} = \frac{\omega_2}{\omega_3} X_{12}$$

$$X_{21} = \frac{\omega_2}{\omega_1} X_{12}$$

$$X_{22} = \frac{1 - \left(\frac{C_1}{C_0} \right)^2}{\omega_2 C_0 \left[1 - \frac{C_2}{C_0} \right] \left[1 + \frac{C_2}{C_0} - 2 \left(\frac{C_1}{C_0} \right)^2 \right]}$$

$$X_{23} = \frac{\left(\frac{C_1}{C_0} \right)^2 - \frac{C_2}{C_0}}{\omega_3 C_0 \left[1 - \frac{C_2}{C_0} \right] \left[1 + \frac{C_2}{C_0} - 2 \left(\frac{C_1}{C_0} \right)^2 \right]}$$

$$X_{31} = X_{21}$$

$$X_{32} = \frac{\omega_3}{\omega_2} X_{23}$$

$$X_{33} = \frac{\omega_2}{\omega_3} X_{22}$$

We must now solve the following set of simultaneous equations

$$\begin{bmatrix} V_1 \\ V_2^* \\ V_3 \end{bmatrix} = \begin{bmatrix} Z_{11} & Z_{12} & Z_{13} \\ Z_{21} & Z_{22} & Z_{23} \\ Z_{31} & Z_{32} & Z_{33} \end{bmatrix} \begin{bmatrix} I_1 \\ I_2^* \\ I_3 \end{bmatrix}$$

subject to the assumed lossless load impedances Z_{L2} and Z_{L3} . (Any loss can be absorbed in series resistances R_{S2} and R_{S3} , respectively.) Also, the signal circuit source impedance Z_G is assumed due to a lossless Z-port network (which includes any multiple tuning) terminated in an ideal circulator (not shown). The gain, noise temperature, and input impedance of the device may be determined as follows.

The power gain is given by the following expression:

$$G = \left| \frac{Z_G - Z_{IN}^*}{Z_G + Z_{IN}} \right|^2$$

The asterisk here and in the above matrix denotes complex conjugate. The input impedance is

$$Z_{IN} = \frac{V_1}{I_1}$$

The noise temperature is found as follows:

$$T_e = \frac{N_0}{G k B}$$

where

T_e = effective input noise temperature

G = power gain

k = Boltzmann's constant

B = bandwidth

N_0 = noise power developed in Z_G due to internal noise sources

$$N_0 = \left[\frac{1}{V_{N1}^2} \left| \frac{I_1}{V_{G1}} \right|^2 + \frac{1}{V_{N2}^2} \left| \frac{I_1}{V_{G2}^*} \right|^2 + \frac{1}{V_{N3}^2} \left| \frac{I_1}{V_{G3}} \right|^2 \right] \text{Re} [Z_G]$$

where

$$\frac{1}{V_{N1}^2} = 4 k B T_D R_{s1}$$

$$\frac{1}{V_{N2}^2} = 4 k B T_D R_{s2}$$

$$\frac{1}{V_{N3}^2} = 4 k B T_D R_{s3}$$

and T_D is the physical temperature of the diode. Ratios I_1/V_{G1} , I_1/V_{G2} , and I_1/V_{G3} are evaluated by substituting generator voltages V_{G1} , V_{G2} , and V_{G3} in place of the corresponding noise source voltages. Solution for T_e and Z_{IN} in terms of the diode parameters gives:

$$T_e = T_D \left[1 - \frac{1}{G} \right] \left[\frac{R_{s1}}{-R_e(Z_{IN})} \right] \left[1 + \frac{R_{s2}}{R_{s1}} \left| \frac{\omega_2}{\omega_1} \right|^2 + \frac{R_{s3}}{R_{s1}} \left| \frac{\omega_3}{\omega_1} \right|^2 \right]$$

$$Z_{IN} = Z_{11} + \frac{jX_{21}(\omega_3 - \omega_2)}{\omega_1}$$

~~UNREPRODUCIBLE PAGE BLANK NOT FILMED~~

where

$$\omega_1 = (Z_{22} + Z_{L2}^*) (Z_{33} + Z_{L3}) - X_{23} X_{32}$$

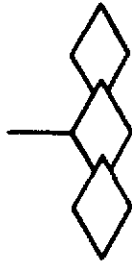
$$\omega_2 = -jX_{12} (Z_{33} + Z_{L3}) + X_{13} X_{32}$$

$$\omega_3 = -X_{13} (Z_{22} + Z_{L2}^*) - X_{12} X_{23}$$

The asterisk denotes complex conjugate.

A computer program to find the solution to these equations was developed by modeling the load impedances Z_{L2} and Z_{L3} to include varactor package capacitance and the dimensions of the waveguide mount. Similar modeling of the coaxial signal circuit was included. "Tuning up" of the parametric amplifier on the computer for symmetrical responses and the proper gain can be accomplished by proper choice of parameter values. The program is basically intended for the balanced parametric amplifier, where the signal circuit is geometrically isolated from the idler and sum circuits. Slight modifications are necessary for other types of mounts (single-ended, all waveguide, etc.).

~~PRECEDING PAGE INFORMATION DELETED~~



APPENDIX B

GAIN CHANGES AS A FUNCTION OF CIRCULATOR ISOLATION CHANGES

The active gain of the parametric amplifier depends critically on the interaction between the complex reflection coefficient looking into the amplifier port of the circulator and the inherent reflection coefficient of the amplifier. For an almost lossless circulator with high isolation, the net reflection coefficient (complex voltage gain) is approximately given by:

$$\Gamma = |\Gamma| e^{j\theta} = \frac{\Gamma_{\text{nom}}}{1 - \frac{\Gamma_{\text{nom}} e^{j\theta}}{L_i^{\frac{1}{2}}}} \quad (\text{B-1})$$

where

Γ_{nom} = nominal value of Γ for unity SWR of the circulator

L_i = nominal magnitude of port-to-port circulator isolation

θ = net phase difference between circulator and amplifier

$|\Gamma|$ = magnitude of $\Gamma = K^{\frac{1}{2}}$

θ = phase of Γ

Differentiating equation H-1 yields the fractional change:

$$\frac{\Delta\Gamma}{\Gamma} = \left[\frac{K}{L_i} \right]^{\frac{1}{2}} \left[\frac{1}{2} \frac{\Delta L_i}{L_i} - j\Delta\theta \right] e^{j(\theta+\theta)} \quad (\text{B-2})$$

From equation H-1, the general expression for fractional change of power gain K ($K = |\Gamma|^2$) is:

$$\frac{\Delta K}{K} = \frac{2\Delta|\Gamma|}{|\Gamma|} = \frac{\Delta\Gamma}{\Gamma} + \left(\frac{\Delta\Gamma}{\Gamma}\right)^* \quad (\text{B-3})$$

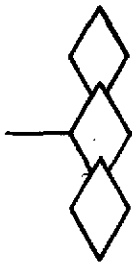
where the asterisk denotes complex conjugate.

Substitution of equation H-1 into equation H-3 yields:

$$\frac{\Delta K}{K} = - \left[\frac{K}{L_i} \right]^{\frac{1}{2}} \left[\left(\frac{\Delta L_i}{L_i} \right) \cos(\theta + \phi) + 2\Delta\phi \sin(\theta + \phi) \right] \quad (\text{B-4})$$

Dealing with a relatively narrow band situation, where θ and ϕ will not vary appreciably over the band, it is possible to operate with either $(\theta + \phi) \sim \pi/2$ or π , which would mitigate gain changes due to ΔL_i or $\Delta\phi$, respectively. Assuming the latter case, equation H-4 reduces to:

$$\frac{\Delta K}{K} \approx \left(\frac{K}{L_i} \right)^{\frac{1}{2}} \frac{\Delta L_i}{L_i}. \quad (\text{B-5})$$



APPENDIX C

NOISE TRANSFER ANALYSIS--SINGLE STAGE PARAMETRIC AMPLIFIER

1. INTRODUCTION

Since the noise of a pump source will cause a random fluctuation in instantaneous pump power, the varactor capacitance will fluctuate accordingly. Because of this it will be shown that the pump noise is downconverted into the signal frequency domain, thereby degrading the tangential sensitivity of the amplifier.

For normal operation, even with a noisy pump, this degradation is often negligible. However, it has been observed that when a strong interfering signal is present in close proximity of the received frequency, a severe degradation in tangential sensitivity occurred. In this case, the pump-derived noise side bands of the strong interfering signal increase the input noise level at the received frequency. This phenomenon will be explained, and an expression for the degradation of the tangential sensitivity as a function of the strength of the interfering signal will be derived.

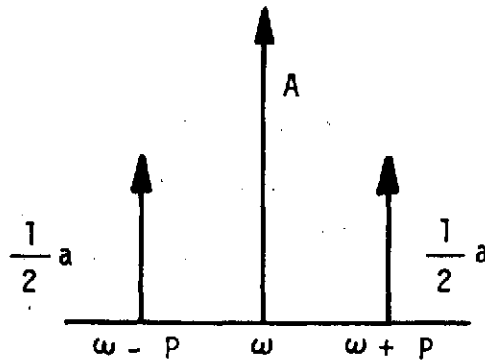
2. ANALYSIS

Consider an amplitude modulated signal,

$$A \left(1 + \frac{a}{A} \cos pt \right) \sin \omega t$$

where A and a denote peak amplitudes.

As is well known the frequency spectrum of this signal is given by Figure C -1.



3-1025

FIGURE C -1. FREQUENCY SPECTRUM OF AMPLITUDE MODULATED SIGNAL

Assuming for simplicity a 1-ohm impedance level, the total power in the side bands is given by $P_{sid} = a^2/4$, while the carrier power is $P = 1/2 A^2$. The total power of the modulated signal fluctuates according to $1/2 A^2 (1 + a/A \cos pt)^2$. For $a/A \ll 1$, this reduces to $\approx 1/2 A^2 (1 + 2 a/A \cos pt) = P (1 + \Delta P/P \cos pt)$, where $\Delta P/P$ equals $2 a/A$. As $a = 2\sqrt{P_{sid}}$ and $A = \sqrt{2P}$, it follows,

$$\frac{\Delta P}{P} = 4 \sqrt{\frac{P_{sid}}{2P}} \quad (C-1)$$

Equation C -1 gives a direct relation between the power fluctuation and the corresponding sideband power of an AM signal with small modulation depth. However, a phase-modulated signal also has sidebands, while exhibiting a constant signal power.

Consider now a carrier of power P , with two corresponding sidebands with a total sideband power P_s . Assume that P_s is split up into two parts σP_s and $(1 - \sigma) P_s$, ($\sigma \leq 1$) causing AM and PM, respectively; then the fluctuation of the signal power, according to equation C -1, can be expressed as:

$$\frac{\Delta P}{P} = 4 \sqrt{\frac{\sigma P_s}{2P}} \quad (C-2)$$

Pure AM or FM can only be obtained when there is a 100 percent correlation between the corresponding sidebands. They have to be of equal amplitude and must have a specific phase relation to make it either pure AM or pure FM.

When there is no correlation between the two sidebands, for example, when the sidebands consist of noise components with random phase and amplitude characteristics, we can assume that the average total sideband power will be equally distributed between AM and FM which means that in equation C-2, $\sigma = 1/2$.

When passing this spectrum through a nonlinear device, however, the nonlinearity will generally cause the sidebands of the output spectrum to be correlated to some degree.

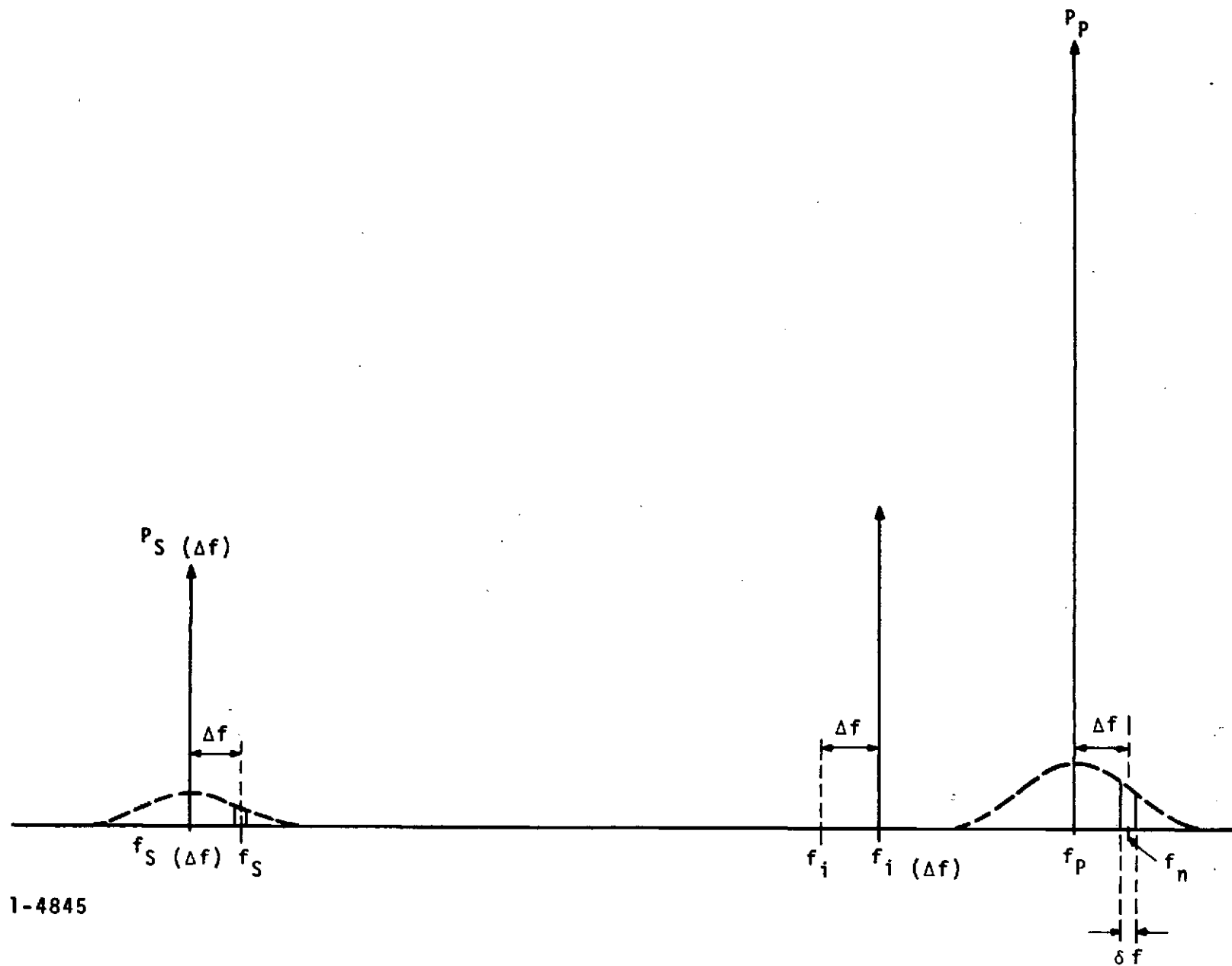
As an oscillator is basically a nonlinear device, it is to be expected that there will be some correlation between its noise sidebands ($\sigma \neq 1/2$).

The proper value of σ will be determined by the physical mechanism of frequency generation.

Assume a parametric amplifier with a pump source P_p (watts) at frequency f_p and tuned to a signal frequency f_s so that the idler frequency $f_i = f_p - f_s$. These frequencies are indicated on a spectral diagram Figure C-2. Also indicated is the noise spectrum of the pump source and a strong interfering signal $f_s(\Delta f) = f_s - \Delta f$ of power $P_s(\Delta f)$, and the corresponding idler frequency $f_i(\Delta f)$.

Consider a noise packet around the frequency $f_n = f_p + \Delta f$ of width δf and containing a power ΔP_n . The spectral noise power density is then $p(f) = \Delta P_n / \delta f$ watts/Hz.

As was explained above, this noisy power quantity with its corresponding sideband (ΔP_n at $f_p - \Delta f$) will cause amplitude as well as frequency modulation of the pump signal. Frequency variations of the pump signal cause corresponding frequency changes in the idler. If the bandwidth of the idler circuit is large, however, these frequency variations will not be noticed in the signal circuit.



1-4845

Figure C-2. Frequency Spectral Diagram

Thus, only the amplitude modulation of the pump is of interest.

The amplitude, ΔP , of the variation in instantaneous pump-power (noise around frequency FM) can be found from equation C-2. With $P_S = 2 \Delta P_n$ (ΔP_n represents only one sideband) we find:

$$\frac{\Delta P_p}{P_p} = 4 \sqrt{\frac{\sigma \Delta P_n}{P_p}} \quad (C-3)$$

The change in gain of a parametric amplifier as a result of a change in pump power is given by (reference 1, equation 10:40)

$$\frac{\Delta K}{K} = K^{1/2} \frac{\Delta P_p}{P_p} \quad (C-4)$$

The equivalent change of the input power of the interfering signal $P_S(\Delta f)$ is therefore:

$$\Delta P_{S(\Delta f)} = K^{1/2} \frac{\Delta P_p}{P_p} P_{S(\Delta f)} \quad (C-5)$$

Substitution of C-3 into C-5 yields:

$$\frac{\Delta P_{S(\Delta f)}}{P_{S(\Delta f)}} = 4 K^{1/2} \sqrt{\frac{\sigma \Delta P_n}{P_p}} \quad (C-6)$$

This induced noise modulation of $P_{S(\Delta f)}$ is pure AM giving two correlated noise sidebands at $f_{S(\Delta f)} - \Delta f = f_s - 2 \Delta f$ and $f_{S(\Delta f)} + \Delta f = f_s$, thus degrading the tangential sensitivity at $f = f_s$.

The corresponding induced noise power ΔP_{n_i} in each sideband can be found with the aid of equation C-2. With $\sigma = 1$ and $P_S = 2 \Delta P_{n_i}$

$$\frac{\Delta P_{S(\Delta f)}}{P_{S(\Delta f)}} = 4 \sqrt{\frac{\Delta P_{n_i}}{P_{S(\Delta f)}}} \quad (C-7)$$

Equating C-6 and C-7 yields:

$$\Delta P_{n_i} = K \frac{\sigma \Delta P_n}{P_p} P_{S(\Delta f)} \quad (C-8)$$

If the noise temperatures of the amplifier and the signal source are T_A and T_S , respectively, the operational temperature is defined as

$$T_{op} = T_A + T_S$$

The tangential sensitivity in the absence of an interfering signal is:

$$P_{T(f_s)} = k T_{op} \cdot B$$

where:

B = system bandwidth

k = Boltzman's constant = 1.38×10^{-23} Joules/K

As was pointed out, the interfering signal $P_{S(\Delta f)}$ increases the noise background at $f = f_s$ from:

$$k T_{op} B \text{ to } k T_{op} B + K \frac{\sigma(\Delta P_n)}{P_p} B P_{S(\Delta f)}$$

where $(\Delta P_n)_B$ is the noise power content of the noise spectrum between the frequencies $f_n - B/2$ and $f_n + B/2$ is:

$$(\Delta P_n)_B = \int_{f_n - B/2}^{f_n + B/2} \rho(f) df$$

This, for small B , can be approximated by:

$$(\Delta P_n)_B \approx P_{(f_n)} B$$

so that the tangential sensitivity at $f = f_s$ in the presence of the interfering signal can be written as:

$$P_{T(f_s \Delta f)} = k T_{op} B + K \frac{\sigma \rho(f_n)^B}{P_p} \cdot P_{s(\Delta f)}$$

The tangential sensitivity, therefore, is degraded by the factor:

$$\frac{P_{T(f_s \Delta f)}}{P_{T(f_s)}} = 1 + K \frac{\sigma \rho(f_n)}{k T_{op} P_p} \cdot P_{s(\Delta f)}$$

Defining the normalized spectral power density as:

$$W_{(\Delta f)} = \frac{\sigma \rho(f_n)}{P_p} \text{ (second)}$$

$$\frac{P_{T(f_s \Delta f)}}{P_{T(f_s)}} = 1 + \frac{K}{T_{op}} F_{(\Delta f)} P_{s(\Delta f)}$$

where

$$F_{(\Delta f)} = \frac{W_{(\Delta f)}}{k}$$

can be regarded as a figure of merit for the pump source of a parametric amplifier.

3. CONCLUSION

It has been derived that the degradation in tangential sensitivity for a single-stage paramp at $f = f_s$ as a result of a strong interfering signal Δf away, is given by:

$$\frac{P_{T(f_s \Delta f)}}{P_{T(f_s)}} = 1 + \left[\frac{K}{T_{op}} F(\Delta f) \right] P_{s(\Delta f)}$$

where

$P_{T(f_s \Delta f)}$ = tangential sensitivity at $f = f_s$ in the presence of an interfering signal Δf away

$P_{T(f_s)}$ = tangential sensitivity at $f = f_s$

K = power gain of amplifier

T_{op} = operational temperature
($T_{op} = T_{\text{amplifier}} + T_{\text{signal-source}}$)

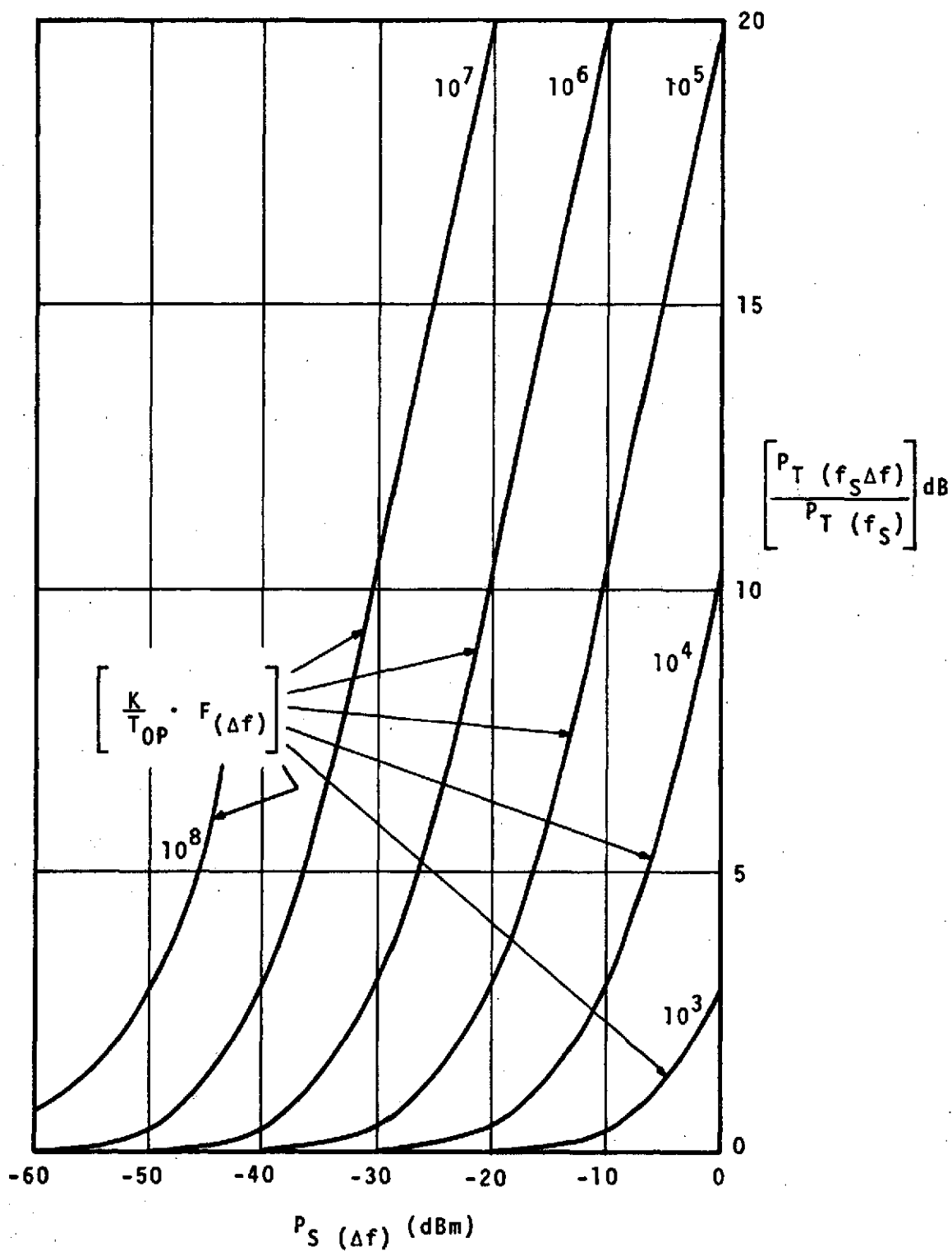
$F(\Delta f) = \frac{W(\Delta f)}{k}$ = figure of merit of pump source

$W(\Delta f)$ = normalized AM spectral noise power density of pump oscillator Δf away from carrier

k = Boltzmann's constant = 1.38×10^{-23} Joules/K

$P_{s(\Delta f)}$ = power of interfering signal Δf away from f_s

In Figure C -3, this relation $P_{T(f_s \Delta f)} / P_{T(f_s)}$ is shown graphically as a function of $P_{s(\Delta f)}$ with $\left(\frac{K}{T_{op}} \right) F(\Delta f)$ as parameter.

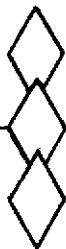


1-4846R1

Figure C-3. Degradation of Tangential Sensitivity as a Function of Absolute Power of Interfering Signal

APPENDIX D

TEST PROCEDURE FOR EVALUATION OF NON-HERMETICALLY SEALED GALLIUM ARSENIDE VARACTOR



1.0 PURPOSE OF TEST

This document formulates the test procedures that will be followed for the Evaluation of the Non-Hermetically Sealed Gallium Arsenide Varactor, AIL Part No. 381701.

The order of the tests are to be followed as indicated with no deviations.

AIL PROPRIETARY INFORMATION

AIL a division of
CUTLER-HAMMER
DEER PARK, LONG ISLAND, NEW YORK 11729



SIZE

A

CODE IDENT NO.

00752

381722

SCALE

SHEET 2

REV

2.0 INITIAL PERFORMANCE TESTS - ELECTRICAL PARAMETERS

2.1 Using the test set-up shown in Figure 1, measure V vs I_p at several points in the forward direction and several in the reverse direction around the breakdown points. The measurements are to be performed at the following current settings and the voltage recorded.

A. Forward Region

I_p (μ amps)

1 μ amps

5 μ amps

10 μ amps

20 μ amps

B. Reverse Region

I_p (μ amps)

1 μ amps

5 μ amps

10 μ amps

20 μ amps

2.2 Measure the capacitance of the varactor at the following voltages using the test set-up shown in Figure 2.

Voltages (volts)

0 volts

+0.2 volts

-1.0 volts

2.3 The following tests are to be performed 100 percent and in the sequence as listed.

2.3.1 Temperature Cycling as per MIL-STD-202-Method 107. The units will be subjected to 5 cycles of Test Condition B (-65°C to 100°C)

AIL a division of CUTLER-HAMMER <small>DEER PARK, LONG ISLAND, NEW YORK 11765</small>	SIZE	CODE IDENT NO.		
	A	00752	381722	
SCALE		SHEET 3		REV

in the non-operating condition.

2.3.1.2 Repeat measurements 2.1 and 2.2 listed above. The measurements are not to be performed less than 1 hour after removed from the temperature chamber. Calculate ΔV_p and ΔC .

2.3.2 High Temperature Reverse Bias

The test is to be performed using the test set-up shown in Figure 1. The varactor is to be placed in an ambient temperature of 100°C for 96 hours and a reverse voltage of approximately 80% of breakdown (defined to be 1 μ amp point) shall be applied to the varactor.

2.3.2.1 Repeat measurements 2.1 and 2.2 listed above. The measurements are not to be performed less than 1 hour after removal from the temperature chamber. Calculate ΔV_p and ΔC .

2.3.3. Operating Burn-In

The varactor is to be operated at rated power dissipation at room temperature for 96 hours.

Rated power dissipation is defined to be:

50 MW D.C.

2.3.3.1 Repeat measurements 2.1 and 2.2 listed above. Calculate ΔV_p and ΔC .

AIL a division of CUTLER-HAMMER <small>DEER PARK, LONG ISLAND, NEW YORK 11759</small>	SIZE	CODE IDENT NO.		
	A	00752	381722	
SCALE		SHEET 4 REV		

AIL PROPRIETARY INFORMATION

2.4 This series of tests are then concluded. The varactor will then be subjected to either the Operating Life Test or the Storage Life Test. This shall be so indicated on the Test Data Sheets.

2.5 Operating Life Test

The varactor shall be operated at rated power dissipation and an ambient temperature of 25°C for 50 minutes ON and 10 minutes OFF for a total time of 960 hours. Measurements shall be made per 2.1 and 2.2 at 0, 160, 480, and 960 hours. Calculate ΔV_p and ΔC .

2.6 Storage Life

The varactor shall be subjected to a storage life test of +100°C without power applied for a period of 960 hours. Measurement shall be made per 2.1 and 2.2 at 0, 160, 480, and 960 hours. Calculate ΔV_p and ΔC . The measurements are not to be performed less than 1 hour after removal from the temperature chamber.

AIL a division of
CUTLER-HAMMER 
DEER PARK, LONG ISLAND, NEW YORK 11759

SIZE

A

CODE IDENT NO.

00752

381722

SCALE

SHEET 5

REV

3.0 TEST EQUIPMENT

	<u>MANUFACTURER</u>	<u>MODEL NO.</u>
1. Direct Capacitance Bridge	Boonton Electronic Corporation	75D
2. DC Differential Voltmeter	John Fluke	871A
3. Transistor Curve Tracer	Tektronix	575
4. DC Meter	John Fluke	871A
5. DC Microvolt-Ammeter	Hewlett-Packard	425A

AIL a division of
CUTLER-HAMMER
OSER PARK, LONG ISLAND, NEW YORK 11720

SIZE

A

CODE IDENT NO.

00752

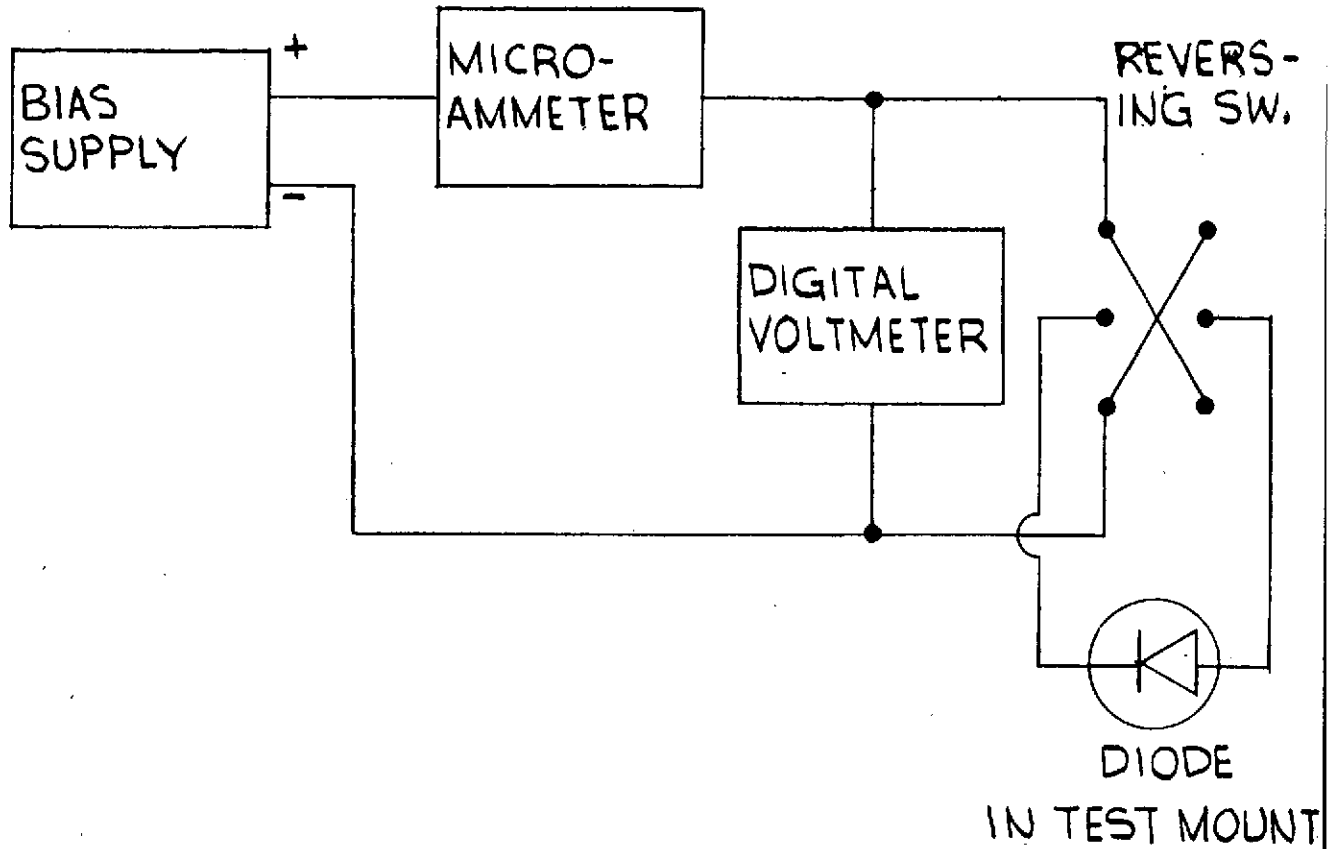
381722

SCALE

SHEET 6

REV

AIL PROPRIETARY INFORMATION



TEST SET-UP FOR I vs. V MEASUREMENT

FIGURE 1.

AIL a division of
CUTLER-HAMMER

DEER PARK, LONG ISLAND, NEW YORK 11760

SIZE

A

CODE IDENT NO.

00752

381722

SCALE

SHEET

REV

AIL PROPRIETARY INFORMATION

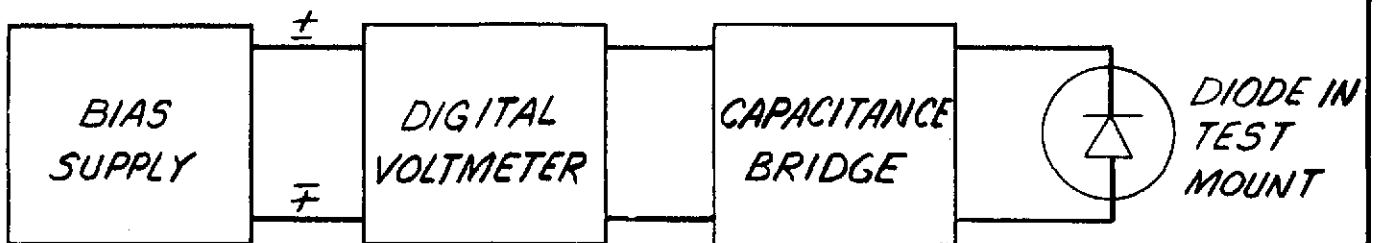


FIGURE 2
TEST SET-UP FOR C vs V MEASUREMENT

AIL a division of
CUTLER-HAMMER
DEER PARK, LONG ISLAND, NEW YORK 11729



SIZE

A

CODE IDENT NO.

00752

381722

SCALE

SHEET **9**

REV

AIL PROPRIETARY INFORMATION

TEST DATA SHEET

Varactor Serial No. _____

2.0 INITIAL PERFORMANCE TESTS-ELECTRICAL PARAMETERS

2.1 DC Characteristics

A. Forward Region

Reverse Region

<u>Ip (uamps)</u>	<u>Vp (volts)</u>	<u>Ip (uamps)</u>	<u>Vp (volts)</u>
<u>1</u>	<u> </u>	<u>1</u>	<u> </u>
<u>5</u>	<u> </u>	<u>5</u>	<u> </u>
<u>10</u>	<u> </u>	<u>10</u>	<u> </u>
<u>20</u>	<u> </u>	<u>20</u>	<u> </u>

2.2 Capacitance Measurement

<u>Vp (volts)</u>	<u>C(v) (pf)</u>
<u>0</u>	<u> </u>
<u>+0.2</u>	<u> </u>
<u>-1.0</u>	<u> </u>

Test Engineer: _____

QA: _____

AIL a division of
CUTLER-HAMMER
DEER PARK, LONG ISLAND, NEW YORK 11766

SIZE CODE IDENT NO.

A 00752

381722

SCALE

SHEET 10 REV

Varactor Serial No. _____

2.3.1 Temperature Cycling

A. DC Characteristics

1. Forward Region

<u>Ip (μamps)</u>	<u>Vp (volts)</u>	<u>Vp (volts) (per 2.1)</u>	<u>ΔVp (volts)</u>
<u>1</u>	_____	_____	_____
<u>5</u>	_____	_____	_____
<u>10</u>	_____	_____	_____
<u>20</u>	_____	_____	_____

2. Reverse Region

<u>Ip (μamps)</u>	<u>Vp (volts)</u>	<u>Vp (volts) (per 2.1)</u>	<u>ΔVp (volts)</u>
<u>1</u>	_____	_____	_____
<u>5</u>	_____	_____	_____
<u>10</u>	_____	_____	_____
<u>20</u>	_____	_____	_____

B. Capacitance

<u>Vp (volts)</u>	<u>C(v) (pf)</u>	<u>C (pf) (per 2.2)</u>	<u>ΔC (pf)</u>
<u>0</u>	_____	_____	_____
<u>+0.2</u>	_____	_____	_____
<u>-1.0</u>	_____	_____	_____

Test Engineer: _____

QA: _____

AIL a division of CUTLER-HAMMER <small>DEER PARK, LONG ISLAND, NEW YORK 11766</small>	SIZE	CODE IDENT NO.	381722
	A	00752	
SCALE			SHEET 11 REV

AIL PROPRIETARY INFORMATION

Varactor Serial No. _____

2.3.2 High Temperature Reverse Bias

A. DC Characteristics

1. Forward Region

<u>I_p (μamps)</u>	<u>V_p (volts)</u>	<u>V_p (volts) (per 2.1)</u>	<u>ΔV_p (volts)</u>
<u>1</u>	_____	_____	_____
<u>5</u>	_____	_____	_____
<u>10</u>	_____	_____	_____
<u>20</u>	_____	_____	_____

2. Reverse Region

<u>I_p (μamps)</u>	<u>V_p (volts)</u>	<u>V_p (volts) (per 2.1)</u>	<u>ΔV_p (volts)</u>
<u>1</u>	_____	_____	_____
<u>5</u>	_____	_____	_____
<u>10</u>	_____	_____	_____
<u>20</u>	_____	_____	_____

B. Capacitance

<u>V_p (volts)</u>	<u>C(v) (pf)</u>	<u>C (pf) (per 2.2)</u>	<u>ΔC (pf)</u>
<u>0</u>	_____	_____	_____
<u>+0.2</u>	_____	_____	_____
<u>-1.0</u>	_____	_____	_____

Test Engineer: _____

QA: _____

AIL a division of
CUTLER-HAMMER
DEER PARK, LONG ISLAND, NEW YORK 11765



SIZE

A

CODE IDENT NO.

00752

381722

SCALE

SHEET 12

REV

AIL PROPRIETARY INFORMATION

Varactor Serial No. _____

Rated

$V_p =$ _____ $P_D =$ _____

Power

$I_p =$ _____

Dissipation

2.3.3 Operating Burn-In

A. DC Characteristics

1. Forward Region

I_p (μ amps)	V_p (volts)	V_p (volts) (per 2.1)	ΔV_p (volts)
<u>1</u>	_____	_____	_____
<u>5</u>	_____	_____	_____
<u>10</u>	_____	_____	_____
<u>20</u>	_____	_____	_____

2. Reverse Region

I_p (μ amps)	V_p (volts)	V_p (volts) (per 2.1)	ΔV_p (volts)
<u>1</u>	_____	_____	_____
<u>5</u>	_____	_____	_____
<u>10</u>	_____	_____	_____
<u>20</u>	_____	_____	_____

B. Capacitance

V_p (volts)	$C(v)$ (pf)	C (pf) (per 2.2)	ΔC (pf)
<u>0</u>	_____	_____	_____
<u>+0.2</u>	_____	_____	_____
<u>-1.0</u>	_____	_____	_____

Test Engineer: _____

OA: _____

AIL a division of
CUTLER-HAMMER
DEER PARK, LONG ISLAND, NEW YORK 11729

SIZE

A

CODE IDENT NO.

00752

381722

SCALE

SHEET 13 REV

AIL PROPRIETARY INFORMATION

Varactor Serial No. _____

Test To Be Performed

1. Operation Life Test: ☐

2. Storage Life Test: ☐

AIL a division of
CUTLER-HAMMER 
DEER PARK, LONG ISLAND, NEW YORK 11720

SIZE

A

CODE IDENT NO.

00752

381722

SCALE

SHEET 14 REV

ALL PROPRIETARY INFORMATION

Varactor Serial No: _____

Rated Vp = _____ PD = _____
Power Ip = _____
Dissipation

2.5 Operating Life Test

Time: 0 Hours

A. DC Characteristics

1. Forward Region

<u>Ip (μamps)</u>	<u>Vp (volts)</u>	<u>Vp (volts) (per 2.1)</u>	<u>ΔVp (volts)</u>
<u>1</u>	_____	_____	_____
<u>5</u>	_____	_____	_____
<u>10</u>	_____	_____	_____
<u>20</u>	_____	_____	_____

2. Reverse Region

<u>Ip (μamps)</u>	<u>Vp (volts)</u>	<u>Vp (volts) (per 2.1)</u>	<u>ΔVp (Volts)</u>
<u>1</u>	_____	_____	_____
<u>5</u>	_____	_____	_____
<u>10</u>	_____	_____	_____
<u>20</u>	_____	_____	_____

B. Capacitance

<u>Vp (volts)</u>	<u>C (v) (pf)</u>	<u>C (pf) (per 2.2)</u>	<u>ΔC (pf)</u>
<u>0</u>	_____	_____	_____
<u>+0.2</u>	_____	_____	_____
<u>-1.0</u>	_____	_____	_____

Test Engineer: _____

QA: _____

AIL a division of
CUTLER-HAMMER
DEER PARK, LONG ISLAND, NEW YORK 11728

SIZE
A

CODE IDENT NO.
00752

381722

SCALE

SHEET 15 REV

ALL PROPRIETARY INFORMATION

Varactor Serial No. _____

Rated Power Dissipation $V_p =$ _____ $P_D =$ _____
 $I_p =$ _____

Time: 168 Hours

A. DC Characteristics

1. Forward Region

<u>I_p (μamps)</u>	<u>V_p (volts)</u>	<u>V_p (volts) (per 2.1)</u>	<u>ΔV_p (volts)</u>
<u>1</u>	_____	_____	_____
<u>5</u>	_____	_____	_____
<u>10</u>	_____	_____	_____
<u>20</u>	_____	_____	_____

2. Reverse Region

<u>I_p (μamps)</u>	<u>V_p (volts)</u>	<u>V_p (volts) (per 2.1)</u>	<u>ΔV_p (volts)</u>
<u>1</u>	_____	_____	_____
<u>5</u>	_____	_____	_____
<u>10</u>	_____	_____	_____
<u>20</u>	_____	_____	_____

B. Capacitance

<u>V_p (volts)</u>	<u>$C(v)$ (pf)</u>	<u>C (pf) (per 2.2)</u>	<u>ΔC (pf)</u>
<u>0</u>	_____	_____	_____
<u>+0.2</u>	_____	_____	_____
<u>-1.0</u>	_____	_____	_____

Test Engineer: _____

QA: _____

AIL a division of **CUTLER-HAMMER**
DEER PARK, LONG ISLAND, NEW YORK 11729

SIZE

A

CODE IDENT NO.

00752

381722

SCALE

SHEET 16

REV

ALL PROPRIETARY INFORMATION

Varactor Serial No. _____

Rated Power Dissipation $V_p =$ _____ $P_D =$ _____
 $I_p =$ _____

Time: 480 Hours

A. DC Characteristics

1. Forward Region

<u>I_p (μamps)</u>	<u>V_p (volts)</u>	<u>V_p (volts) (per 2.1)</u>	<u>ΔV_p (volts)</u>
<u>1</u>	_____	_____	_____
<u>5</u>	_____	_____	_____
<u>10</u>	_____	_____	_____
<u>20</u>	_____	_____	_____

2. Reverse Region

<u>I_p (μamps)</u>	<u>V_p (volts)</u>	<u>V_p (volts) (per 2.1)</u>	<u>ΔV_p (volts)</u>
<u>1</u>	_____	_____	_____
<u>5</u>	_____	_____	_____
<u>10</u>	_____	_____	_____
<u>20</u>	_____	_____	_____

B. Capacitance

<u>V_p (volts)</u>	<u>$C(v)$ (pf)</u>	<u>C (pf) (per 2.2)</u>	<u>ΔC (pf)</u>
<u>0</u>	_____	_____	_____
<u>+0.2</u>	_____	_____	_____
<u>-1.0</u>	_____	_____	_____

Test Engineer: _____

QA: _____

AIL a division of **CUTLER-HAMMER**
DEER PARK, LONG ISLAND, NEW YORK 11765

SIZE

A

CODE IDENT NO.

00752

381722

SCALE

SHEET 17

REV

AIL PROPRIETARY INFORMATION

Varactor Serial No. _____

Rated Vp = _____ P_D = _____
Power
Dissipation Ip = _____

Time: 960 Hours

A. DC Characteristics

1. Forward Region

<u>Ip (μamps)</u>	<u>Vp (volts)</u>	<u>Vp (volts) (per 2.1)</u>	<u>ΔVp (volts)</u>
<u>1</u>	_____	_____	_____
<u>5</u>	_____	_____	_____
<u>10</u>	_____	_____	_____
<u>20</u>	_____	_____	_____

2. Reverse Region

<u>Ip (μamps)</u>	<u>Vp (volts)</u>	<u>Vp (volts) (per 2.1)</u>	<u>ΔVp (volts)</u>
<u>1</u>	_____	_____	_____
<u>5</u>	_____	_____	_____
<u>10</u>	_____	_____	_____
<u>20</u>	_____	_____	_____

B. Capacitance

<u>Vp (volts)</u>	<u>C (v) (pf)</u>	<u>C (pf) (per 2.2)</u>	<u>ΔC (pf)</u>
<u>0</u>	_____	_____	_____
<u>+0.2</u>	_____	_____	_____
<u>-1.0</u>	_____	_____	_____

Test Engineer: _____

QA: _____

AIL a division of
CUTLER-HAMMER
OSER PARK, LONG ISLAND, NEW YORK 11753



SIZE

A

CODE IDENT NO.

00752

381722

SCALE

SHEET 18 REV

Varactor Serial No. _____

2.6 Storage Life Test

Time: 0 Hours

A. DC Characteristics

ALL PROPRIETARY INFORMATION

1. Forward Region

<u>Ip (μamps)</u>	<u>Vp (volts)</u>	<u>Vp (volts) (per 2.1)</u>	<u>ΔVp (volts)</u>
<u>1</u>	_____	_____	_____
<u>5</u>	_____	_____	_____
<u>10</u>	_____	_____	_____
<u>20</u>	_____	_____	_____

2. Reverse Region

<u>Ip (μamps)</u>	<u>Vp (volts)</u>	<u>Vp (volts) (per 2.1)</u>	<u>ΔVp (volts)</u>
<u>1</u>	_____	_____	_____
<u>5</u>	_____	_____	_____
<u>10</u>	_____	_____	_____
<u>20</u>	_____	_____	_____

B. Capacitance

<u>Vp (volts)</u>	<u>C(v) (pf)</u>	<u>C (pf) (per 2.2)</u>	<u>ΔC (pf)</u>
<u>0</u>	_____	_____	_____
<u>+0.2</u>	_____	_____	_____
<u>-1.0</u>	_____	_____	_____

Test Engineer: _____

QA: _____

AIL a division of
CUTLER-HAMMER
DEER PARK, LONG ISLAND, NEW YORK 11735



SIZE
A

CODE IDENT NO.
00752

381722

SCALE

SHEET 19 REV

Varactor Serial No. _____

Time: 168 Hours

A. DC Characteristics

AIL PROPRIETARY INFORMATION

1. Forward Region

<u>Ip (μamps)</u>	<u>Vp (volts)</u>	<u>Vp (volts) (per 2.1)</u>	<u>ΔVp (volts)</u>
<u>1</u>	_____	_____	_____
<u>5</u>	_____	_____	_____
<u>10</u>	_____	_____	_____
<u>20</u>	_____	_____	_____

2. Reverse Region

<u>Ip (μamps)</u>	<u>Vp (volts)</u>	<u>Vp (volts) (per 2.1)</u>	<u>ΔVp (volts)</u>
<u>1</u>	_____	_____	_____
<u>5</u>	_____	_____	_____
<u>10</u>	_____	_____	_____
<u>20</u>	_____	_____	_____

B. Capacitance

<u>Vp (volts)</u>	<u>C(v) (pf)</u>	<u>C (pf) (per 2.2)</u>	<u>ΔC (pf)</u>
<u>0</u>	_____	_____	_____
<u>+0.2</u>	_____	_____	_____
<u>-1.0</u>	_____	_____	_____

Test Engineer: _____

QA: _____

AIL a division of
CUTLER-HAMMER
6888 PARK, LONG ISLAND, NEW YORK 11788

SIZE

A

CODE IDENT NO.

00752

381722

SCALE

SHEET 20 REV

Varactor Serial No. _____

Time: 480 Hours

AIL PROPRIETARY INFORMATION

A. DC Characteristics

1. Forward Region

<u>Ip (μamps)</u>	<u>Vp (volts)</u>	<u>Vp (volts) (per 2.1)</u>	<u>ΔVp (volts)</u>
<u>1</u>	_____	_____	_____
<u>5</u>	_____	_____	_____
<u>10</u>	_____	_____	_____
<u>20</u>	_____	_____	_____

2. Reverse Region

<u>Ip (μamps)</u>	<u>Vp (volts)</u>	<u>Vp (volts) (per 2.1)</u>	<u>ΔVp (volts)</u>
<u>1</u>	_____	_____	_____
<u>5</u>	_____	_____	_____
<u>10</u>	_____	_____	_____
<u>20</u>	_____	_____	_____

B. Capacitance

<u>Vp (volts)</u>	<u>C(v) (pf)</u>	<u>C (pf) (per 2.2)</u>	<u>ΔC (pf)</u>
<u>0</u>	_____	_____	_____
<u>+0.2</u>	_____	_____	_____
<u>-1.0</u>	_____	_____	_____

Test Engineer: _____

QA: _____

AIL a division of
CUTLER-HAMMER
DEER PARK, LONG ISLAND, NEW YORK 11729

SIZE

A

CODE IDENT NO.

00752

381722

SCALE

SHEET 21 REV

Varactor Serial No. _____

Time: 960 Hours

A. DC Characteristics

AIL PROPRIETARY INFORMATION

1. Forward Region

<u>Ip (μamps)</u>	<u>Vp (volts)</u>	<u>Vp (volts) (per 2.1)</u>	<u>ΔVp (volts)</u>
<u>1</u>	_____	_____	_____
<u>5</u>	_____	_____	_____
<u>10</u>	_____	_____	_____
<u>20</u>	_____	_____	_____

2. Reverse Region

<u>Ip (μamps)</u>	<u>Vp (volts)</u>	<u>Vp (volts) (per 2.1)</u>	<u>ΔVp (volts)</u>
<u>1</u>	_____	_____	_____
<u>5</u>	_____	_____	_____
<u>10</u>	_____	_____	_____
<u>20</u>	_____	_____	_____

B. Capacitance

<u>Vp (volts)</u>	<u>C(v) (pf)</u>	<u>C (pf) (per 2.2)</u>	<u>ΔC (pf)</u>
<u>0</u>	_____	_____	_____
<u>+0.2</u>	_____	_____	_____
<u>-1.0</u>	_____	_____	_____

Test Engineer: _____

QA: _____

AIL a division of
CUTLER-HAMMER
DEER PARK, LONG ISLAND, NEW YORK 11765

SIZE

A

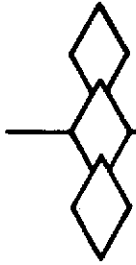
CODE IDENT NO.

00752

381722

SCALE

SHEET 22 REV



APPENDIX E
SUMMARY OF DIODE EVALUATION DATA

SUMMARY OF EVALUATION DATA

VARACTOR NO. 1-1

LIFE TEST
* 100°C STORAGE
— OPERATING LIFE, 50mw

	I-42	INITIAL	THERMAL SHOCK -65 TO +100°C	96 HOURS EACH		LIFE TEST *		
				100°C V _R	50mw V _f	HOURS		
						168	480	960
		VOLTS						
FORWARD BIAS	+1	.508	.510	.071				
	+5	.559	.562	.267				
	+10	.585	.586	.392				
	+20	.610	.611	.512				
REVERSE BIAS	-1	15.16	15.13	.082				
	-5	15.20	15.17	.372				
	-10	15.21	15.19	.632				
	-20	15.23	15.20	1.014				
		CAPACITANCE - pF						
BIAS VOLTAGE	C _j							
	0	.145	.148					
	+2	.160	.163					
	-10	.113	.116	.50FT				

VARACTOR NO. 1-2

LIFE TEST
* 100°C STORAGE
— OPERATING LIFE, 50mw

	I-42	VOLTS						
FORWARD BIAS	+1	.508	.508	.500	.497	.515	.518	.514
	+5	.557	.560	.557	.556	.565	.564	.561
	+10	.583	.586	.582	.584	.604	.582	.581
	+20	.607	.612	.608	.619	.678	.606	.605
REVERSE BIAS	-1	12.91	12.91	12.92	12.91	12.94	12.91	12.87
	-5	13.07	13.05	13.05	13.06	13.11	13.06	13.08
	-10	13.09	13.08	13.08	13.10	13.15	13.09	13.10
	-20	13.12	13.10	13.10	13.13	13.18	13.10	13.12
		CAPACITANCE - pF						
BIAS VOLTAGE	C _j							
	0	.138	.138	.141	.133	.136	.138	.140
	+2	.152	.152	.151	.148	.148	.151	.152
	-10	.111	.111	.111	.107	.108	.110	.110

ALL PROPRIETARY INFORMATION

SUMMARY OF EVALUATION DATA

LIFE TEST

VARACTOR NO. 1-3

* 100°C STORAGE
— OPERATING LIFE, 50mw

	I-42	INITIAL	THERMAL SHOCK -65 TO +100°C	96 HOURS EACH		LIFE TEST *		
				100°C V _R	50 mw V _f	HOURS		
						168	480	960
		VOLTS						
FORWARD BIAS	+1	.515	.520	.501	.497	.520	.513	.515
	+5	.585	.564	.556	.554	.570	.570	.561
	+10	.588	.587	.581	.580	.597	.587	.581
	+20	.609	.611	.608	.611	.635	.620	.604
REVERSE BIAS	-1	12.01	11.99	11.98	11.98	11.95	11.91	10.68
	-5	12.23	12.20	12.18	12.22	12.23	12.20	11.47
	-10	12.26	12.23	12.23	12.27	12.29	12.23	11.72
	-20	12.29	12.25	12.26	12.32	12.35	12.26	11.95
		CAPACITANCE - pF						
BIAS VOLTAGE	C _j							
	0	.147	.148	.149	.148	.152	.148	.149
	+2	.161	.162	.161	.161	.166	.162	.162
	-10	.119	.119	.118	.118	.122	.118	.119

VARACTOR NO. 1-4

* 100°C STORAGE
— OPERATING LIFE, 50mw

	I-42	VOLTS						
FORWARD BIAS	+1	.522	.528	.508	.505	.522	.518	.523
	+5	.570	.573	.563	.560	.572	.568	.570
	+10	.592	.594	.589	.581	.591	.587	.590
	+20	.615	.617	.615	.610	.619	.612	.612
REVERSE BIAS	-1	16.43	16.37	16.35	16.37	16.41	16.35	16.38
	-5	16.45	16.39	16.39	16.41	16.45	16.41	16.44
	-10	16.46	16.40	16.41	16.43	16.40	16.42	16.45
	-20	16.47	16.41	16.42	16.45	16.47	16.43	16.46
		CAPACITANCE - pF						
BIAS VOLTAGE	C _j							
	0	.139	.135	.137	.138	.138	.138	.138
	+2	.151	.148	.151	.151	.151	.151	.150
	-10	.109	.108	.109	.110	.110	.110	.110

ALL PROPRIETARY INFORMATION

SUMMARY OF EVALUATION DATA

VARACTOR NO. 1-5

LIFE TEST
* 100°C STORAGE
— OPERATING LIFE, 50mw

	I-42	INITIAL	THERMAL SHOCK -65 TO +100°C	96 HOURS EACH		LIFE TEST *		
				100°C V _R	50mw V _f	HOURS		
						168	480	960
				VOLTS				
FORWARD BIAS	+1	.524	.528	.508	.504	.518	.522	.521
	+5	.568	.578	.563	.558	.577	.568	.569
	+10	.590	.607	.589	.584	.585	.590	.588
	+20	.616	.641	.615	.611	.611	.614	.613
REVERSE BIAS	-1	13.39	13.35	13.33	13.34	13.38	13.34	13.35
	-5	13.45	13.45	13.40	13.41	13.45	13.42	13.44
	-10	13.47	13.49	13.42	13.44	13.46	13.43	13.45
	-20	13.48	13.55	13.44	13.46	13.48	13.45	13.46
				CAPACITANCE - pfd				
BIAS VOLTAGE	C _j							
	0	.138	.139	.136	.138	.139	.137	.138
	+2	.151	.151	.148	.151	.151	.150	.151
	-10	.112	.112	.108	.112	.112	.111	.112

VARACTOR NO. 1-6

LIFE TEST
* 100°C STORAGE
— OPERATING LIFE, 50mw

	I-42	VOLTS						
FORWARD BIAS	+1	.528	.531	.513	.508	.525	.526	.525
	+5	.574	.577	.566	.560	.567	.571	.570
	+10	.596	.599	.593	.587	.590	.592	.593
	+20	.619	.622	.618	.612	.612	.617	.616
REVERSE BIAS	-1	16.43	16.38	16.38	16.40	16.45	16.43	16.44
	-5	16.46	16.42	16.42	16.44	16.48	16.44	16.46
	-10	16.48	16.43	16.44	16.46	16.49	16.45	16.47
	-20	16.50	16.45	16.46	16.48	16.51	16.47	16.49
				CAPACITANCE - pfd				
BIAS VOLTAGE	C _j							
	0	.114	.113	.110	.114	.112	.113	.113
	+2	.125	.124	.120	.126	.124	.124	.123
	-10	.090	.090	.086	.091	.088	.090	.088

SUMMARY OF EVALUATION DATA

VARACTOR NO. 1-7

LIFE TEST
* 100°C STORAGE
— OPERATING LIFE, 50mw

	I-4q	INITIAL	THERMAL SHOCK -65 TO +100°C	96 HOURS EACH		LIFE TEST *		
				100°C V _R	50 mw V _f	HOURS		
						168	480	960
VOLTS								
FORWARD BIAS	+1	.508	.510	.495	.488	.505	.508	.507
	+5	.555	.557	.549	.544	.543	.549	.551
	+10	.576	.579	.575	.569	.573	.574	.575
	+20	.600	.603	.600	.596	.595	.600	.599
REVERSE BIAS	-1	12.19	12.15	12.19	12.18	12.21	12.19	12.01
	-5	12.47	12.44	12.43	12.44	12.47	12.49	12.45
	-10	12.51	12.48	12.48	12.49	12.51	12.57	12.50
	-20	12.54	12.51	12.52	12.52	12.54	12.66	12.53
CAPACITANCE - pF								
BIAS VOLTAGE	C _j							
	0	.188	.188	.188	.185	.187	.190	.188
	+2	.206	.206	.208	.204	.207	.212	.205
	-10	.145	.145	.145	.143	.145	.150	.144

ALL PROPRIETARY INFORMATION

VARACTOR NO. 1-8

LIFE TEST
* 100°C STORAGE
— OPERATING LIFE, 50mw

	I-4q	VOLTS					
FORWARD BIAS	+1	.518	.523	.505	.497	0	
	+5	.566	.569	.558	.552	P	
	+10	.585	.589	.585	.578	E	
	+20	.610	.612	.612	.604	N	
REVERSE BIAS	-1	13.87	13.86	13.20	13.66		
	-5	13.97	13.94	13.18	13.62		
	-10	13.99	13.96	13.19	13.61		
	-20	14.00	13.97	13.20	13.63		
CAPACITANCE - pF							
BIAS VOLTAGE	C _j						
	0	.140	.142	.141	.137		
	+2	.155	.157	.155	.152		
	-10	.109	.110	.110	.106		

SUMMARY OF EVALUATION DATA

VARACTOR NO. 1-9

LIFE TEST

* 100°C STORAGE
— OPERATING LIFE, 50mw

	I-U _q	INITIAL	THERMAL SHOCK -65 TO +100°C	96 HOURS EACH		LIFE TEST *		
				100°C V _R	50 mw V _f	HOURS		
						168	480	960
		VOLTS						
FORWARD BIAS	+1	.517	.519	.501	.499	.511	.512	.513
	+5	.564	.565	.556	.554	.560	.567	.563
	+10	.585	.587	.583	.578	.582	.583	.584
	+20	.608	.610	.609	.604	.603	.606	.608
REVERSE BIAS	-1	15.44	15.40	15.37	15.40	15.42	15.41	15.43
	-5	15.46	15.42	15.41	15.44	15.47	15.43	15.45
	-10	15.47	15.43	15.44	15.46	15.48	15.44	15.46
	-20	15.48	15.44	15.45	15.47	15.49	15.45	15.48
		CAPACITANCE - pF						
BIAS VOLTAGE	C _j							
	0	.156	.154	.151	.157	.155	.155	.156
	+2	.173	.170	.167	.173	.172	.170	.170
	-10	.122	.120	.117	.122	.120	.122	.120

ALL PROPRIETARY INFORMATION

VARACTOR NO. 1-10

LIFE TEST

* 100°C STORAGE
— OPERATING LIFE, 50mw

	I-U _q	VOLTS						
FORWARD BIAS	+1	.527	.528	.510	.523	.526	.523	.524
	+5	.575	.578	.564	.561	.580	.572	.573
	+10	.594	.596	.591	.588	.586	.591	.598
	+20	.619	.619	.618	.615	.616	.620	.624
REVERSE BIAS	-1	16.36	16.33	16.31	16.37	16.40	16.35	16.37
	-5	16.38	16.35	16.35	16.39	16.41	16.37	16.40
	-10	16.39	16.36	16.37	16.40	16.42	16.38	16.41
	-20	16.40	16.37	16.39	16.41	16.43	16.40	16.43
		CAPACITANCE - pF						
BIAS VOLTAGE	C _j							
	0	.128	.127	.128	.126	.131	.125	.127
	+2	.140	.139	.140	.138	.145	.137	.138
	-10	.103	.101	.103	.100	.106	.098	.102

SUMMARY OF EVALUATION DATA

VARACTOR NO. 3-1

LIFE TEST
100°C STORAGE
* OPERATING LIFE, 50mw

	I-42	INITIAL	THERMAL SHOCK -65 TO +100°C	96 HOURS EACH		LIFE TEST *		
				100°C	50mw	HOURS		
				V _R	V _f	168	480	960
VOLTS								
FORWARD BIAS	+1	.524	.525	.507	.507	S		
	+5	.572	.569	.561	.559	O		
	+10	.595	.593	.587	.584	F		
	+20	.624	.616	.613	.611	T		
REVERSE BIAS	-1	18.02	18.00	17.98	18.01			
	-5	18.06	18.03	18.02	18.06			
	-10	18.07	18.04	18.04	18.08			
	-20	18.09	18.05	18.06	18.09			
CAPACITANCE - pF								
BIAS VOLTAGE	C _j							
	0	.117	.119	.139	.119			
	+2	.128	.131	.152	.130			
	-10	.097	.095	.115	.094			

VARACTOR NO. 3-2

LIFE TEST
100°C STORAGE
* OPERATING LIFE, 50mw

	I-42	VOLTS						
FORWARD BIAS	+1	.528	.533	.511	.509	S		
	+5	.573	.576	.567	.563	O		
	+10	.597	.598	.593	.587	F		
	+20	.620	.622	.619	.615	T		
REVERSE BIAS	-1	17.96	17.93	17.90	17.95			
	-5	17.97	17.94	17.93	17.98			
	-10	17.98	17.95	17.95	17.99			
	-20	17.99	17.96	17.96	18.01			
		CAPACITANCE - pF						
BIAS VOLTAGE	C _j							
	0	.110	.108	.110	.111			
	+2	.121	.119	.121	.121			
	-10	.088	.085	.087	.088			

SUMMARY OF EVALUATION DATA

LIFE TEST

VARACTOR NO. 3-3

100°C STORAGE

* OPERATING LIFE, 50mw

	I-42	INITIAL	THERMAL SHOCK -65 TO +100°C	96 HOURS EACH		LIFE TEST *		
				100°C	50 mw	HOURS		
				V _R	V _f	168	480	960
		VOLTS						
FORWARD BIAS	+1	.547	.515	.498	.495	S		
	+5	.559	.562	.554	.550	O		
	+10	.583	.585	.580	.577	F		
	+20	.606	.608	.607	.607	T		
REVERSE BIAS	-1	12.17	12.16	12.14	12.16			
	-5	12.33	12.33	12.30	12.32			
	-10	12.36	12.35	12.34	12.36			
	-20	12.37	12.36	12.36	12.39			
		CAPACITANCE - pfd						
BIAS VOLTAGE	C _j							
	0	.159	.159	.167	.157			
	+2	.174	.175	.184	.173			
	-10	.122	.122	.132	.121			

ALL PROPRIETARY INFORMATION

VARACTOR NO. 3-4

LIFE TEST

100°C STORAGE

* OPERATING LIFE, 50mw

	I-42	VOLTS						
FORWARD BIAS	+1	.526	.530	.511	.501	S		
	+5	.574	.574	.566	.561	O		
	+10	.596	.597	.592	.587	F		
	+20	.621	.620	.618	.613	T		
REVERSE BIAS	-1	17.61	17.59	17.55	17.60			
	-5	17.63	17.60	17.59	17.64			
	-10	17.64	17.62	17.61	17.66			
	-20	17.66	17.63	17.62	17.67			
		CAPACITANCE - PFD						
BIAS VOLTAGE	C _j							
	0	.109	.108	.107	.106			
	+2	.120	.116	.116	.116			
	-10	.087	.086	.087	.085			

SUMMARY OF EVALUATION DATA

VARACTOR NO. 3-5

LIFE TEST
100°C STORAGE
* OPERATING LIFE, 50mw

	I-4q	INITIAL	THERMAL SHOCK -65 TO +100°C	96 HOURS EACH		LIFE TEST *		
				100°C V _R	50 mw V _f	HOURS 168 480 960		
← VOLTS →								
FORWARD BIAS	+1	.523	.524	.506	.507			
	+5	.569	.570	.561	.558			
	+10	.590	.592	.587	.582			
	+20	.614	.615	.613	.609			
REVERSE BIAS	-1	17.25	17.23	17.19	17.24			
	-5	17.27	17.24	17.23	17.27			
	-10	17.28	17.25	17.24	17.29			
	-20	17.29	17.26	17.26	17.30			
← CAPACITANCE - pfd →								
BIAS VOLTAGE	C _j							
	0	.126	.126	.128	.126			
	+2	.138	.138	.140	.139			
	-10	.100	.099	.102	.100			

VARACTOR NO. 3-6

LIFE TEST
100°C STORAGE
* OPERATING LIFE, 50mw

	I-4q	VOLTS						
FORWARD BIAS	+1	.536	.538	.518	.518	.535	.576	.532
	+5	.587	.581	.573	.574	.580	.582	.577
	+10	.614	.603	.600	.607	.599	.603	.599
	+20	.650	.626	.629	.644	.623	.630	.622
REVERSE BIAS	-1	16.83	16.81	16.78	16.83	16.84	16.82	16.84
	-5	16.86	16.83	16.81	16.87	16.86	16.84	16.86
	-10	16.87	16.84	16.83	16.89	16.87	16.85	16.88
	-20	16.89	16.85	16.85	16.93	16.89	16.87	16.89
		CAPACITANCE - pfd						
BIAS VOLTAGE	C _j							
	0	.126	.112	.117	.115	.115	.126	.112
	+2	.137	.122	.128	.127	.127	.136	.121
	-10	.101	.087	.091	.091	.092	.102	.088

ALL PROPRIETARY INFORMATION

SUMMARY OF EVALUATION DATA

LIFE TEST

VARACTOR NO. 3-7

100°C STORAGE
* OPERATING LIFE, 50mw

	I-42	INITIAL	THERMAL SHOCK -65 TO +100°C	96 HOURS EACH		LIFE TEST *		
				100°C V _R	50 mw V _f	HOURS		
				168			480	960
VOLTS								
FORWARD BIAS	+1	.512	.517	.498	.497	.510	.513	.513
	+5	.560	.559	.553	.548	.558	.559	.555
	+10	.582	.584	.580	.575	.580	.579	.580
	+20	.606	.608	.605	.602	.604	.604	.603
REVERSE BIAS	-1	12.93	12.93	12.95	12.97	12.97	12.96	12.97
	-5	13.08	13.07	13.06	13.09	13.10	13.09	13.10
	-10	13.11	13.09	13.09	13.11	13.11	13.11	13.12
	-20	13.12	13.11	13.10	13.13	13.13	13.12	13.13
CAPACITANCE - pF								
BIAS VOLTAGE	C _j							
	0	.148	.147	.143	.148	.148	.149	.150
	+2	.163	.162	.157	.163	.163	.163	.164
	-10	.116	.115	.110	.116	.116	.116	.117

ALL PROPRIETARY INFORMATION

VARACTOR NO. 3-8

LIFE TEST
* OPERATING LIFE, 50mw

	I-42	VOLTS						
FORWARD BIAS	+1	.531	.532	.515	.516	.529	.530	.524
	+5	.578	.578	.570	.564	.575	.575	.575
	+10	.599	.601	.597	.593	.595	.599	.596
	+20	.622	.624	.623	.617	.620	.622	.621
REVERSE BIAS	-1	17.33	17.31	17.28	17.33	17.34	17.33	17.35
	-5	17.35	17.32	17.31	17.36	17.36	17.35	17.36
	-10	17.36	17.33	17.33	17.38	17.37	17.36	17.37
	-20	17.38	17.35	17.35	17.39	17.38	17.37	17.39
CAPACITANCE - pF								
BIAS VOLTAGE	C _j							
	0	.113	.111	.113	.113	.110	.111	.112
	+2	.123	.120	.123	.123	.119	.121	.121
	-10	.092	.090	.092	.092	.089	.090	.090

SUMMARY OF EVALUATION DATA

VARACTOR NO. 3-9

LIFE TEST
100°C STORAGE
* OPERATING LIFE, 50mw

	I-4a	INITIAL	THERMAL SHOCK -65 TO +100°C	96 HOURS EACH		LIFE TEST *		
				100°C	50mw	HOURS		
				V _R	V _f	168	480	960
VOLTS								
FORWARD BIAS	+1	.532	.533	.512	.509	.532	.530	.505
	+5	.577	.578	.568	.565	.577	.576	.574
	+10	.599	.599	.594	.593	.599	.596	.595
	+20	.623	.623	.621	.618	.629	.622	.619
REVERSE BIAS	-1	17.74	17.72	17.70	17.74	17.76	17.74	17.77
	-5	17.77	17.74	17.74	17.78	17.78	17.77	17.78
	-10	17.78	17.76	17.76	17.80	17.79	17.78	17.79
	-20	17.80	17.78	17.78	17.82	17.81	17.81	17.80
CAPACITANCE - pF								
BIAS VOLTAGE	C _j							
	0	.114	.113	.115	.113	.113	.111	.114
	+2	.125	.124	.126	.124	.124	.120	.123
	-10	.093	.091	.092	.091	.091	.087	.091

ALL PROPRIETARY INFORMATION

VARACTOR NO. 3-10

LIFE TEST
100°C STORAGE
* OPERATING LIFE, 50mw

	I-4q	VOLTS						
FORWARD BIAS	+1	.529	.532	.513	.507	.531	.527	.511
	+5	.575	.578	.567	.564	.573	.574	.570
	+10	.598	.597	.595	.590	.595	.597	.598
	+20	.620	.622	.620	.616	.618	.619	.625
REVERSE BIAS	-1	17.90	17.88	17.85	17.90	17.90	17.91	17.92
	-5	17.93	17.90	17.90	17.94	17.93	17.92	17.94
	-10	17.94	17.91	17.91	17.95	17.95	17.93	17.95
	-20	17.96	17.93	17.93	17.97	17.96	17.95	17.97
BIAS VOLTAGE	C _j							
	0	.114	.115	.114	.116	.115	.113	.115
	+2	.125	.125	.123	.126	.126	.123	.124
	-10	.093	.093	.092	.093	.092	.090	.092



SPEC NO. 00752- ENV-72-2
CODE NO.



RANDOM VIBRATION TEST REPORT
ON
C.R.G. VARACTOR DIODE

PREPARED BY: H. Grumm
H. Grumm

DATE: 2-14-72



SPEC NO. 00752 - ENV-72-2
CODE NO.

REV.

TABLE OF CONTENTS

	<u>PAGE</u>
1.0 SCOPE	3
2.0 APPLICABLE DOCUMENTS	3
3.0 TEST CONDITIONS	3
4.0 SEQUENCE OF TESTS	3
5.0 TEST PROCEDURE	4
6.0 RESULTS	6

APPENDIX A - PHOTOGRAPHS OF g^2 /cps Vs. Channel No.



1.0 SCOPE

This document defines the Vibration testing performed on four C.R.G. Varactor Diodes at A.I.L.

2.0 APPLICABLE DOCUMENTS

The document listed below forms a part of this report.

<u>Document No.</u>	<u>Title</u>
MIL-STD-810B Notice 1	Environmental Test Methods

3.0 TEST CONDITIONS

Unless otherwise specified the vibration testing was conducted at ambient temperature 75°F in the X axis, 102°F in the Z axis, and ambient pressure of 760 mm of Hg.

3.1 Test Equipment Calibration

All equipment used for testing had been calibrated. All equipment used for testing exhibited calibration labels stating date of last calibration, date of next calibration and property number.

4.0 SEQUENCE OF TESTS

- 4.1 Random vibration X & Y axis at 5.4 to 16.0 grms.
- 4.2 Electrical check.
- 4.3 Random vibration Z axis 5.4 to 46.4 grms.
- 4.4 Random vibration X axis 20.7 to 46.4 grms.
- 4.5 Electrical check.

5.0 TEST PROCEDURE

5.1 Vibration Equipment Used

- a. Vibration Exciter MB Electronics, Model C60.
- b. Power Amplifier, MB Electronics, Model T452-B
- c. Equalization Console, MB Electronics, Model T485
- d. Spectrum Analyzer, MB Electronics, Model T491
- e. Accelerometer, MB Electronics, Model 302
- f. Oscilloscope, Tektronics, Model 535A
- g. Accelerometer Amplifier, Unholtz, Model 8PMCVA
- h. Camera, Dumont, Model 2614
- i. Automatic Exciter Control, MB Electronics, Model N575/N576
- j. True R.M.S. Meter, MB Electronics, Model N120

5.2 Test Setup

5.2.1 X&Y Axis

The four diodes were placed symmetrically on a $1\frac{1}{2}$ inch thick aluminum plate 7 inches in diameter. This plate was attached to the horizontal slip plate. The slip plate was floated on an oil film table. The input was colinear to the X axis. One accelerometer was oriented to detect vibration in the same axis.

5.2.2 Z Axis

For this axis the aluminum plate was bolted directly to the moving element of the shaker.

5.3 Random Vibration Equalization

With the accelerometer attached to the vibration fixture but without the diodes the exciter fixture was equalized via the Spectrum Analyzer and Random Console to the following power spectral densities which was test curve AE of MIL-STD-810B.

20 to 100 cps at 6 db per octave roll on

100 to 1000 cps at .02 g²/cps

1000 to 2000 cps at 6 db per octave roll off.

This energy had a overall of 5.4 grms. The on-the-line Spectrum Analyzer together with the rms meters monitored the accelerometer. None of the 48 DC level energy had less than 50 cps bandwidth. When the system was equalized the levels were brought to zero and the diodes on the fixture were mounted.

5.4 Random Vibration Test

5.4.1 Paragraph 5.3 was repeated with the diodes in place according to the following:

Test Curve	Spectral Density	Grms	Time (min)	Axis
AE	0.02	5.4	3	X & Y
AF	0.04	7.6	3	X & Y
AG	0.06	9.3	3	X & Y
AH	0.10	12.0	3	X & Y
AJ	0.20	16.9	3	X & Y

Test Curve	Spectral Density	Grms	Time (min.)	Axis
AE	0.02	5.4	3	Z
AF	0.04	7.6	3	Z
AG	0.06	9.3	3	Z
AH	0.10	12.0	3	Z
AJ	0.20	16.9	3	Z
AK	0.30	20.7	3	Z
AL	0.40	23.9	3	Z
AM	0.60	29.3	3	Z
AN	1.00	37.9	3	Z
AP	1.50	46.4	30	Z
AK	0.30	20.7	3	X & Y
AL	0.40	23.0	3	X & Y
AM	0.60	29.3	3	X & Y
AN	1.00	37.9	3	X & Y
AP	1.50	46.4	30	X & Y

6.0 RESULTS

Appendix A contains the on-the-line random vibration data. All electrical tests were performed by project.

Appendix B contains the electrical test results.

APPENDIX A

The key to the on-the-line Spectrum Analyzer, MB-T491 is the bank of 48 crystal filters resulting in 48 dc voltages displayed on an oscilloscope indicating proportional g^2/cps energy. A complete plot of spectral density over a 2000 cps band is displayed in each photograph.

Vertical Calibration

→ The 48 dc voltages are calculated from the photos using millivolt per cm given times the number of cm shown in the photo. A graph for g^2/cps vs. voltage then converts voltage to g^2/cps . ←

Horizontal Calibration

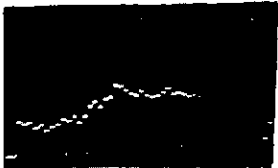
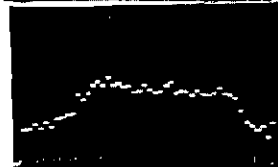
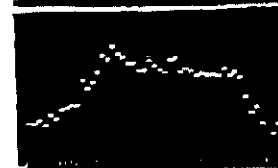

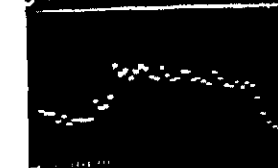
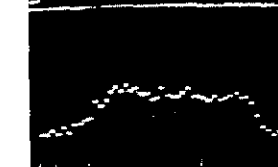
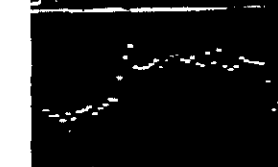
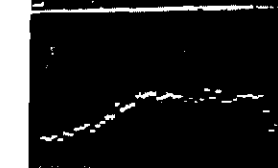
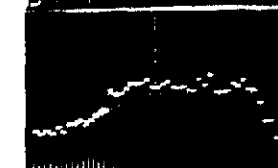

Every one of the 48 dc voltage markers is assigned one horizontal graticule marker.

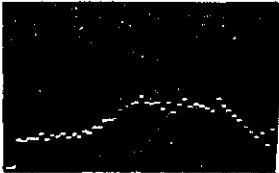
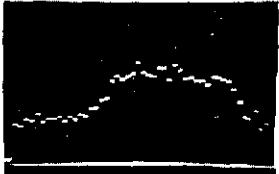
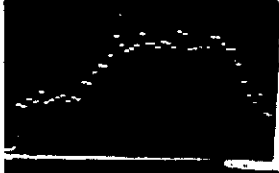
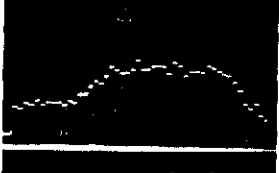

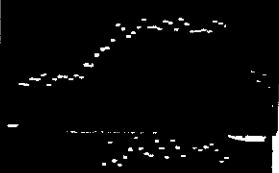

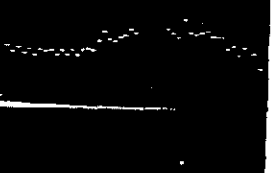


Channel 1 (12.5 cps) thru 8 (100 cps) are 12.5 cps wide.

Channel 8 (100 cps) thru 25 (200 cps) are 25 cps wide.

Channel 25 (200 cps) thru 48 (2000 cps) are 50 cps wide.

X-Y Axis

<u>Photo</u>	<u>Vert. Scale</u>	<u>Test Curve</u>
	.1 mv/cm	AE
	.1 mv/cm	AF
	.1 mv/cm	AG
	.1 mv/cm	AH
	.2 mv/cm	AJ
	.2 mv/cm	AK
	.2 mv/cm	AL
	.5 mv/cm	AM
	.5 mv/cm	AN
	.5 mv/cm	AP

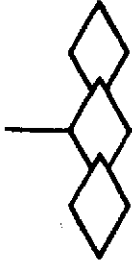
<u>Photo</u>	<u>Vert. Scale</u>	<u>4 AX19</u> <u>Test Curve</u>
	.1 mv/cm	AE
	.1 mv/cm	AF
	.1 mv/cm	AG
	1 mv/cm	AH
	.2 mv/cm	AJ
	.2 mv/cm	AK
	.2 mv/cm	AL
	.5 mv/cm	AM
	.5 mv/cm	AN
	.5 mv/cm	AP

APPENDIX B

The four diodes mounted in the vibration test fixture were optically as well as electrically examined prior to; initial testing, after completion of X & Y axis up to 16.0 g rms, and completion of X, Y, & Z axis at 46.4 g rms, with no failures.

The forward and reverse voltage drops prior to and at the conclusion of vibration testing is as follows:

<u>Unit</u>	<u>Prior</u>		<u>Conclusion</u>	
	<u>V_f</u>	<u>V_r</u>	<u>V_f</u>	<u>V_r</u>
1	.56V	10.2V	.565V	10.2V
2	.51	15.6	.51	15.7
3	.59	10.8	.60	10.9
4	.59	12	.59	11.9



APPENDIX F

NOISE TRANSFER ANALYSIS--GENERAL CASE FOR MULTISTAGE PARAMETRIC AMPLIFIER SYSTEM

The analysis in Appendix C was based upon the interfering signal being in the passband of the amplifier.

Referring to equation C-8,

$$\Delta P_{ni} = K \frac{\sigma \Delta P_n}{P_p} \cdot P_{s_{\Delta f}}$$

K really represents the gain for the frequency of the interfering signal $f_{s(\Delta f)}$

In case K represents the gain in the passband and the interfering signal $f_{s(\Delta f)}$ is outside the passband, so that the gain at $f - f_{s(\Delta f)} = \rho K$ ($\rho < 1$), the general formula should read

$$\Delta P_{in} = \rho K \frac{\sigma \Delta P_n}{P_p} P_{s(\Delta f)} \quad (F-1)$$

Assume now n cascaded stages with:

K_n = mid-band gain of n^{th} stage

$\rho_n K_n$ = gain of n^{th} stage at $f = f_{s(\Delta f)}$

$\frac{\sigma \Delta P_n}{P_p}$ = noise quantity of the pump of the n^{th} stage

The transferred noise to the input of the n^{th} stage can now be written as:

$$\left(\Delta P_{ni} \right)_N = \rho_n K_n \left[\frac{\sigma \Delta P_n}{P_p} \right]_n \left(P_{s(\Delta f)} \right)_N \quad (\text{F-2})$$

where the suscript N refers to the fact that those quantities are taken at the input of the n^{th} stage.

For the noise components falling inside the passband, the noise contribution of the n^{th} stage can be transferred to the input of the first stage according to:

$$\left(\Delta P_{ni} \right)_n = \frac{\left(\Delta P_{ni} \right)_N}{\prod_{p=1}^{p=n-1} K_p} = \rho_n K_n \left[\frac{\sigma \Delta P}{P_p} \right]_n \left(P_{s(\Delta f)} \right)_N \cdot \frac{1}{\prod_{p=1}^{p=n-1} K_p} \quad (\text{F-3})$$

with:

$$\left(P_{s(\Delta f)} \right)_N = \left[\prod_{p=1}^{p=n-1} \rho_p K_p \right] P_{s(\Delta f)} \quad (\text{F-4})$$

it follows:

$$\left(\Delta P_{ni} \right)_n = \prod_{p=1}^{p=n} \rho_p \cdot K_n \left[\frac{\sigma \Delta P_n}{P_p} \right]_n P_{s(\Delta f)} \quad (\text{F-5})$$

Thus, the total input noise

$$\Delta P_{ni} = \sum_{p=1}^{p=n} \left[\prod_{q=1}^{q=n} \rho_q \right] K_p \left[\frac{\sigma \Delta P_n}{P_p} \right]_p P_s(\Delta f) \quad (F-6)$$

If identical pumps are used so that

$$\left[\frac{\sigma \Delta P_n}{P_p} \right]_n = \frac{\sigma \Delta P_n}{P_p} \quad (F-7)$$

$$\Delta P_{ni} = K_{eff} \cdot \frac{\sigma \Delta P_n}{P_p} \cdot P_s(\Delta f)$$

where:

$$K_{eff} = \sum_{p=1}^{p=n} \left[\prod_{q=1}^{q=n} \rho_q \right] K_p$$

thus for

$$n=2 \quad K_{eff} = \rho_1 K_1 + \rho_1 \rho_2 K_2$$

$$n=3 \quad K_{eff} = \rho_1 K_1 + \rho_1 \rho_2 K_2 + \rho_1 \rho_2 \rho_3 K_3$$

In the case when all stages are identical ($K_n = K$ and $\rho_n = \rho$), $K_{eff} = npK$; in the case when the interfering signal is inside the passband ($\rho = 1$), $K_{eff} = nK$.

The foregoing derived expressions and graphs can thus be applied for n cascaded stages by simply substituting the specific K_{eff} for K .